Cyclic Deformation and Fatigue Behaviour in Cancellous Bone

zur Erlangung des akademischen Grades eines
DOKTORS DER INGENIEURWISSENSCHAFTEN (Dr.-Ing.)
der Fakultät für Maschinenbau
der Universität Paderborn

vorgelegte
DISSERTATION

von
M.Sc. Sebastian Dendorfer
aus Regensburg

Datum des Kolloquiums: 11.01.2008
Erster Gutachter: Prof. Hans Jürgen Maier
Zweiter Gutachter: Prof. David Tylor

Publications

S. Dendorfer, J. Hammer and H.J. Maier, Strain evolution during compressive fatigue of bovine cancellous bone, edited by J. Hozman and P. Kneppo, IFMBE Proceedings of the 3rd European Medical & Biological Engineering Conference, EMBEC 05, November 20-25 2005, Prague, Cz, 11(1), No. 2628

S. Dendorfer, J. Hammer and H.J. Maier, Deformation behaviour of bovine cancellous bone, Technol Health Care. 2006;14(6): 549–56

S. Dendorfer, H.J. Maier and J. Hammer, How do age and anisotropy affect the fatigue behaviour of cancellous bone?, Studies in Health Technologies and Informatics, accepted

S. Dendorfer, H.J. Maier, D. Taylor and J. Hammer, Anisotropy of the fatigue behaviour of cancellous bone, Journal of Biomechanics, in press

Contents

Abstract

The fatigue behaviour of materials is of particular interest for the failure prediction of materials and structures exposed to cyclic loading. For trabecular bone structures only a few sets of lifetime data have been reported in the literature and structural measures are commonly not considered. The influence of load contributions which are not aligned with the main physiological axis remains unclear. Furthermore site and species dependent relationships are not well described. In this study seven different groups of trabecular bone, defined in terms of orientation, species and site were exposed to cyclic compression. In total, 108 fatigue tests were analysed with respect to lifetimes, deformation behaviour and damage accumulation. Furthermore, damage mechanisms were derived from novel measurement methods for the optical strain analysis on the apparent and tissue level. The lifetimes were found to decrease drastically when off-axis loads were applied. Additionally, species and site strongly affect fatigue lifetimes. While the characteristics of cyclic deformation were found to be similar for all groups, large deviations were observed for the fatigue lifetimes. Bovine specimens did reveal higher lifetimes compared to human samples and lifetimes decreased with increasing deviation of the specimens' axis from the physiological bone axis. Already small deviations cause a large reduction, whereas deviations above 45° result in a similar fatigue behaviour. Strains at failure were found to be dependent on specimen orientation (with respect to the physiological bone axis). The whole cyclic deformation process as well as damage evolution until defined failure could be shown to be a function of normalised stress and group. The corresponding functional relationships were derived. Damage acceleration was found to be constant for all specimens and different damage mechanisms are acting for on-axis and off-axis groups. Likewise, load thresholds were found, at which damage mechanisms change from low-cycle to high-cycle fatigue. Age

appeared to have a large influence on the initial modulus of the specimens. Deformation analysis on the apparent and the trabecular level could be linked to macroscopic damage and microdamage was found to contribute to residual strain accumulation. Concluding, the axis of loading appears to contribute dominantly to fatigue and cyclic deformation, which may be even more pronounced in cases of increased anisotropy (Osteoporosis). Therefore, local morphological information has to be included in risk of fracture predictions in order to achieve a higher reliability.

Kurzfassung

Das Ermüdungsverhalten von Materialien ist von grosser Bedeutung für die Beurteilung des Versagensrisikos von Bauteilen und Strukturen die zyklischer Belastung ausgesetzt sind. In Analogie zu technischen Bauteilen können Ermüdungsscäden auch bei Knochen beobachtet werden. Im Gegensatz zu kortikalen Knochen, bei dem das Ermüdungsverhalten weitgehend untersucht ist existieren nur sehr wenige Daten für spongiösen Knochen. In allen verfügbaren Studien wurde die starke Anisotropie der Knochenstruktur nicht berücksichtigt und nur Proben entlang der physiologischen Achse verwendet. Weiter ist der Einfluss von verschiedenen Spongiosa-Arten (human, bovin) sowie des Alters noch nicht geklärt. In dieser Studie wurden sieben Gruppen von Spongiosaproben, insgesamt 108 Proben, unterschiedlich bezüglich der Spezies (human, bovin), des Entnahmeortes (Wirbelkörper, distale Femurkondyle) sowie der Abweichung von der physiologischen Hauptachse hinsichtlich des Verformungsverhaltens unter zyklischer Druckbelastung untersucht. Neben der Analyse des integralen Materialverhaltens wurde ein optisches Verformungsmesssystem verwendet, mit dessen Hilfe die Entwicklung von Dehnungen auf der Probenoberfläche sowie auf Knochenbälkchenebene gemessen wurde. Proben deren Hauptachse nicht mit der physiologischen Hauptachse übereinstimmte zeigten stark reduzierte Lebensdauern. Ebenso haben Spezies sowie der Entnahmeort einen grossen Einfluss auf das Ermüdungsverhalten. Dies war auch der Fall wenn die unterschiedlichen Anfangssteifigkeiten der Proben berücksichtigt wurden. Die Rinderproben zeigten eine höhere Ermüdungsfestigkeit als die menschlichen Proben. Die Lebensdauern reduzierten sich mit grösseren Abweichungen von der physiologischen Hauptachse. Bereits kleine Winkelabweichungen resultierten in einem starken Abfall der Ermüdungsfestigkeit, bei Abweichungen grösser 45° wurden annähernd gleiche Lebensdauern gemessen. Die Versagensdehnungen sind

ebenfalls gruppenabhängig und steigen mit steigender Abweichung von der Hauptachse. Das zyklische Verformungsverhaltens konnte ebenso wie die Entwicklung der integralen Schädigung in Abhängigkeit der normalisierten Spannung (σ/E_0) und der Gruppenzugehörigkeit dargestellt werden. Die entsprechenden mathematischen Zusammenhänge wurden abgeleitet. Verschiedene Schädigungsmechanismen wurden für die Gruppen parallel zur Hauptachse und die Gruppen mit Abweichungen von der Achse gefunden. Das Alter der Spender hatte einen grossen Einfluss auf die Anfangssteifigkeit der Proben und somit auf das zyklische Verformungsverhalten sowie die Lebensdauern. Ein weiterer Einfluss des Alters konnte jedoch nicht gezeigt werden. Die optische Verformungsmessung konnte erfolgreich auf die spongiösen Proben angewendet werden. Die hierbei gefunden lokalen Dehnungskonzentrationen, sowohl auf der (integralen) Probenoberfläche als auch auf der Oberfläche einzelner Trabekel konnten mit dem integralen Verformungsverhalten korreliert werden. So kann gezeigt werden, dass die Entwicklung bleibender Verformungen direkt mit der Bildung und dem Wachstum von Mikrorissen verknüpft ist. Zusammenfassend konnte der starke Einfluss der verschiedenen Spongiosa-Arten auf die Versuchsergebnisse gezeigt werden. Bereits geringe Abweichungen von der physiologischen Hauptachse resultieren in einer starken Abnahme der Ermüdungsfestigkeit. Bedingt durch den Anstieg der Anisotropie in älteren Knochen wird dieser Effekt noch weiter verstärkt. Deshalb ist gerade bei der Abschätzung des klinischen Versagensrisikos die Berücksichtigung von Strukturkennwerte unabdingbar um die Genauigkeit der Methoden zu erhöhen. Mit den abgeleiteten Funktionen für die Entwicklung der Verformungen sowie der Schädigung und zyklischer Belastung stehen wichtige Werkzeuge zur Verfügung, welche direkt in numerischen und analytischen Studien verwendet werden können.

Nomenclature

$\dot{\varepsilon}$ ..... Strain rate, s^{-1}

σ ..... Nominal or 1st Piola-Kirchhoff stress, MPa

σ_c ..... Compressive strength, MPa

σ_f ..... Fatigue strength coefficient

ε ..... Nominal strain, mm/mm

ε_f ..... Fatigue ductility coefficient

ε_{max} ..... Maximum strains (accumulated total strains), mm/mm

$\varepsilon_{max\ f}$ ..... Maximum strains at failure (D=0.1), mm/mm

$\varepsilon_{max\ t}$ ..... Maximum strains at end of the transient, mm/mm

ε_{res} ..... Residual strains (accumulated residual strains), mm/mm

$\varepsilon_{res\ f}$ ..... Residual strains at failure (D=0.1), mm/mm

$\varepsilon_{res\ t}$ ..... Residual strains at end of the transient, mm/mm

E_0 ..... Initial secant modulus, MPa

N/N_f ..... Normalised cycle numbers

N_f ..... Number of cycles to failure (D=0.1)

a ..... Fatigue strength coefficient, Equation 4.14

B ..... Basquin exponent

b ..... Fatigue strength exponent, Equation 4.14

BMD ..... Bone Mineral Density, g/ccm

BMU ..... Basic Multicellular Unit

C ..... Fatigue ductility exponent

c, d ..... Regression coefficients for Equation 4.2

D ..... Damage parameter: $1-(E_{sec}/E_0)$

d ..... Density, g/ccm

e, f ..... Regression coefficients for Equation 4.3

g, h ..... Regression coefficients for Equation 4.4

i, j ..... Regression coefficients for Equation 4.5

in vitro ..... Latin: in the glass

in vivo ..... Latin: in the living

k, l ..... Regression coefficients for Equation 4.9

LM ..... Light Microscopy

m, n ..... Regression coefficients for Equation 4.10

MIL ..... Mean Intercept Length

PBA ..... Physiological bone axis

SEM ..... Scanning Electron Microscopy

1 Introduction

1.1 Background

In recent years, increasing research efforts were made in the field of biomechanics and bone mechanics. These activities are mainly driven by social and economical needs. The economic burden (only direct costs) in Germany attributable to Osteoporosis alone was estimated as high as euros 5.4 billion based on data from 2003 (Haeussler et al., 2007). As demography changes with the consequence of a higher amount of elderly people as well as the increase in the individual lifespan, life sciences will be confronted with major challenges (Borgström et al., 2007). Additionally, the level of activity of older people nowadays is high, which results in high requirements on implants and prostheses. The trend of degeneration in tissue quality (in the body) with increasing age sets demand for steady improvements. Furthermore, the timespan in which patients are bedridden in general should be reduced in order to improve the outcome of healing, but also to reduce health-related absenteeism. Besides these rather ambitious and noble aims, from a scientist's point of view, the fascination of this reseach field lays in the complexity of the problems, requiring a thorough interdisciplinary cooperation of (among others) medics, biologists and engineers. For example, the idea of a self-maintaining (and optimising) spatial structure is especially attractive for structural engineers and therefore one of the reasons for this work in the field of bone mechanics.

A proper understanding of the mechanics of bones is required for multiple reasons. The diagnosis to what extent certain bones are at risk of failing gets increasingly important as the population of elderly people increases. In today's clinical practise Osteoporosis and

therefore fracture risk is determined by measuring the Bone Mineral Density (BMD). This integral value provides only information on the quantity of bone available, but whereas it has been shown in numerous studies that density is related to (monotonic) strength in bone (Gibson and Ashby, 1997), its dependency is rather weak as it neglects other components contributing substantially to bone strength such as morphological information. Current research tries to improve imaging techniques to allow a more precise prediction of these parameters and therefore of bone quality (Friedman, 2006). Therefore, also knowledge about the mechanical behaviour of bone structures with respect to bone architecture is needed. Further, (micro-)damage is supposed to act as a stimulus for repair and adaption processes (remodeling) in bone (Burr et al., 1985; Lee et al., 2002). Understanding how damage in bone evolves may therefore also shed light on the underlying mechanobiology. This knowledge is essential to investigate treatment options for bone diseases like Osteoporosis. Treatment options are also needed for the increasingly complicated fractures due to declined bone quality of elderly people as well as for the so-called critical size defect, where bone is not able to bridge the defect region. Research is conducted on artificial bone substitutes which may be used to bridge critical defects in bones with or without the expression of drugs. So highly porous Ti6Al4V constructs have been developed which show apparent mechanical properties similar to cancellous bone (Li et al., 2006). Other approaches are mainly based on hydroxylapatite and calcium, using osteoconductive and degradable properties of the materials (Englert et al., 2007). In order to successfully apply these materials also knowledge of the initial, unharmed bone tissue is required. Finally, of course the further refined development of implants and prostheses takes advantage of an improved understanding of bone mechanics.

1.2 Objectives

Bone tissue can be divided in two types, mainly differing in apparent density: high density bone called cortical or compact bone and less dense bone showing a framework structure named cancellous or trabecular bone. On a micro- and ultrastructural level bone exhibits

many of the characteristics of an engineering composite or fibre-reinforced concrete. It is well known for engineering structures that cyclic loading may induce fatigue failure. In fact, a vast majority of structural collapses in loaded structures are fatigue induced (Suresh, 1998). Fatigue damage is also known to cause fractures in bones (Snyder et al., 2006; Niemeyer et al., 2006) and is associated with age-related fragility fractures (Burr et al., 1997) as well as the loosening of implants (Bauer and Schils, 1999). Despite these clinical observed fractures only few studies are available concerning the fatigue behaviour of cancellous bone (Michel et al., 1993; Moore and Gibson, 2003b; Haddock et al., 2004; Yamamoto et al., 2006). All of these studies were conducted using bone specimens cored parallel to the main structural axis of the trabecular bone architecture and only few using human donor material. But loading *in vivo* may not always be aligned with this axis. A change in local loading conditions, e.g. through structural implants (Fig. 1.2) or even through habitual motion, may result in load components in off-axis directions. Further, the influence of off-loads may be much more pronounced with increasing anisotropy of the structure, which is one of the main characteristics of Osteoporosis. Information of direction-dependent fatigue properties may therefore contribute essentially to our understanding of failure in bones and for example assist in the proper placement of implants.

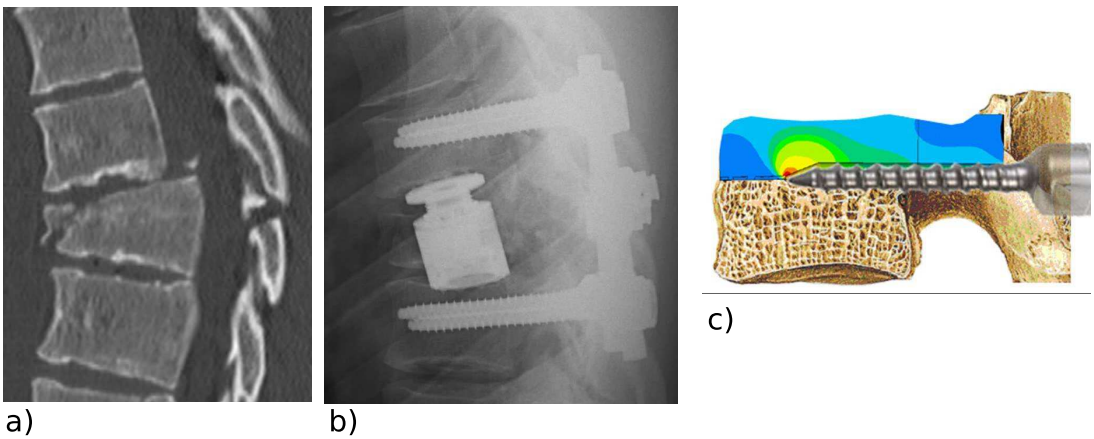

Figure 1.1: Fracture and treatment of a spine injury. a) Compression fracture with torsional components of a thoracic vertebra (T8), b) Post-operation (with kind permission of M. Nerlich, Clinical Center of the University Regensburg), b) Stress distribution (schematically) around a pedicle screw under loading.

Whereas some principal mechanisms of the damage process during cyclic loading are reported for bovine bone (Moore and Gibson, 2003a; Ganguly et al., 2004), still, a full understanding of the failure and cyclic deformation mechanisms, especially concerning human bone, is missing. Even if it has been proposed that fatigue in cancellous bone is governed by ultrastructural mechanisms as two very different cancellous bone types (bovine and human) did show very similar lifetime behaviour under cyclic loading conditions (Haddock et al., 2004), the influence of different bone architectures on the cyclic deformation behaviour has not been addressed yet. But especially the increasing application of advanced numerical models (Homminga et al., 2004; Yeni et al., 2001; Hernandez et al., 2006) as well as theoretical modelling of deformation processes in general sets a demand for a strong experimental base of the deformation processes. Damage in cancellous bone due to cyclic loading has been identified using post-testing microscopic analyses (Moore and Gibson, 2003a). Damage evolution during loading has only been investigated in step-wise compression experiments (Nazarian and Muller, 2004). The direct link between microscopic and macroscopic damage is still not known. Additionally, the effect of age on the fatigue behaviour of cancellous bone remains obscure.

Therefore, the main research questions in this study were defined as:

- What is the influence of the axis of loading on the fatigue and cyclic deformation behaviour of cancellous bone?
- How do different types of cancellous bone (species, site) and age influence the fatigue behaviour?
- How do damage evolution and cyclic deformation depend on loading and orientation?
- Furthermore, methods should be established to study the underlying damage mechanism in order to possibly link microscopic and macroscopic damage.

2 Trabecular Bone: Morphology and Mechanics

2.1 Structural Properties

2.1.1 Bone Composition

Bone tissue in mammals is present in very different configurations. The main function of bone is to provide the mechanical stability for body and motion as well as to protect vital parts of the body. Apart from these rather obvious facts bone is essential for mineral homoeostasis, storing and providing minerals. At first glance, bones seem to be rather compact and homogeneous. But on the macroscopic, microscopic and nanoscopic scale a highly heterogeneous composite can be found. The outer layer of all bones and the diaphysis (the mid section/shaft) of long bones are built of high density ($\sim 1.0 - 1.8\ g/cm^3$) compact (or cortical) bone. This hard shell encloses a low density ($< 1.0\ g/cm^3$) network of plates and struts named trabecular (cancellous, spongy) bone (Fig. 2.1).

Marrow and cells are located in-between the trabeculae. Apart from the differing structural architecture, the tissue composition (and tissue density) is almost similar in both, cortical and cancellous bone. It consists of a mineral (~ 65 %) and an organic phase (~ 35 %). The mineral component is mainly built of impure hydroxyapatite, $Ca_{10}(PO_4)_6(OH)_2$, in form of needles, plate and rod-like crystals. Furthermore, minerals like carbonate, citrate, magnesium and fluoride are present, mainly for homoeostasis. About 90 % of the organic matrix proteins are collagen type 1, organised in helix-like fibres. Other components are various non-collagenous proteins and water. The collagen

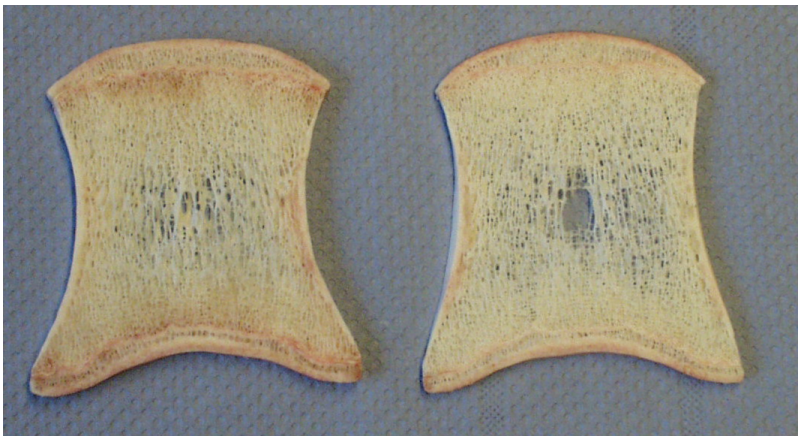

Figure 2.1: Bovine vertebral body sections from two different positions. A thin outer layer, cortical bone, encloses a foam structure, cancellous bone.

fibrils possess a two-phase, viscoelastic material behaviour with a high tensile strength. And due to its structural composition as well as its high length to diameter ratio their primary mechanical function is to withstand tension loading. The combination of the stiff mineral and the high rupture strength of the fibres builds up an efficient composite, similar to technical composite materials and reinforced concrete (see e.g. Cowin (2001)).

The predominant structures in cortical bone are osteons. In the middle of an osteon lays the Haversian canal, which is surrounded by concentric layers of (collagen) lamellae. Interconnected Osteocytes are found between the lamellae, canalaculi enable the exchange of nutrients. Fig. 2.2 shows a section of cortical bone taken from a human femur. The boundary between osteons and surrounding bone is referred to as the cement line. The diameter of a osteon is about 200 μm and their longitudinal axis is mainly aligned with the main axis of long bones. Trabeculae are built of segments of parallel lamellae (built of fibres of collagen) preferentially aligned with the longitudinal axis of the trabeculae. These groupings of lamellae are separated by cement lines (amorphous substance deficient in collagen) and called trabecular packets (Fig. 2.3).

Unlike engineering material, the living body has the ability to react to altered loading conditions and (micro-)damage, which may be induced by cyclic or isolated loadings, with adaptation and repair processes referred to as remodeling (Frost, 2003; Lee et al., 2002) (Fig. 2.3). A combination of bone resorbing (Osteoclasts) and bone forming (Osteoblasts)

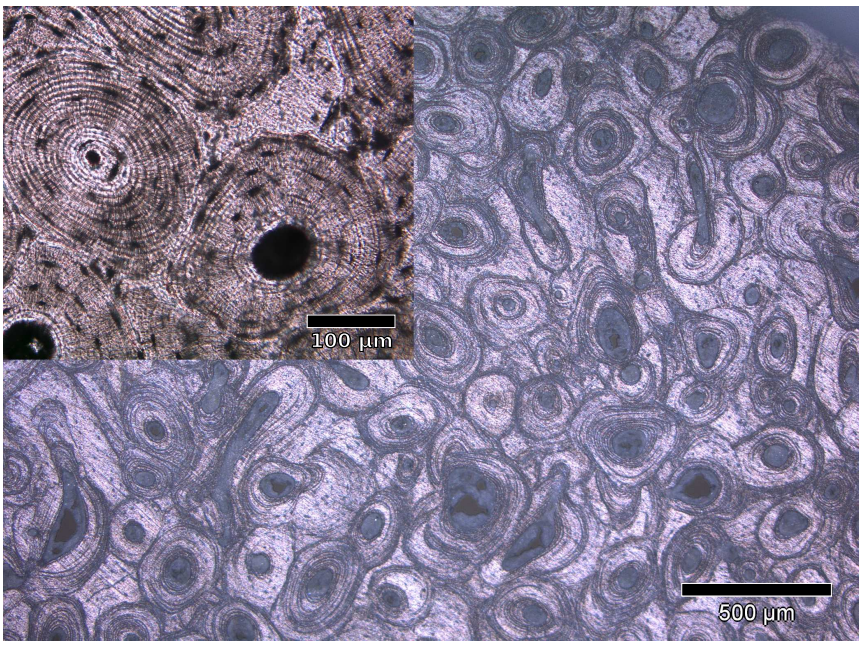

Figure 2.2: Microstructural composition of cortical bone. Osteons in a transverse section through human femoral cortical bone.

cells, organised in Basic Multicellular Units (BMU), is involved in this remodeling process. Whereas in cortical bone BMUs 'tunnel' through the bone with a diameter of approximately 200 μm, at a speed of 40 μm/day and resorb and build new bone in so-called secondary osteons, in trabecular bone remodeling occurs on the trabeculae surface by resorbing the old bone and filling the cavity with a new trabecular packet. Due to the large surface to volume ratio in cancellous bone the bone turnover is much more active compared to cortical bone. The turnover rate is reported as high as 26 %/year in cancellous bone, compared to 3 %/year in cortical bone (Jess, 1990). These remodeling processes enable bones to operate under high loading conditions, taking into account damage from daily activities, but having the advantage of a mimimum weight design and the ability to transform and adapt to altered loading conditions. A drastic example for a change in the latter are space flights which are known to reduce bone mass (LeBlanc et al., 2007). But also misuse (alcohol, smoking, imbalance in dietary intake) as well as physical inactivity in general are known to reduce the ability to remodel (Sowers, 2000). Numerous researchers proposed different theories on remodeling processes and models to predict these (Prendergast and Taylor, 1994; Fyhrie and Schaffler, 1995; Levenston and Carter, 1998; Lee et al.,

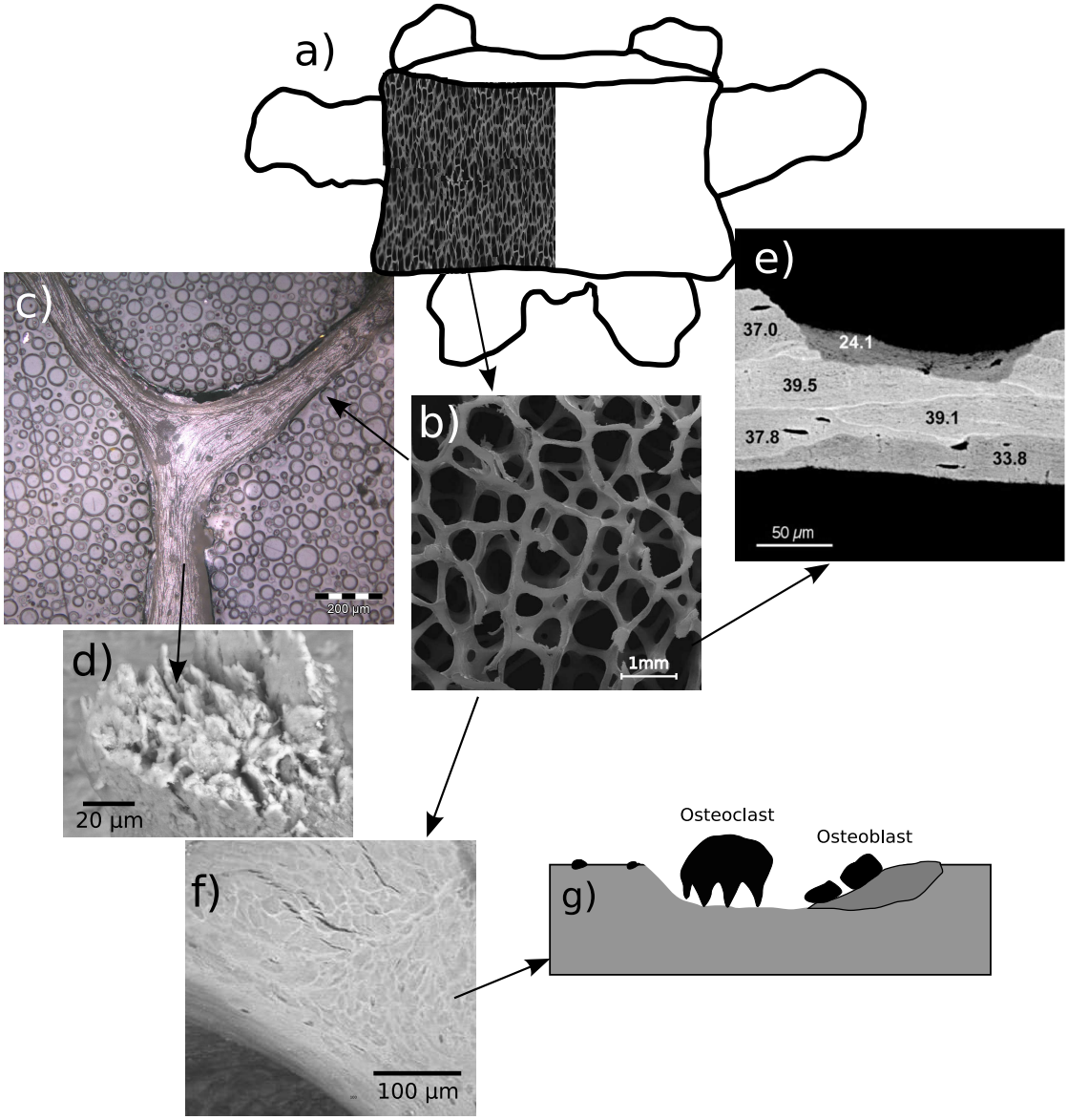

Figure 2.3: Overview of the structural composition of trabecular bone on different scale levels. a) Sketch of a vertebral body, b) low magnification microscopy of the (human vertebral) cancellous bone structure, c) sectioned trabeculae showing the underlying lamenar structure, d) lamenar bundles on a fracture surface of a trabecula, e) quantitative backscattered electron imaging of a sectioned trabecula, individual bone packets, separated by cement lines are visible, the numbers refer to the average mineral content given in vol% within each packet (Fratzl et al. (2004), with kind permission), f) Osteoclastic (bone resorbing) activity on the surface of trabecula, g) basic mechanism of trabecular remodeling with bone resorbing (Osteoclasts) and formation (Osteoblasts) cells.

2002; Frost, 2003; Taylor et al., 2003a). But the precise mechanism by which the living bone detects damage and in consequence adapts to loading are still unknown (Taylor et al., 2007).

2.1.2 Morphology of Cancellous Bone

The cellular nature of cancellous bone is visible from low-magnification microscopy (Whitehouse et al., 1971; Whitehouse and Dyson, 1974). Cancellous bone can be classified as a open (pore) polyhedral cellular solid (Gibson, 2005). Typical dimensions are: pore sizes 0.3 - 1.5 mm, strut dimensions 0.1 - 0.3 mm. These hold regardless of the species (Martin et al., 1998). The architecture of the trabecular network appears to be inhomogeneously oriented. Many authors found striking evidence that bone grows in response to loading (Wolff, 1892; Roux, 1895; Frost, 1987). That means, the architecture of the trabeculae network follows the trajectories of the main loading direction so that bending is minimised. The structural anisotropy may therefore depend on the ratios of the acting principal stresses (Gibson and Ashby, 1997). Higher loading results in more platelike trabeculae in the main loading direction with interconnecting small trabeculae as spacers (Fig. 2.4), whereas lower loaded regions exhibit a more truss-like framework (Fig. 2.3 b)) (Whitehouse and Dyson, 1974).

Several structural measures for the degree of anisotropy have been developed. The most established method is the Mean Intercept Length (MIL) (Whitehouse and Dyson, 1974; Whitehouse, 1974; Harrigan and Mann, 1984). Furthermore, the Volume Orientation (VO) (Odgaard et al., 1990), Star Volume Distribution (SVD) (Cruz-Orive et al., 1992) and fast Fourier transformation-based measures (Brunet-Imbault et al., 2005) are, among others, reported. Cowin defined the fabric tensor as a measure for the degree of anisotropy, which is based on the inverse of the MIL tensor, and set up a general theory which relates the structural anisotropy to the elasticity tensor (Cowin, 1985).

The open cell structure of trabecular bone requires a distinction between the apparent properties, referring to the whole specimen, and the tissue properties, referring to the bone

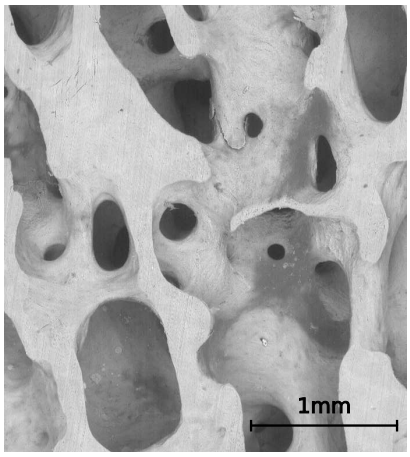

Figure 2.4: SEM image of a bovine vertebral cancellous bone. Plate-like structure in the main physiological axis (vertical) direction.

tissue/trabeculae itself. The mechanical properties referred to in this study are analysed on the apparent level. In order to fulfil the assumption of a continuum for the experimental investigation of the apparent properties an adequate specimen size has to be chosen. The minimum continuum length has been estimated to be about five trabecular spacings and therefore $5 - 10\ mm$ (Fung, 1993).

2.2 Mechanical Properties

The mechanical response of cancellous bone has been characterised by numerous researchers. Several approaches to model the deformation behaviour have been performed on an analytical, numerical and experimental base. Analytical models include structural analysis of unit cells and density-based methods assuming the cell geometry as similar at different degrees of density (Gibson, 2005). By means of numerical methods the deformation behaviour of regular or random cellular structures has been investigated (Vajjhala et al., 2000; Schaffner et al., 2000; Makiyama et al., 2002). Recently, due to increased computational power and improved imaging techniques also numerical studies on almost exact geometries of trabecular bone samples have been performed (Yeni et al., 2001; Homminga et al., 2004; Hernandez et al., 2006). However, most of the published work on the biome-

chanics of trabecular bone during the last 40 years is based on experimental studies, which do also make up the majority of the following review. Most studies discussed below deal with cancellous bone, if not stated explicitly that other materials have been used. As material testing on highly inhomogeneous structures like cancellous bone is quite complicated and no real standard for the experimental boundary conditions are given in terms of specimen size, rate of loading, load application and surrounding media, results from literature are also very heterogeneous. Some of the variations in mechanical data may be ascribed to experimental effects, introduced by ignoring the structural anisotropy, the proper boundary conditions (e.g. end artefact errors) (Linde and Hvid, 1989; Keaveny et al., 1993, 1997) and size effects (Taylor, 1998). But there is also a natural heterogeneity which complicates the analysis of bone. For example, compressive stiffness was found to vary up to 100-fold within a single proximal tibia (Goldstein et al., 1983).

2.2.1 Monotonic Loading

Monotonic trabecular bone properties have been investigated by numerous researchers (Keaveny et al., 2001). The compressive stress-strain behaviour of cancellous bone is typical of that of a cellular solid. Following a linear regime, plastic collapse occurs with subsequent failure of struts, resulting in a rather long stress plateau, and an increase of stresses at higher strains due to densification effects (Gibson and Ashby, 1997) (see Fig. 4.3). Several studies indicate that bending of trabeculae is the dominant deformation mode in linear elastic deformations (van Rietbergen et al., 1995; Nazarian and Muller, 2004). Depending on the slenderness ratio trabeculae can fail either by elastic buckling or by progressive microfracture (Townsend et al., 1975). At lower degrees of density elastic buckling dominates, at higher density rates the trabeculae have lower slenderness ratios and fail by progressive microfracturing (Gibson and Ashby, 1997). Yield strength in tension was found to be smaller than in compression (Kaplan et al., 1985). Typical values for yield strength and modulus of cancellous bone are shown in Tab. 2.1. Strains at failure were also found to be higher in compression than tension (Kopperdahl and Keaveny, 1998). The absolute value of the yield strain can vary between sites (Kopperdahl and Keaveny, 1998; Morgan

et al., 2001) whereas they seem to be almost constant within one site. Typical failure strains (0.2% offset strain) are reported to be 1.09% for bovine tibia (Keaveny et al., 1994) and 0.79% for human vertebral cancellous bone (Haddock et al., 2004). As strains at failure are constant, at least in bone taken from the same site, but modulus and strength may vary by order of magnitudes, it has been suggested that the damage behaviour and therefore the failure criterion for cancellous bone is strain-based (Moore and Gibson, 2003b). The mechanical performance of cancellous bone under monotonic loading seems to be rather poor, compared to engineering material (Fig. 2.5), but in relationship to its density it reveals to be an extraordinary composite.

The oriented architecture of the cancellous bone structure is also reflected in the mechanical properties. The mechanical anisotropy of trabecular bone has been tested under monotonic loading conditions and isotropy of yield strains has been suggested, whereas modulus and strength vary with orientation (Turner, 1989; Ford and Keaveny, 1996; Nicholson et al., 1997; Bayraktar et al., 2004). Modulus as well as strength were found to decrease in off-axis directions, depending on the structual anisotropy. Nicholson et al. (1997) found an approximately 4-fold higher stiffness in superior-inferior direction in human vertebral cancellous bone compared to lateral values. A recent study shows that specimens taken from the radius with a high structural anisotropy exhibit a significant lower value in yield strain than specimens from other sites with lower anisotropy (Matsuura et al., 2007). Furthermore, cancellous bone is reported to have at least orthotropic symmetry in the elastic properties (Williams and Lewis, 1982; Turner and Cowin, 1988; Yang et al., 1998). The multiaxial behaviour of cancellous bone has been studied and yield criteria like the Tsai-Wu criterion have been applied to model the deformation behaviour (Stone et al., 1983; Keaveny et al., 1999).

Due to the porous structure of cancellous bone also the influence of marrow, in terms of pore fluid, on the mechanical behaviour may be regarded. It has been shown that this is negligible for strain rates below 10/s (Carter and Hayes, 1977). Further, bone is known to possess viscoelastic properties. But with a strain rate coefficient of 0.06 this dependency is rather weak (see Equation 2.1). Under physiological loading conditions, daily activities,

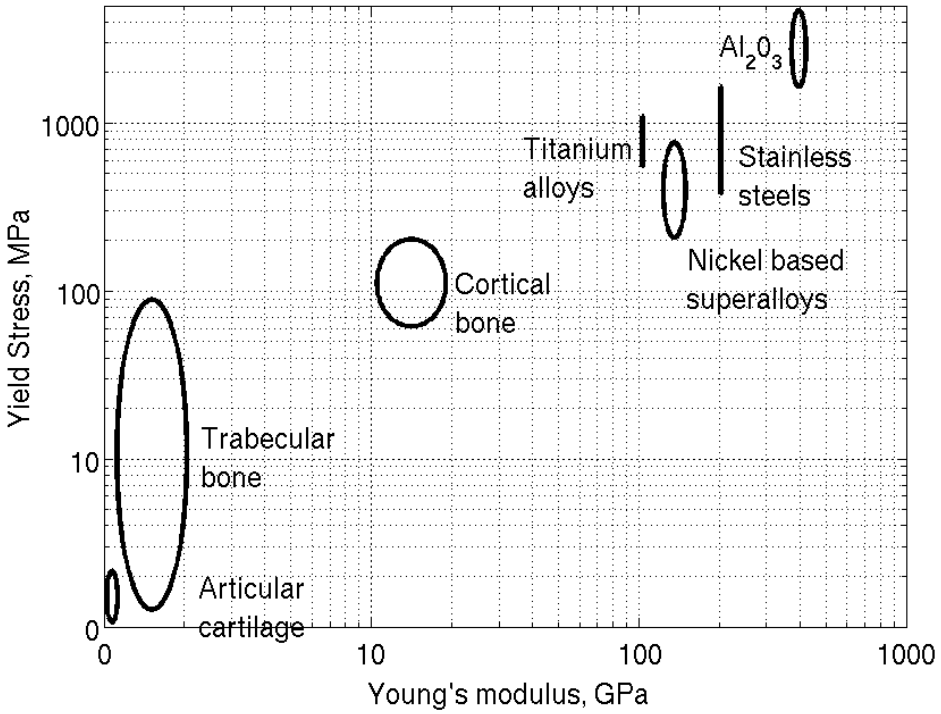

Figure 2.5: Comparison of the range of modulus and yield strength for biological and engineering materials.

strain rates below 0.015 s^{-1} are reported (Martin et al., 1998). Of course, this may not hold for trauma situations. With increasing rate of loading yield strength as well as modulus increase, whereas strain at failure decreases. Therefore, bone tissue can withstand in trauma situation higher loadings, but does also fail in very high speed impacts in a very brittle manner and complex fracture patterns are observed in these cases. The transition from physiological frequencies (0.5-2 Hz) to high frequencies (30 - 125 Hz) were observed to affect the fatigue strength in experimental situations by a factor of 1.33 (Taylor, 1998). Moisture also influences the mechanical behaviour of bone and is an essential boundary condition in the experimental setup. Wet bone exhibits an increased ductility whereas dry bone has a higher modulus and yield strength.

The determination of density - mechanical properties correlations is the scope of numerous research activites as bone density measurements can be applied in clinical praxis. As structural cell modelling suggests both elastic modulus and yield strength depend on

Table 2.1: Compressive modulus and compressive strength of cancellous bone

Anatomic site	Modulus, MPa	Strength, MPa	
Human vertebra	70 to 90	1.37 to 1.86	(Yamada, 1970)
Human proximal tibia	489 ± 331	2.22 ± 1.42	(Rohl et al., 1991)
Human proximal tibia	445 ± 257	5.33 ± 2.93	(Lotz and Hayes, 1990)
Human vertebra	67 ± 44	2.45 ± 1.52	(Mosekilde and Mosekilde, 1986)
Human vertebra	291 ± 113	2.23 ± 0.95	(Kopperdahl and Keaveny, 1998)
Bovine tibia	2690 ± 900		(Bowman et al., 1998)

apparent density, even if the precise relationship remains controversial. The measurement of Bone Mineral Density (BMD) is a non-invasive standard procedure in clinics. Different methods have been developed in order to measure the density of minerals in bones (e.g. X-ray, computed tomography or ultrasound). Correlation between elastic modulus and density were found to be linear (loaded in physiological axis, from one site) (Kopperdahl and Keaveny, 1998), quadratic (Rice et al., 1987) or cubic (Carter and Hayes, 1977). The latter authors' relationships are frequently used in the following forms:

$$\sigma_c = 68 \times \dot{\varepsilon}^{0.06} \times d^2 \tag{2.1}$$

$$E = 3790 \times \dot{\varepsilon}^{0.06} \times d^3 \tag{2.2}$$

$\dot{\varepsilon}$: strain rate, s^{-1}

d: density, g/ccm

σ_c: compressive strength, MPa

E: modulus, MPa

Recently, there seems to be evidence that no universal modulus - density relationship for on-axis loading is present (Morgan et al., 2003). Correlations between mechanical properties and BMD were found to be highest if loads were applied aligned with the main physiological axis (Augat et al., 1998). Alternative formulations for the prediction of the mechanical properties which include microstructural information are also under investigation (Rajapakse et al., 2004). Despite the fact that most of these relationships show

good correlations (from a statistical point of view), the quality of the data seems to be unacceptable for precise fracture prediction. Therefore, attempts are made to increase the predictability power with morphological information. Several authors used successfully different combinations of volume fraction and measures for structural anisotropy in order to increase the predictability strength of the elastic properties (Hodgskinson and Currey, 1990; Zysset and Curnier, 1996; Yang et al., 1998; Zysset, 2003). Furthermore, ultrasonic techniques were applied to measure the elastic constants in cancellous bone (Ashman and Rho, 1988), having the advantage of excluding many experimental artefacts but lacking the opportunity to predict the mechanical behaviour precisely in the in vivo situation. Taken together, approaches exist to determine the mechanical behaviour non-invasively but today's knowledge leaves plenty of space for improvements.

Finite element models developed from micro computer tomography have been applied to detect failure mechanism and local strain fields (Homminga et al., 2004; Hernandez et al., 2006). Microdamage initiation was found to occur prior to apparent yield using image-based finite element models with local principal strains of $0.46 - 0.63\%$ in compression (Nagaraja et al., 2005). Further numerical studies demonstrated also that damage is already visible below the apparent compressive yield strain. The authors suggest that local tissue yielding can in fact initiate at very low apparent strains and that the apparent mechanical properties are degenerated through these localised effects (Morgan et al., 2005).

The behaviour of microcracks in bone is a highly active research field (Hazenberg et al., 2007). Most of the research has been addressed to cortical bone. It has been shown that fracture toughness increases with crack length (Vashishth, 2004). Multiple mechanisms were suggested to contribute to this effect. Microstructural barriers were found to arrest crack growth. Cracks below a critical length are supposed to be stopped, whereas above a certain threshold crack energy is large enough for further propagation and initiation of macroscopic damage. Microcracks of less then 100 μm were found to arrest at cement lines, which surround the osteons, whereas medium microcracks of $100 - 300$ μm were deflected at the cement lines' boundary. Longer microcracks (greater than 400 μm)

did cross the cement lines (Mohsin et al., 2006). Furthermore, bridging of microcracks (through collagen fibres) (Yeni and Fyhrie, 2003; Nalla et al., 2003) as well as diffuse damage in front of larger microcracks (Vashishth, 2004) are supposed to raise the fracture toughness with increasing crack length. The exact connection between microstructural composition of trabecular bone and its mechanical behaviour is still under discussion. A mechanical role of the cement lines with respect to microfractures in trabecular tissue has been suggested (Choi and Goldstein, 1992), as well as the importance of the non-uniform mineral distribution in trabeculae on the apparent mechanical properties was emphasised (van der Linden et al., 2001). The microstructural properties itself, lamellar-level elastic modulus, hardness and extracellular matrix have been suggested not to depend on age, gender or increased bone mass maintenance (known to occur in heavier individuals) (Hoffler et al., 2000). Likewise, studies on crystal length and crystal thickness in the mineral phase of the bone tissue did not reveal significant differences between normal and osteoporotic trabecular bone (Rubin et al., 2003). But nevertheless, more data is needed to reveal the exact relationship between the micro- and ultrastructural composition and the mechanical properties.

It has been suggested that damage in human cancellous bone is at least of orthotropic nature. Transverse damage components for on-axis (0°) specimens were found to be on average 1.9% of the damage components aligned with the stress axis, whereas transversal oriented specimens (90°) did reveal transverse components of 6.5% (Bredbenner and Davy, 2006). In contrast, other attempts to characterise the damage effects in bovine tibial trabecular bone used high-resolution finite element models resulted in much higher transverse damage values for the off-axis specimens and much higher magnitudes of the damage parameters (up to 36% of the loading axis components) (Bredbenner (2003) as cited in Bredbenner and Davy (2006)). Although damage was found to be anisotropic in cancellous bone, the material coordinate system did not lose alignment with the structural orientation (fabric tensor) (Liu et al., 2003).

2.2.2 Cyclic Loading

The majority of failure cases in mechanical engineering resulting from mechanical loading, are fatigue-induced (Suresh, 1998). In contrast to failure under monotonic loading (in ductile materials), where failure is associated with macroscopic plastic deformation under cyclic load exposure, fractures appear almost sudden and unexpected without visible distinctive deformation. Additionally, this may happen at stress levels much below the monotonic yield strength. Therefore, severe accidents may result, which did cause serious damage in the past. The main stages of damage evolution during fatigue following the description of Mugrabi (1985) are shown in Fig. 2.6.

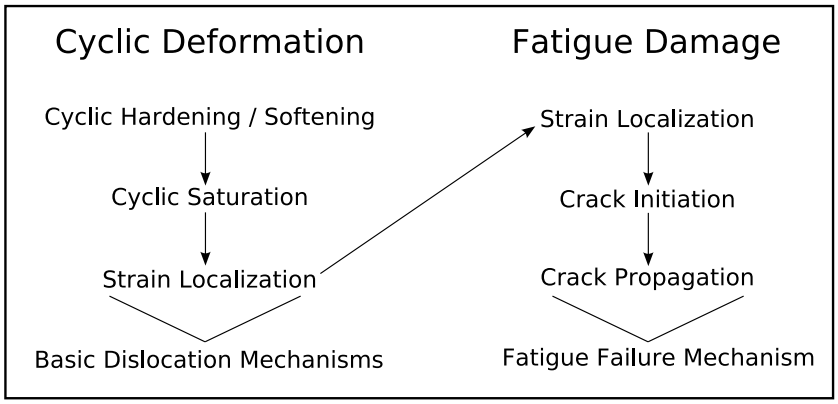

Figure 2.6: Main stages of fatigue damage evolution (Mugrabi, 1985).

The cyclic deformation process is started with a transient, characterised by cyclic softening/hardening during the first few load cycles followed by cyclic saturation. In this region the structural response on the loading is stabilised. As strains localise cracks are initiated which do subsequently propagate and finally cause macroscopic failure. Lifetimes are frequently analysed using the concept of S-N (Woehler) curves. Basquin (1910) established a relationship between the stress amplitude $\Delta\sigma/2$ and the number of cycles to failure N_f:

$$\frac{\Delta\sigma}{2} = \sigma_f (2N_f)^B \tag{2.3}$$

σ_f: fatigue strength coefficient

B: Basquin exponent

Some decades later, Manson (1954) and Coffin (1954) found that cyclic damage in metallic materials is caused by plastic strains:

$$\frac{\Delta\varepsilon}{2} = \varepsilon_f (N_f)^C \tag{2.4}$$

ε_f: Fatigue ductility coefficient

C: Fatigue ductility exponent

Therefore, Equation 2.4 is valid in the low-cycle fatigue regime, as high stress is necessary in order to cause plastic deformation whereas Basquin's relationship is governed by elastic deformations and is used in high-cycle, low stress fatigue. Details are not further discussed here as most of the published work in this field refers to metallic materials and is therefore not directly applicable to bone tissue. Comprehensive information on cyclic deformation and fatigue can be found in standard textbooks (Hertzberg, 1995; Suresh, 1998).

Cyclic failures of bones due to the accumulation of fatigue damage are clinically known as overuse injuries or stress fractures which are observed in athletes (Snyder et al., 2006; Niemeyer et al., 2006) and military recruits (Sormaala et al., 2006) and are also associated with age-related fragility fractures (Burr et al., 1997). Cyclic loading-induced damage accumulation is also reported to weaken vertebrae (Burr et al., 1997) and is often associated with loosening of implants (Bauer and Schils, 1999). It has been suggested that microdamage induced due to fatigue loading does initiate remodeling processes (Burr et al., 1985; Lee et al., 2002).

The investigation of fatigue failure has a rather long history in traditional material sciences, starting in the late 18^{th} century (Schuetz, 1996). King and Evans (1967) were the first to measure lifetime (S-N) curves for (cortical) bone in the sixties. Subsequently, different authors analysed mechanical fatigue concerning compact and trabecular bone. Whereas the fatigue strength of cortical bone is extensively reported in the literature (Carter et al., 1981; Zioupos and Casinos, 1998; Yeni and Fyhrie, 2002; O'Brien et al., 2003; Taylor

et al., 2003b; George and Vashishth, 2006) only few data is available for trabecular bone (Michel et al., 1993; Moore and Gibson, 2003b; Haddock et al., 2004; Yamamoto et al., 2006). Most studies concentrate on bovine and human trabecular bone specimens cored in the main (on-axis) direction and analysed in cyclic compression (with varying mean stress). The studies showed a considerable scatter for the same bone type between different research groups which may also result from differing experimental boundary conditions in terms of specimen size, surrounding media and embedding.

In order to reduce the large scatter of the results applied stresses are usually normalised by the initial modulus of each specimen, which is also a standard procedure in the testing of cellular solids. Analysing this normalised stress (σ/E_0) as a function of the cycles to failure results in Basquin type relationships (Equation 2.3). A more recent approach showed that a normalisation of the applied stress by (bone) volume fraction and the axial fabric eigenvalue (Cowin, 1985) can improve the estimation of fatigue life for cancellous bone in axial cyclic compression (Rapillard et al., 2006). Maximum strains at failure as well as accumulated residual strains (Fig. 4.4) were found to depend linearly on the applied normalised stress (Moore and Gibson, 2003b). A fatigue endurance limit at a normalised stress level of $\sigma/E_0 = 0.0035$ has been suggested based on microdamage evaluation in bovine trabecular bone (Moore and Gibson, 2003b), whereas modeling of the fatigue behaviour hints at a lower endurance limit as low as $\sigma/E_0 = 0.0024$ (Ganguly et al., 2004).

The characteristics for fatigue in cancellous bone were found to be comparable to the principles derived for metals. Beside the earlier mentioned three stages of deformations, stress strain hysteresis were found to move along the strain axis during cyclic compression. This observed cyclic creep effect is also associated with a decrease of the secant modulus and a broadening of the hysteresis loops (Haddock et al., 2004; Moore and Gibson, 2003b). The physical effect of the translation has been associated with damage in form of microcracks, which do not fully close during unloading in bovine trabecular bone (Moore and Gibson, 2003a). The exact influence of creep remains somehow controversial (Bowman et al., 1998; Moore et al., 2004), but recently there seems to be some evidence that creep

effects are negligible in low-cycle fatigue tests (Moore et al., 2004). Nevertheless it was suggested that creep effects may be dominant on physiological load levels and be therefore related to non-traumatic vertebral fractures (Yamamoto et al., 2006) whereas, higher loadings may result in residual strains due to microcracking. The observed decrease in secant modulus of equine and canine cortical bone exposed to cyclic loading was also shown to be mainly due to the formation and growth of microcracks (Burr et al., 1998; Fleck and Eifler, 2003). The same mechanism was observed in cancellous bone, the reduction in secant modulus was also found to be related to increasing microcracking and fractured trabeculae (Moore and Gibson, 2003a). Increasing strains during fatigue testing were observed to be associated with a reduction in secant modulus for both cortical and trabecular bone respectively (Moore and Gibson, 2003b; Ganguly et al., 2004; Cotton et al., 2005).

Cotton et al. (2005) found that damage rate (the rate of change in secantmodulus per load cycle) is a good predictor of fatigue life for human cortical bone exposed to pure tensile fatigue. The authors took the (constant) damage rate from the rather linear damage behaviour between 10 % and 90 % of the specimen's lifetime and showed that correlations between this damage rate and cycles to failure were better than for normalised stress vs. cycles to failure. The damage rate did also appear to be a function of normalised stress σ/E_0. Fatigue damage in cancellous bone has been quantified with numerical and experimental means. 2-D and 3-D cellular solids were modeled and analysed with finite element methods (Guo et al., 1994; Schaffner et al., 2000; Makiyama et al., 2002). The models failed to predict the real response of cancellous bone under cyclic loading but showed principle mechanisms, which may also hold for the biological material. So the failure of only few trabeculae resulted in a largely reduced modulus and macroscopic damage was initiated by the subsequent failure of only few struts. Furthermore, crack growth and propagation was observed to be the primary failure mechanism for low-stress, high-cycle fatigue of trabecular bone, while the primary failure mechanism for high-stress, low-cycle fatigue was suggested to be creep deformation and fracture (Guo et al., 1994).

Ganguly et al. (2004) did model the reduction in secant modulus during compression fatigue loading of bovine cancellous bone as a function of the maximum strain. They ap-

proximated upper and lower bounds for this reduction within normalised stress ranges. The authors suggest that damage is governed by maximum strain, and determined the relationships between strain and reduction in secant modulus with monotonic compression tests, whereas the secondary residual strain accumulation rate was governed by the normalised stress and was taken from cyclic compression experiments. Their model is successful in predicting the experimental data for a given stress range, but these ranges were rather coarsly chosen. Additionally to the exact applied stress level also the initial/transient phase of the cyclic deformation model has been neglected.

A study on the comparability of the fatigue behaviour of bovine and human cancellous bone suggests that fatigue damage occurs at a ultrastructural level as these very different bone types exhibit a rather similar deformation behaviour if the differences in monotonic yield strain are included in the analysis (Haddock et al., 2004).

Of course, all mechanical data on the fatigue behaviour of bone which is established on an experimental basis do not take into account any biological reactions, such as remodeling/healing. So it remains unclear how this repair process influences the overall outcome as there are two contrary ideas. Firstly, these healing processes may prolong fatigue life as microdamage is repaired, but on the other hand, as osteoclastic resorption is preliminary to repair, resorption lacunae may cause local stress concentrations, which can also cause damage acceleration (Martin et al., 1997; Hernandez et al., 2006).

2.3 Age-Related Changes

Age affects the biomechanical and morphological properties of bone resulting in an increased risk of bone fractures with advanced age (Kanis et al., 2004). With increasing age remodeling activity loses its equilibrium with damage and bone quality decreases. A mismatch between bone resorption and formation results in diminishing bone density. The reason for this mismatch may be both mechanically- and biologically-induced. For the diagnosis of severe bone mass reduction (Osteoporosis) density measurements (DXA-based) are used and classifications based on density data from young females is applied to deter-

mine the severity of the disease (the World Health Organisation (WHO) defined a higher reduction in bone density than 2.5 standard deviations below bone peak mass as Osteoporosis (W.H.O., 1994)). But not only the amount of bone available (density) is important, moreover, bone architecture and bone quality have a major impact on the risk of fracture. The determination of this quality is in the focus of many current research activities (Compston, 2006; Nagaraja et al., 2007). Peak bone mass and strength were found to be highest at an age of 20 to 30 years and bone mass and strength was found on average to be higher in men than women (Mosekilde, 2000). Density decreases with age (Fig. 2.7, 2.8).

Mosekilde (1989) reported an approx. 50 % reduction in vertebral cancellous bone density between 20 and 80 years. The compressive strength of human femoral cancellous bone revealed a decrease by 8.5 % each decade (McCalden et al., 1997). For both sexes an extreme decline in vertebral bone strength with ageing could be observed. Whereas men show a certain compensatory increase in bone size with age, no cross-sectional adaptation could be found for women (Mosekilde, 2000). The architecture of cancellous bone structures does also change with age, e.g. in aging tibial bone trabeculae were found to align more strongly with the primary direction-parallel to the longitudinal loading axis (Ding et al., 2002). In general, in cancellous bone structures trabeculae are removed, starting with struts transversally oriented to the physiological load axis and therefore increasing the degree of anisotropy. Women show, especially at ages older than 50 years (menopause), a

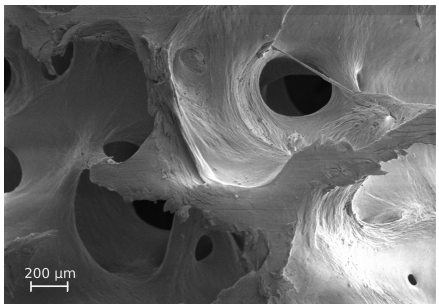

Figure 2.7: Human vertebral cancellous bone, male 46 years, main axis in horizontal direction (SEM).

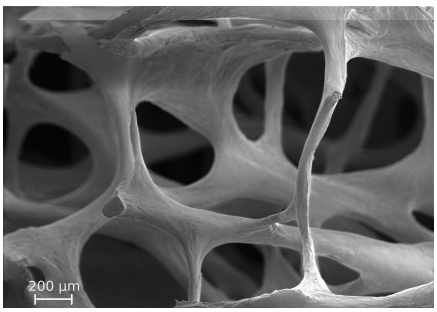

Figure 2.8: Human vertebral cancellous bone, male 80 years, main axis in horizontal direction (SEM).

higher tendency for the perforation of these horizontal (normal to the main physiological axis) struts of the trabeculae network (Mosekilde, 1989, 2000). Trabecular number was found to be reduced in females, whereas in males, strut thickness was reduced (Mullender et al., 2005). Despite these structural changes overall vertebral cancellous bone density was found to be equal for both sexes and compressive stress appeared to be independent of gender (Ebbesen et al., 1999). The microcrack density was observed to increase exponentially with age in human femoral cortical bone (Schaffler et al., 1995). Despite this increase, longer fatigue life in cortical bone could be associated with higher initial crack density when modulus variability was taken into account (Sobelman et al., 2004). Fatigue life in cortical bone decreased exponentially with age, and old bone exhibited a different development of damage in terms of modulus degradation than younger bone (Diab et al., 2005). It has been shown that microdamage may be higher in cancellous rather than cortical bone. Wenzel et al. (1996) found a microcrack density of almost 5 microcracks/mm^2 in human vertebral bone, but in contrast to the findings on cortical bone (Schaffler et al., 1995) they did not find a significant increase with age. Furthermore, fracture toughness of bone was found to decrease with age whereas its microhardness increased. It has been suggested that changes in bone fracture toughness may not be necessarily reflected in its mineral density, porosity, elastic modulus, yield strength and ultimate strength (Wang et al., 1998). The same researchers did not find any significant changes in BMD, elastic modulus and yield strength as a function of time. By contrast (Zioupos and Currey, 1998) found a steady and significant decrease with age for all these mechanical measures. For example, elastic modulus fell by 2.3 % per decade of later life from its value of 15.2 GPa at 35 years of age. Similar declines were also observed for yield strength and fracture toughness. The found deterioration in the elastic properties of the material reduced the critical stress intensity level required to initiate a macrocrack which was preceded by less damage and after initiation needed less energy to propagate (Nalla et al., 2004; Cotton et al., 2005). An increased anisotropy of bone resulting from age effects does also increase the anisotropy of the compressive yield strength. It is unclear how this influences clinically fracture etiology (Keaveny et al., 2001). In summary, the overall effect of age on bone quality (as a

predictor of fracture risk) is still controversial.

2.4 Summary

Despite the availability of the described data some issues remain unsolved. Whereas the fatigue behaviour of cancellous bone has been described for bovine and human trabecular bone for uniaxial cyclic compression in the main physiological axis, the relationship between off-axis loading and lifetime has not been addressed so far. The influence of species and therefore very different architectures has only been partly described. Likewise, the way deformation and damage evolve during cyclic compression with respect to differing load axes and species remains unsolved. Furthermore, the influence of age on the fatigue behaviour of cancellous bone is unclear. Especially the mechanical consequences of an increased anisotropy remain unsolved. The fact that many osteoporotic fractures occur during a fall emphasises the need for a proper understanding of the effect of off-axis loadings on the mechanical properties of cancellous bone. Further, the relationships between localised damage and macroscopic structural integrity are still unknown.

3 Materials and Methods

3.1 Specimens

In order to characterise the behaviour of trabecular bone under monotonic and cyclic loading specimens were prepared using only fresh frozen bones. The use of human donor material was subject to an ethics proposal, which was approved by the ZKS (Zentrum für Klinische Studien) of the Clinical Centre of the University Regensburg. Bovine material was supplied by a butcher. Human cadaveric material was obtained from the Institute for Pathology, Clinical Centre Augsburg.

Bovine bone specimens were used for preliminary studies and for two series of fatigue tests. As bovine bone is frequently used for the mechanical characterisation of trabecular structures (Michel et al., 1993; Moore and Gibson, 2003b) this data may be used in order to facilitate comparison with literature. Furthermore, bovine trabecular bone exhibits a much stronger structure compared to human bone and therefore represents an upper limit of mechanical performance. In total, 27 bovine lumbar spine segments (each L1-L5) were prepared. The animals were 18 to 24 months old. Human bone specimens were dissected from lumbar spine segments (L1-L5) and the distal femoral condyle from 9 donors with an age from 46 to 80 years and a mean of 62.2 $\pm$ 10.7 years (8 male, 1 female). No additional information about the pathological history was available. Vertebrae with deformed endplates were excluded from the study. Specimens used for the fatigue series were cored in different orientations with respect to the physiological whole bone axis. In order to define a local coordinate system for each bone the endplates were chosen as reference for the vertebral body and the distal condyle for the femurs (see Fig. 3.1). The specified angle

refers to the misalignment with the physiological bone axis (PBA) (0° = coincident with PBA). Bovine vertebral samples were drilled in 0° and 90°. Human vertebral specimens were dissected in 0°, 22°, 45°, 90°, and femoral specimens also in 0° (Fig 3.3).

Vertebrae were separated and cores were drilled in the frozen state and then cut to length (Discotom-2, Struers). The bovine specimens were ground at low speed (grit size: 1200) to a rectangular cross section in order to facilitate a rigorous measurement of the two dimensional surface strains, without distortion of the out of plane deformations. For the same reason, marrow was retained for the bovine specimens. Human specimens were kept cylindrical and marrow was fully removed with compressed air and water as in these series deformations at the trabeculae level were of major interest. The resulting cross sections were: Cylindrical: Diameter 11.2 mm $\times$ length 15 mm (human) and cubic: 7.75 mm $\times$ 7.75 mm $\times$ 15 mm (bovine). Specimen dimensions are likely to be large enough to assume continuum behaviour (Harrigan et al., 1988). By microscopic analysis no damage caused by the preparation process was identified. The specimens were again frozen at -20°C. Prior to testing, each specimen has been fully thawed for five hours in 0.9 % *NaCl* solution. For testing, specimens were embedded in specimen holders with methylmethacrylate (KEM 15, ATM, stiffness: 5000 MPa) in order to guarantee a homogeneous load application and avoid end trabeculae breaking, which results in a toe region in the stress strain curve and therefore causes uncertainties in the strain data. These effects are named end artefact errors (Keaveny et al., 1997). End artefacts refer to damage occurring in the specimen's ends due to inhomogeneous boundary conditions. All mechanical experiments were accomplished with a servo-hydraulic testing system (MTS 810 System, Teststar II, 5 kN load cell). In order to supply almost physiological conditions experiments were performed in tempered (37° *C*) 0.9% *NaCl* solution. All bovine specimens and partly the human specimens were scanned for Bone Mineral Density (BMD). BMD was measured along the load axis in 2 mm slices (Stratec XCT-900).

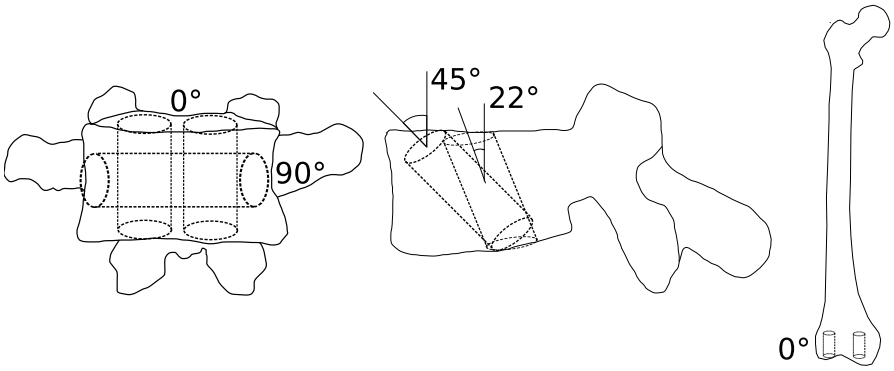

Figure 3.1: Specimen orientations, schematically. The coring angles refer to the physiological coordinate system of each whole bone. The endplates of the vertebrae and the proximal condyle of the femur were chosen as references, the 0 degree direction is in alignment with the physiological axis.

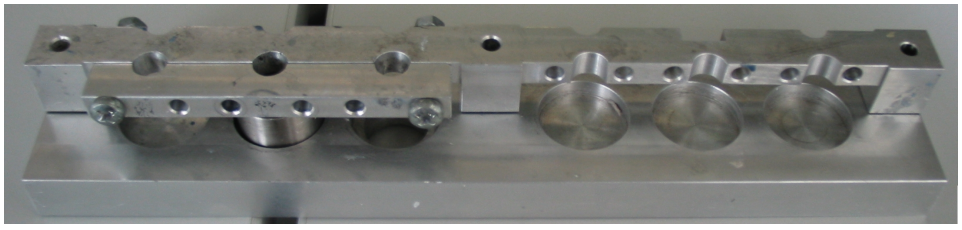

Figure 3.2: Specimen embedding rig.

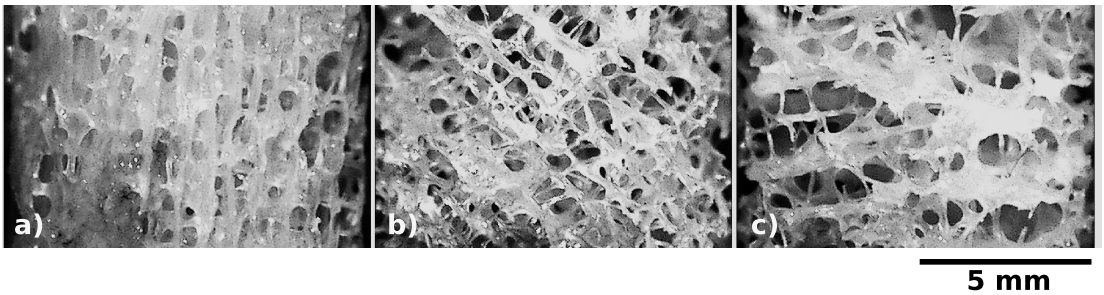

Figure 3.3: Typical samples from different groups of cancellous bone. a) human femoral 0°, b) human vertebral 45°, c) human vertebral 90° (all SEM).

3.2 Testing Conditions

Monotonic compression tests were performed on bovine specimens using a constant (physiological) strain rate $\dot{\varepsilon}$ of 0.015 s^{-1}. All fatigue tests were performed under load control with the same strain rate $\dot{\varepsilon}$ of 0.015 s^{-1} ($0.9-3$ Hz) expect for the bovine tests where the frequency of loading was fixed for reasons of optical deformation measurement at 1 Hz. The specimens were preloaded to a small load level (approx. $1-2\%$ of the static failure load, -2 to -50 N) to ensure full contact (Bowman et al., 1998; Moore and Gibson, 2003b). Prior to fatigue testing, ten cycles from -50 N to -300 N for the bovine bone and from (approximately) -1 N to -5 N for the human bone were applied to determine the initial modulus of the specimen. A triangular wave form from the preload level to a prescribed load value was applied until catastrophic failure occurred. Therefore, a varying mean stress was operating in the different specimens. In order to reduce the scatter of the results the load level was determined by relating the applied stress to the initial modulus of each specimen, which is a common practice in the mechanical testing of spongeous structures (Gibson and Ashby, 1997). Detailed information of the load level range is given in Table 4.1. The initial modulus for the post-analysis was corrected subsequent to the fatigue test because the low load levels of the preconditioning cycles did not always allow for an absolutely exact determination of E_0. Therefore, the secant modulus of the first cycle was determined. Some specimens reveal a slight increase in stiffness in the first few cycles. In these specimens, which were mainly low load $-$ high cycle specimens, secant modulus of the fifth cycle was taken for the analysis. All specimens were stopped as an integral strain of -1.33% was reached. At this value stiffness is already reduced to a large degree but structural integrity is mostly still given, sufficient for microscopic postprocessing. Failure was defined as a ten percent reduction in secant modulus in order to facilitate comparison with literature data (Bowman et al., 1998). Maximum and minimum force and displacement values were measured continuously, full hysteresis loops were recorded with more than 400 data values in at least logarithmic manner. Post-testing microscopic analysis was conducted by means of Scanning Electron Microscopy (SEM) and Stereomicroscopy.

3.3 Deformation Analysis

The integral deformation was measured using the deformation sensor of the test machine, measuring the grip to grip motion. Extensive preliminary studies assured the accuracy of the test setup. Surface strains were measured on two sides of the specimens with the same optical deformation measurement system (Aramis, GOM mbH) for the bovine specimens. This setup allowed for a continuous two-dimensional analysis of surface deformations. Concerning human specimens, mostly single trabeculae were analysed. The optical deformation measurement system is based on the correlation of a pattern of grey values. Therefore, prior to testing a stochastic colour pattern has to be applied. In this work, mostly a pattern of black and white speckles was applied using pressurised dispensers, also other methods were investigated (e.g. black light-(UV-A-)based marker paint). The accuracy of the system depends on the resolution of the CCD-Cameras (1600 $\times$ 1200 pixel), the measurement volume and the applied pattern and is specified to be in the range of 0.01% strain. Especially the pattern is a critical parameter: it has to be applied in a very accurate manner. In the framework of this study different approaches were investigated for the setup of the optical deformation measurement. Because of the highly porous stucture of cancellous bone 3D-methods were found to be rather unstable. Most measurements were done with 2D-methods, neglecting deformations in the depth direction. Therefore, for continuous surface strain analysis specimens with a rectangular cross section (bovine 0° and 90°) were used, whereas microdamage has been detected on single trabeculae (human groups) which were aligned with the analysis plane.

3.4 Data Analysis

The force displacement data was normalised using nominal (1^{st} Piola-Kirchhoff) stress and nominal strain. In order to take into account the stiffening effect of the embedding material, initial height of the specimens was reduced by one half of the layer (1 mm on each side) for strain calculation, therefore resulting in an initial gauge length of 14 mm. Secant modulus

was determined for all hysteresis loops by:

$$E_{sec} = \frac{\sigma_{max} - \sigma_{min}}{\varepsilon_{max} - \varepsilon_{min}} \tag{3.1}$$

The cycle to failure was defined as the cycle where secant modulus has decreased by 10% in relation to the initial modulus. Applied maximum compression stress was normalised with the inital modulus for each specimen (σ/E_0). Maximum strains were defined as the total strain (elastic and residual) components, (accumulated) residual strains as the inelastic deformation (see Fig. 4.4). Various strain and deformational components were differentiated with respect to the number of cycles, the details are shown in the results section. Regression analyses were performed using least square methods. In some cases (which are indicated in the results) a robust algorithm was chosen which takes data outliers into account in order to facilitate reasonable fits. The significance level for statistical tests was chosen to be $p < 0.05$. All analyses were performed using Matlab (R14, The Mathworks). Surface strains were analysed using different methods, which are stated in detail in the corresponding results section.

4 Results – Mechanical Behaviour

4.1 Specimen Characterisation

Bone Mineral Density (BMD) was measured for most of the specimens in order to find relevant correlations of the mechanical data with this clinically important measure. Especially for the bovine specimens also the homogeneity along the specimens' axis was a major concern as the cancellous bone structure shows a relatively large architectural deviation from the physiological bone axis in the middle of the vertebrae (Fig. 2.1). Thus, specifically the two aspects were: a) the homogeneity of the specimens and b) density correlations with mechanical data. The homogeneity of the bovine specimens was verified with 2 mm sliced QCT scans and quantitative stereology. Both measures were found to be reasonably constant for a specimen length of 15 mm. This was valid from both ends (superior and inferior directed) of the bovine vertebra (Fig. 4.1). So only this section of the cores was taken for further analyses.

Bone Mineral Density measurements on 75 specimens from all groups (bovine and human) lead to a correlation of

$$E_0 = 0.0072 \times BMD^{2.09},\ R^2 = 0.68. \tag{4.1}$$

E_0: Initial secant modulus, MPa
BMD: Bone Mineral Density, g/ccm

By taking more detailed analyses correlations for the single groups showed the following strengths: bovine 0°: R^2 = 0.69; bovine 90°: R^2 = 0.30; human 45°: R^2 = 0.33;

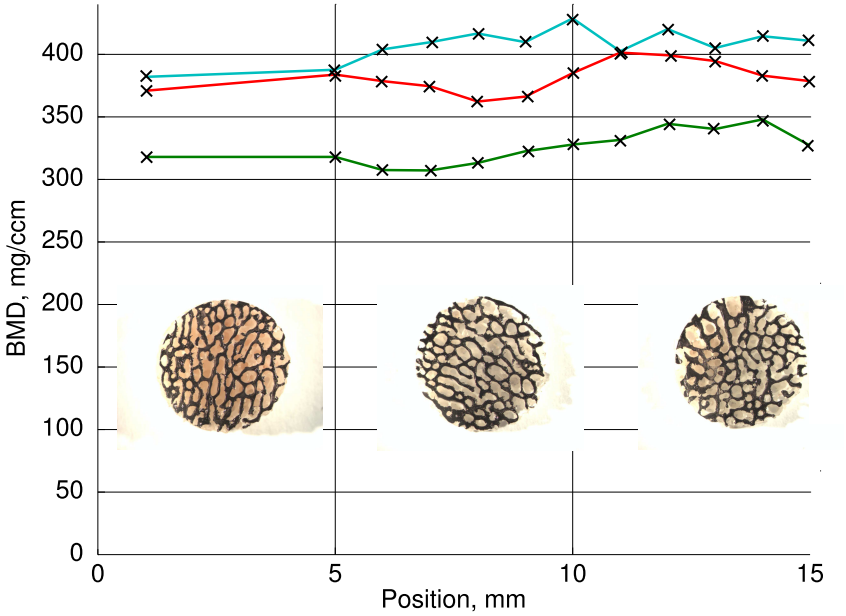

Figure 4.1: BMD as a function of the position in the specimen (Position 0 mm refers to the superior end of the specimen) (Penzkofer, 2005).

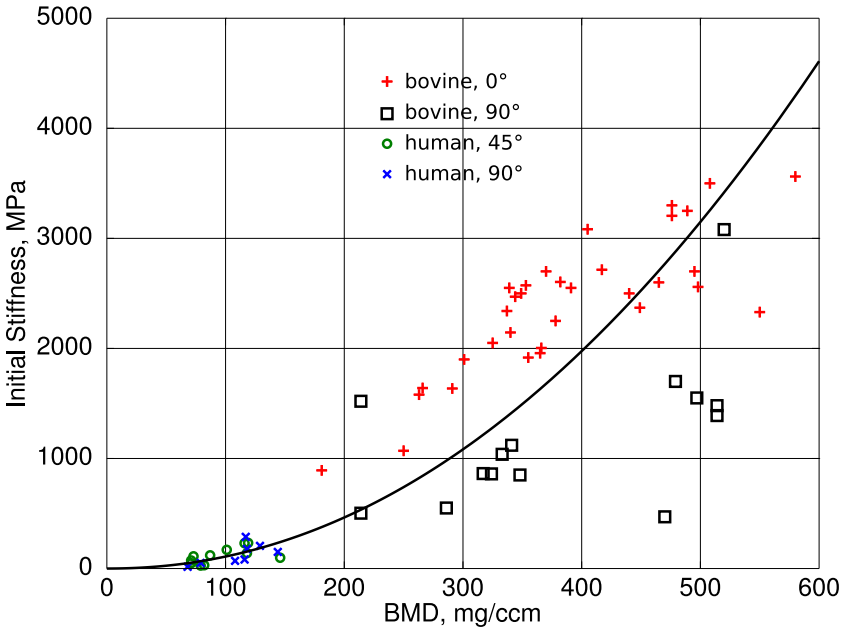

Figure 4.2: Mean BMD values of various specimens and groups.

human 90°: $R^2 = 0.44$. These values were determined with linear functions, as they showed the best fits for these tests in contrast to the combined fit for all specimens (Fig. 4.1).

4.2 Monotonic Compression

Typical for a cellular solid (Gibson and Ashby, 1997), the monotonically loaded cancellous bone specimens' behaviour was found to be linear (in stress-strain space) at the beginning of the compression (Figure 4.3). The linear regime is followed by a decreasing slope, indicating failure and plastic collapse, and an increase (densification) at higher strain values. While the magnitude of the maximum compressive stress varies up to tenfold between the groups, the characteristics of the deformation behaviour are similar. Even if the initial deformation behaviour appears to be rather linear, non-linearities can be found by analysing the deformations with a higher local resolution. The surface deformations of the specimen reveal these inhomogeneous components. Localised strain concentrations can be found already at a small percentage of the maximum stress. These strain concentrations do further localise and increase in value until failure occurs in the same region. Macroscopic damage appears in the form of deformation line across the whole specimen cross section (Fig. 4.3). Due to the limited number of available samples no statistical analyses could be applied to the monotonic compression tests. Nevertheless, in the preliminary studies strains at failure were found to be almost constant for bovine samples.

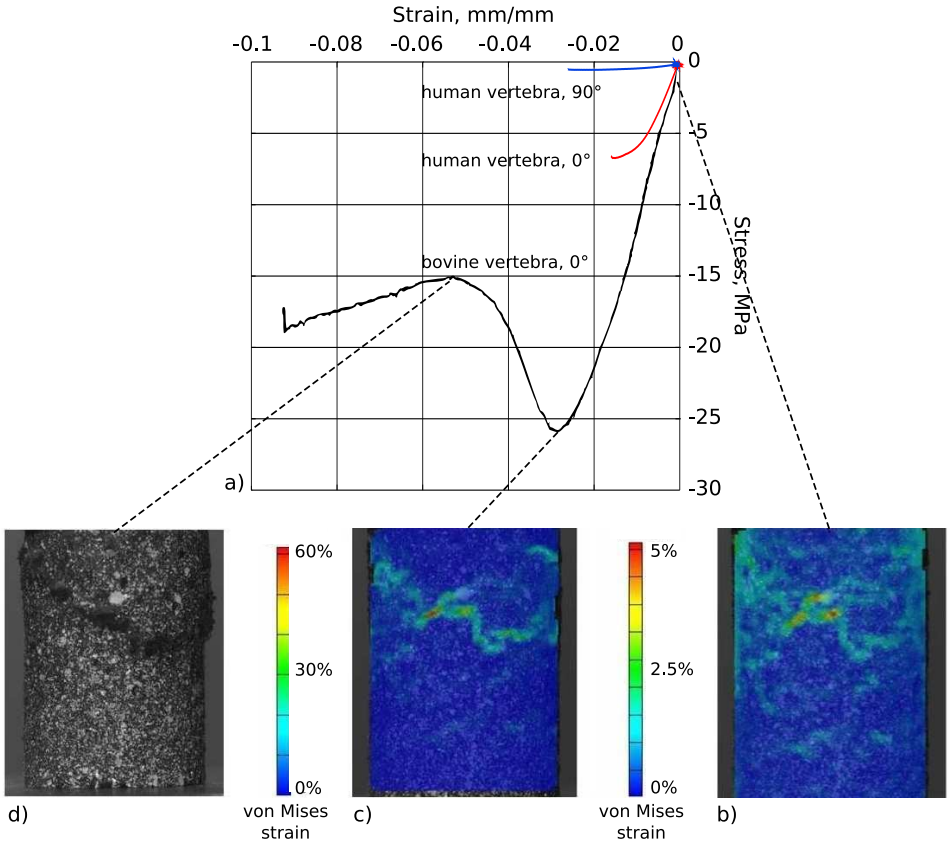

Figure 4.3: Monotonic compression of a human 0°, a human 90° and a bovine vertebral 0° bone specimen. The surface von Mises strains at two different stages were analysed at the bovine sample. b) 0.44 MPa, c) 26 MPa, d) after failure; (The human specimens were compressed to fixed strain values for further investigations, thus only the linear regime and the maximum stress peak is visible. The indicated (surface) strain values are not valid on the tissue level).

4.3 Cyclic Compression

Altogether, 108 specimens were tested in cyclic compression. A summary of the results of the cyclic compression experiments of all specimen groups is given in Table 4.1. Cycles to failure for all specimens in all groups ranged from $1 - 1,000,000$. Seven specimens did not fail and were stopped at a minimum of 240,000 cycles.

Table 4.1: Summary of groups.

Group	N	E_0 [MPa]	Load range σ/E_0, %
Bovine 0°	31	2709 ± 548	$0.39 - 1.47$
Bovine 90°	12	1227 ± 725	$0.33 - 1.06$
Human vertebral 0°	14	447 ± 117	$0.22 - 1.00$
Human vertebral 22°	8	159 ± 11	$0.23 - 0.68$
Human vertebral 45°	13	111 ± 68	$0.17 - 1.25$
Human vertebral 90°	15	98 ± 78	$0.20 - 1.25$
Human femoral 0°	14	1031 ± 461	$0.23 - 0.82$

N: Number of specimens

4.3.1 Deformation Behaviour

The (integral) cyclic deformation behaviour of trabecular bone follows the principle mechanisms of fatigue, which were derived for metallic materials as well as bone tissue (Michel et al., 1993; Moore and Gibson, 2003b; Ohrndorf et al., 2006) both intra- and intergroup-wise. It can be characterised by increasing residual strains (cyclic creep), which causes a shift of the hysteresis loops along the strain axis and a broadening and increasing nonlinearity of the hysteresis. Furthermore, the secant modulus, defined as the slope between the minimum and maximum stress level, decreases with increasing cycle numbers (Fig. 4.4, Equation 3.1).

The cyclic deformation process reveals the three classical stages of fatigue: a transient behaviour characterised by rapid strain increase within the first load cycles, a saturation of strains and a fast increase of deformation (softening) near catastrophic failure (Fig. 4.5). This holds qualitatively for all groups.

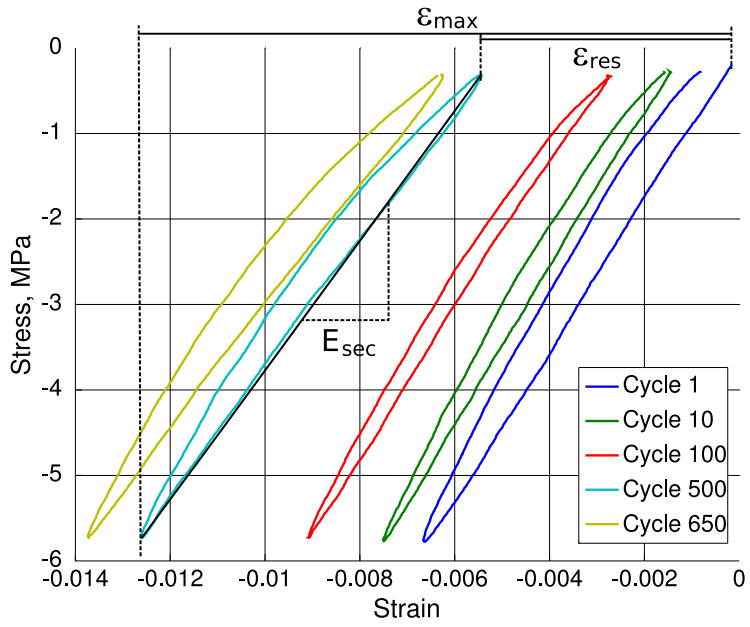

Figure 4.4: Stress strain hysteresis loops (human femoral 0° specimen, $\sigma/E_0 = 0.0060$, $N_f = 300$. Residual strains are defined as the accumulated plastic deformations (shift along strain axis), maximum strains are defined as total strains (residual strains superimposed with the elastic part of the strains).

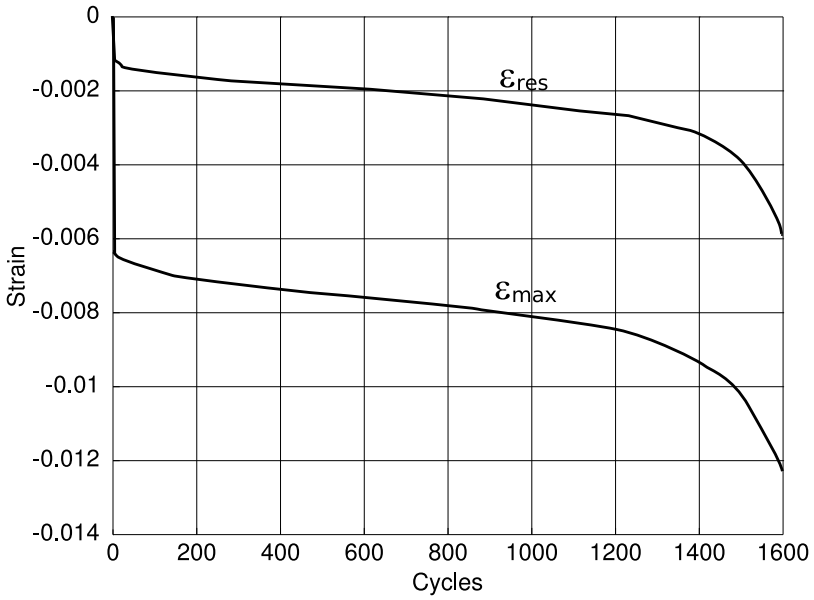

Figure 4.5: Maximum and residual strains for a bovine vertebral 0° specimen.

Analysis of the deformation behaviour

The integral (along the load axis) cyclic deformation process can be separated in several phases: deformations in the initial transient region (ε_t), evolution of the deformations during the pseudo saturation regime (ε_s), deformation at the defined failure criterion (ε_f) and increasing deformations prior to macroscopic failure (Fig. 4.6). The first two stages were analysed with respect to groupwise differences in the deformation behaviour and related to the load level σ/E_0 in order to provide information on the evolution of deformations until failure and the accumulated deformations at a point prior to failure. Therefore, deformations in the inital region are linearized and the deformation rates in the saturation regime are determined.

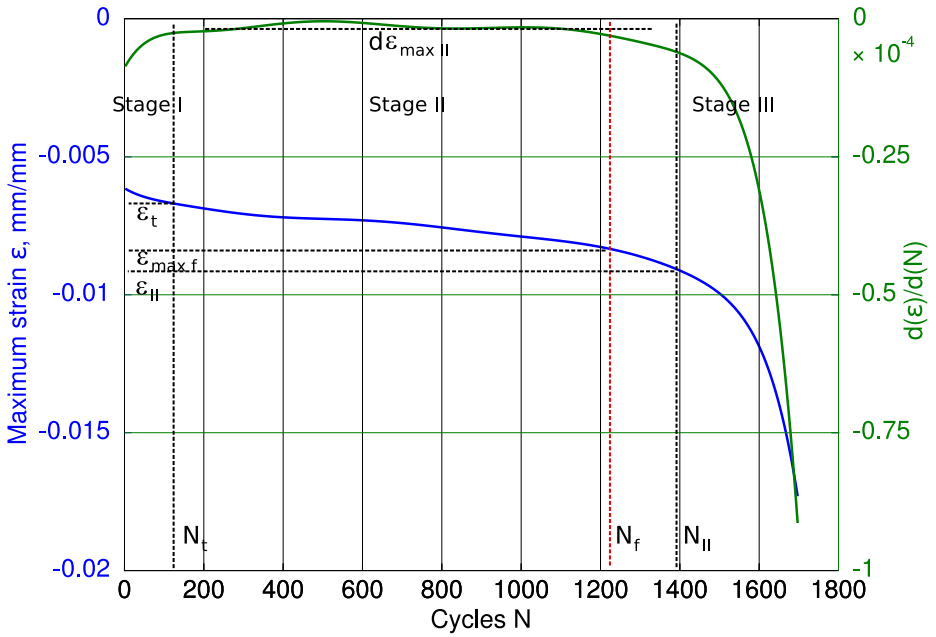

Figure 4.6: Cyclic deformation of a bovine 0° specimen. Shown is the evolution of the maximum strains and the differentiated maximum strains with respect to the number of cycles as well as the characteristic points at which the deformational behaviour was analysed.

Initial transient region

Maximum strains as well as accumulated residual strains were analysed at the end of the transient behaviour. Higher normalised loads σ/E_0 resulted in higher deformations at the end of Stage I. While maximum strains showed a linear dependency on the applied maximum load (σ/E_0), residual strains exhibited only very weak trends. The regression analysis results of the maximum strain vs. load were further assessed by an analysis of covariance test in order to find out statistically relevant differences between the specimen groups. Statistically significant differences were observed for the bovine groups and human 90°. The test between human 0° and human 90° only just failed statistical significance with a p-value of 0.06. Despite the failed statistical significance between all groups results are shown in a groupwise manner. Maximum strains at the end of the transient went up with increasing misalignment of the samples' orientation with respect to the main structural axis of the bone intergroupwise and with increasing load magnitude intragroupwise, respectively.

$$\varepsilon_{max\ t} = c \times (\sigma/E_0) + d \tag{4.2}$$

$\varepsilon_{max\ t}$*: accumulated maximum strain at the end of Stage I*

c, d: regression coefficients (see Table 4.2)

Table 4.2: Regression coefficients for Equation 4.2

Group	c	d	R^2
Human vertebral 0°	0.89	0.003	0.86
Human vertebral 22°	0.89	0.001	0.89
Human vertebral 45°	1.06	0.001	0.78
Human vertebral 90°	1.67	0	0.89
Human femoral 0°	0.97	0	0.92
Bovine vertebral 0°	0.82	0.002	0.62
Bovine vertebral 90°	0.85	0.001	0.84

All analyses were performed with the robust option.

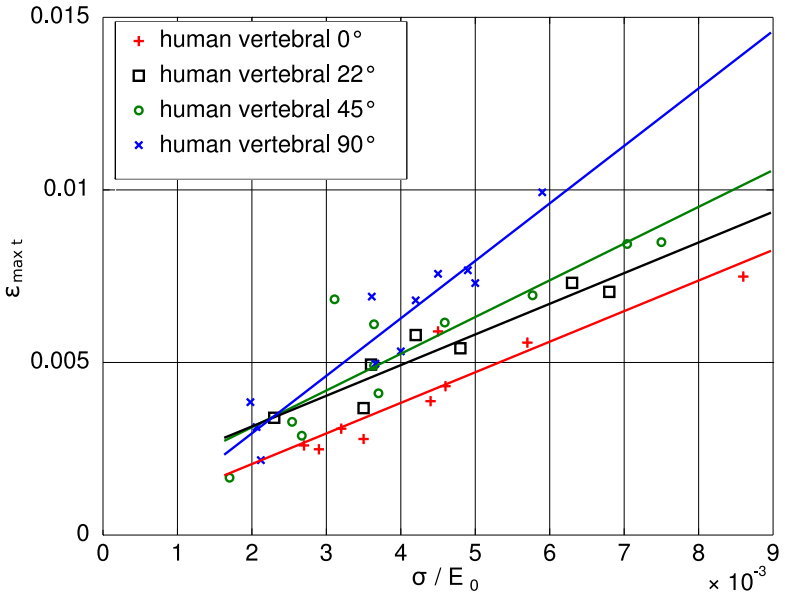

Figure 4.7: Maximum strain at the end of the initial transient as a function of load σ/E_0 for the human vertebral groups.

The functional relationship between the number of cycles in the initial transient phase and the load level σ/E_0 was best represented by exponential approaches (Fig. 4.8).

$$N_t = e \times \exp^{-f \times (\sigma/E_0)} \tag{4.3}$$

N_t: Number of cycles in Stage I

e, f: Regression coefficients (see Table 4.3)

No statistically significant difference was found among the human vertebral groups (even if a trend for differences exists), whereas the bovine groups behaved markably different. At similar load levels, bovine specimens exhibited higher absolute cycle numbers for the transient. Therefore the human vertebral groups were taken as one common group as well as the bovine vertebral groups.

The relation of the number of cycles in the transient and the number of cycles to failure can be seen in Table 4.4. The fraction of lifetime within the transient is going up with increasing deviation from the physiological axis. At the same site, statistical analyses

Table 4.3: Regression coefficients for Equation 4.3.

Group	e	f	R^2
Human vertebral	7.7×10^5	-1864	0.91
Bovine vertebral	9.1×10^7	-2074	0.94

Both analyses were performed with the robust option.

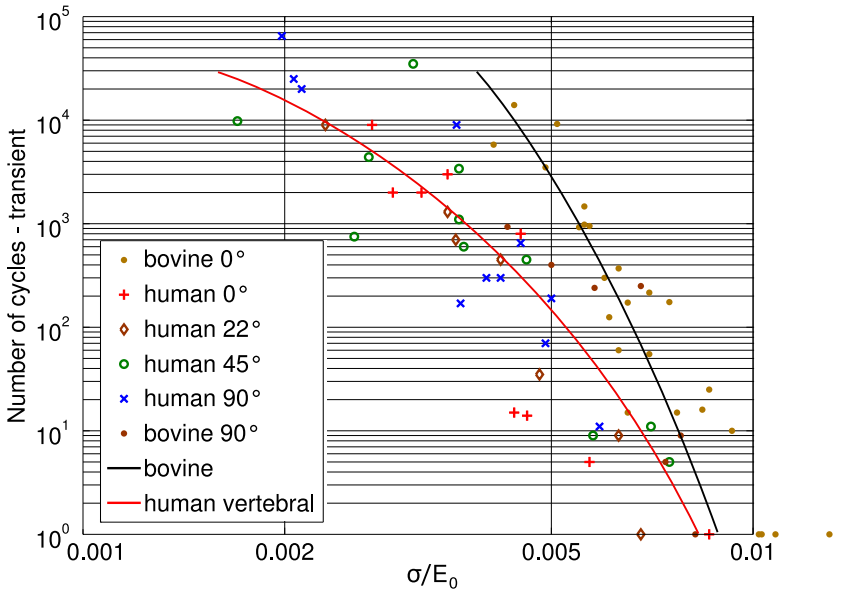

Figure 4.8: Number of cycles at the end of the initial transient as a function of load σ/E_0. Regression curves are shown for the combined human vertebral and combined bovine vertebral group.

revealed significant differences between the human vertebral 0° and the human vertebral 45° and 90° group. Irrespective of the species and site, 0° groups were found to have the smallest relative number of cycles within Stage I.

Saturation Region

The evolution of maximum and accumulated residual strains within the saturation region (Stage II) was analysed with respect to the load level σ/E_0. For this reason, the cyclic deformation curves for the two strain values of each specimen were differentiated with respect to the number of cycles (comp. Fig. 4.6). The mean strain evolution rate was used for the regression analysis. Bovine groups showed once again a remarkably different be-

Table 4.4: Fraction of number of cycles in Stage I (N_t) to number of cycles to failure (N_f).

Group	N_t / N_f
Human vertebral 0°	0.16 ± 0.07
Human vertebral 22°	0.27 ± 0.18
Human vertebral 45°	0.42 ± 0.23
Human vertebral 90°	0.47 ± 0.26
Human femoral 0°	0.17 ± 0.13
Bovine vertebral 0°	0.13 ± 0.05
Bovine vertebral 90°	0.18 ± 0.15

haviour. Groupwise differences were also obtained for the human specimens (Fig. 4.9). At similar load magnitudes, bovine cancellous bone exhibited smaller strain evolution rates, which increased in the off-axis group, nevertheless being smaller than the rates in all human groups. Among the human groups, smallest rates were observed in femoral cancellous bone, whereas in the vertebral groups strain evolution rates increased with increasing specimens' orientation angle. Power-law relationships were established for the groups.

$$\frac{d\varepsilon_{max}}{dN} = g \times (\sigma / E_0)^h \tag{4.4}$$

g, h: Regression coefficients (see Table 4.5)

Table 4.5: Regression coefficients for Equation 4.4.

Group	g	h	R^2
Human vertebral 0°	2×10^{27}	14.07	0.96
Human vertebral 22°	2×10^{18}	10.2	0.96
Human vertebral 45°	9×10^{11}	7.5	0.87
Human vertebral 90°	8×10^{16}	9.53	0.89
Human femoral 0°	2×10^{14}	8.8	0.88
Bovine vertebral 0°	2×10^{21}	12.45	0.91

All analyses were performed with the robust option.

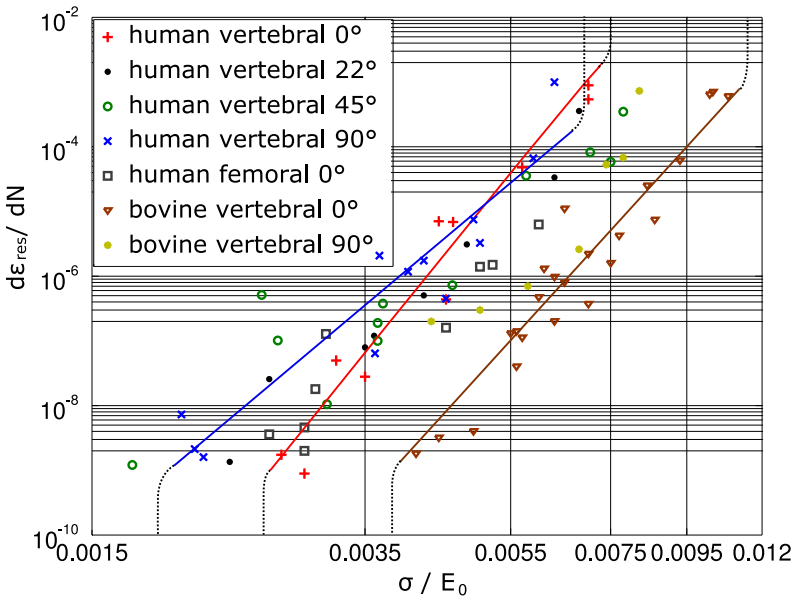

Figure 4.9: Rate of residual strain evolution as a function of the load level σ/E_0. Regression curves are shown for the human vertebral 0°, human vertebral 90° as well as the bovine 0° group. The dotted lines refer to the supposed behaviour beyond the data range.

Strains at failure

Failure was defined as a ten percent reduction in secant modulus. The accumulated residual strains as well as the maximum strains were analysed at this point. Both appear to be linearly dependent on the applied load σ/E_0.

$$\varepsilon_f = i \times \sigma/E_0 + j \tag{4.5}$$

i, j: Correlation coefficients (see Table 4.6)

A linear relationship between maximum strain at failure and the applied load provided an accuracy in the order of $R^2 = 0.80$ when all data, irrespective of the specific group was analysed. Considering the groups separated, the two groups human vertebral 0° and human vertebral 90° represent the upper and lower limits of all specimens (Fig. 4.10), the correlations increased to $R^2 = 0.93$ and $R^2 = 0.85$ respectively. Off-axis specimens tend to have larger strain values at failure. The analysis of covariance (ANOCOVA) between

Table 4.6: Regression coefficients for Equation 4.5.

Group	i	j	R^2
Human vertebral 0°	−1.07	−0.001	0.93
Human vertebral 22°	−1.13	−0.001	0.92
Human vertebral 45°	−1.37	−0.001	0.84
Human vertebral 90°	−1.52	−0.001	0.85
Human femoral 0°	−1.22	−0.001	0.85
Bovine vertebral 0°	−1.23	−0.001	0.84
Bovine vertebral 90°	−1.01	−0.002	0.86

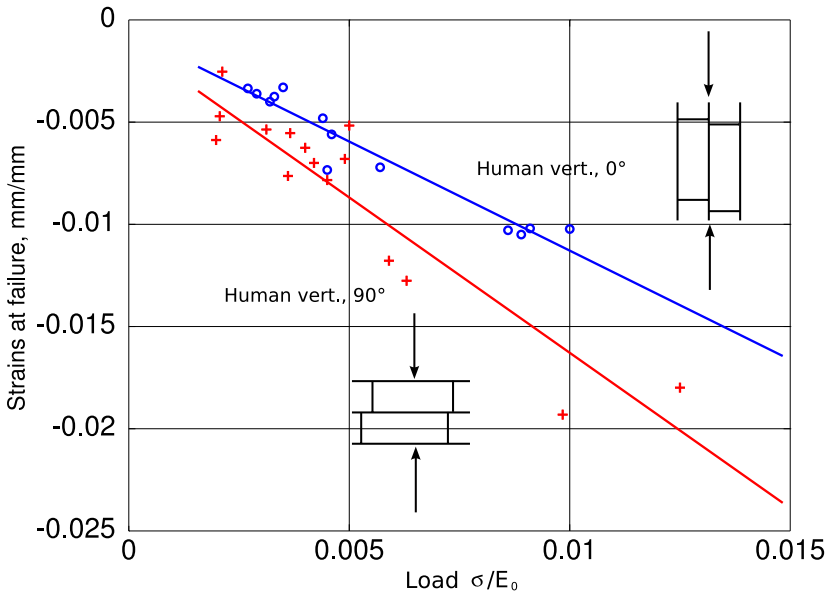

Figure 4.10: Maximum strains at failure for the two bounding groups human 0° and human 90°.

these two groups showed a significance level of $p = 0.02$ and was therefore statistically significant. The other groups failed statistical significance. Detailed information about the relationships is given in Tab. 4.6. Similar relationships were found for the accumulated residual strains with a lower correlational power. As described in Equation 4.14 a power-law relationship between cycles to failure (N_f) and the normalised load (σ/E_0) can be observed. Therefore, also a power-law can be observed by correlating the strains at failure ($\varepsilon_{maxf}, \varepsilon_{resf}$) with N_f.

4.3.2 Damage Mechanisms

In this chapter, quantitative and qualitative analyses of damage and its evolution during cyclic loading are described in order to reveal the principle mechanisms of cyclic failure in cancellous bone structures. Quantitative analyses are shown for the integral damage evolution and certain aspects of two-dimensional damage. The aim of two dimensional (surface) analyses of the damage process was to define the methodology which different scale levels of damage can be detected with and to identify the nature of damage rather than a strict statistical analysis, which is beyond the scope of this work. The main question concerning quantitative damage analyses was if a single variable (load σ/E_0) is capable of predicting damage evolution.

Integral damage

An integral damage parameter can be defined by the decrease of the secant modulus of the hysteresis loops.

$$D = 1 - E_{sec}/E_0 \tag{4.6}$$

Different levels of structural degeneration can therefore be associated with the alteration of this parameter. While a value of 0 is associated with the undamaged initial state, at $D = 1$ the structure has lost all load bearing capability. Fig. 4.11 shows the onset and the evolution of $1 - D$ (which is generally acknowledged in the literature) under cyclic loading for bovine vertebral specimens cored in two different directions (group 1 cored

along the main physiological axis; group 2 cored in the medial-lateral direction of the vertebral body). For all load levels (σ/E_0) the physiologically loaded specimens (group 1) clearly show retarded onset of damage.

Reduction of the normalised secant modulus (and therefore an increase of D) with respect to percentage lifetime appeared to be different among the groups. The bovine vertebral 0° and 90° samples hardly reached normalised lifetime (N/N_f) values greater than 1.2 (as failure is defined at $D = 0.1$ also normalised lifetimes > 1 are possible). Likewise, specimens from human groups aligned with the physiological axis (human vertebral 0° and femoral 0°) failed shortly after $N/N_f = 1.0$. In contrast, off-axis groups revealed a much higher resistance. With increasing misalignment up to 8-fold normalised lifetimes were reached in some cases (Fig. 4.12).

The overall damage evolution for a single specimen could be approximated with a quadratic function for all groups. This holds at least in the range $D < 0.2$. While the qualitative course of damage evolution was similar for the bovine groups and human vertebral 0°, 22° as well as human femoral 0° with an positive quadratic behaviour, some specimens from the human vertebral 45° group and all specimens in the human vertebral 90° group revealed a negative quadratic functional relationship. Fig. 4.13 shows the different damage behaviour.

As D appeared to be quadratic dependent on the number of cycles, damage rate ($\frac{\Delta D}{\Delta N}$) changes in a linear manner and damage acceleration is found to be constant for each specimen:

$$\frac{\Delta^2 D}{\Delta N^2} = const.(for\ one\ specimen) \tag{4.7}$$

If the damage acceleration and the initial damage rate are known, damage evolution can be determined theoretically.

$$D = \frac{\Delta D}{\Delta N}_{initial} \times N + \frac{1}{2} \times \frac{\Delta^2 D}{\Delta N^2} \times N^2 \tag{4.8}$$

Damage acceleration was found to be function of the normalised load σ/E_0. The

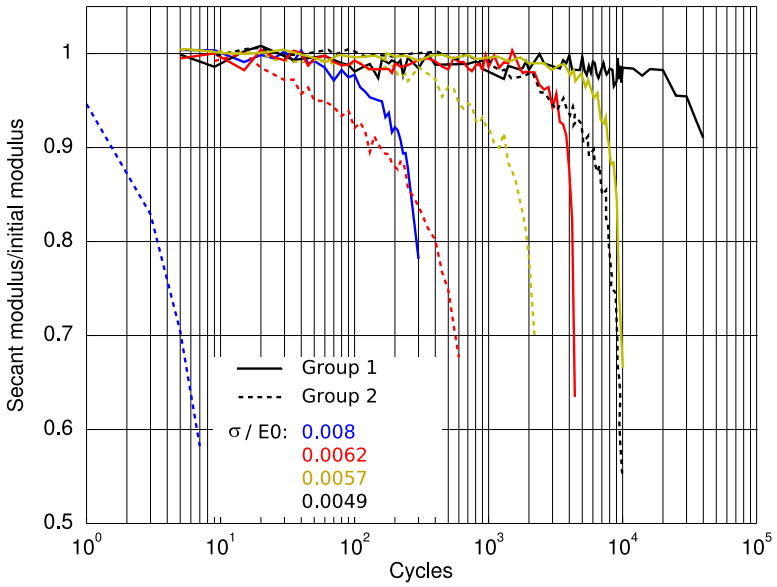

Figure 4.11: Evolution of damage ($1 - D$) in two different groups of bovine trabecular bone where specimens of each group were loaded with equivalent σ/E_0. Group 1: cored along physiological axis, Group 2 cored perpendicular (medial-lateral) to the physiological axis.

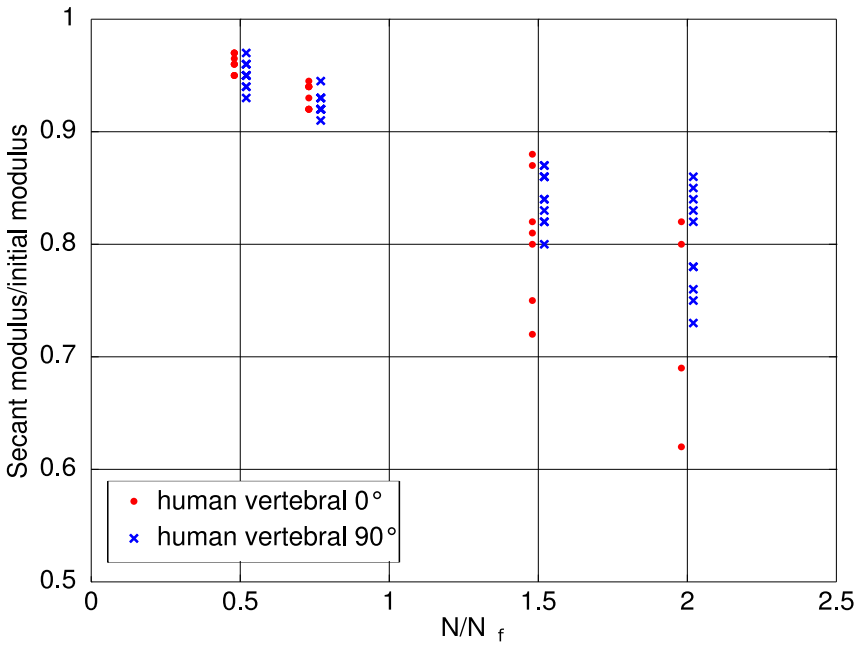

Figure 4.12: Reduction in normalised secant modulus ($1 - D$) as a function of percentage lifetime for the groups human vertebral $0°$ and human vertebral $90°$.

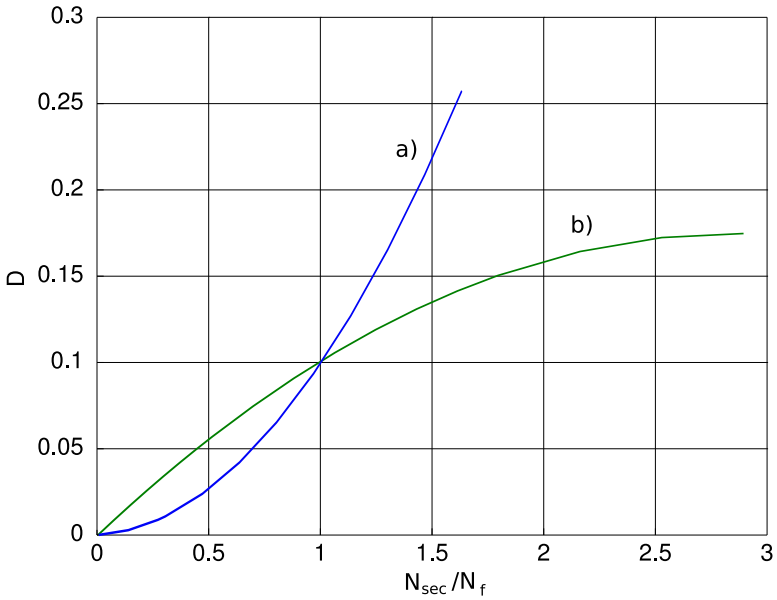

Figure 4.13: Qualitative course of damage in the different groups. a) all groups except human vertebral 90° and parts of human vertebral 45°, their course is shown in b).

relationship could be best approximated with a power law function:

$$\frac{\Delta^2 D}{\Delta N^2} = k \times (\sigma / E_0)^l \tag{4.9}$$

k, l: Regression coefficients (see Table 4.7)

While damage acceleration was positive for most of the specimens, also a few were observed to have negative damage acceleration values. This effect could be increasingly observed with larger deviation from the physiological axis. In detail, human vertebral 22°

Table 4.7: Regression coefficents for Equation 4.9.

Group	k	l	R^2
Human vertebral 0°	7×10^{40}	20.36	0.90
Human vertebral 45° ◊	3×10^{14}	7.5	0.94
Human vertebral 90° ♦	2×10^{32}	16.5	0.90
Human femoral 0°	4×10^{29}	15.55	0.93
Bovine vertebral 0°	8×10^{33}	18.84	0.89

◊ correlations only for positive damage acceleration values
♦ correlations for $-\sigma/E_0$

contained 2 specimens with a negative trend out of 8 analysed, human vertebral 45° 4 out of 11, human vertebral 90° 10 out of 12 with the remaining two having values close to zero. Therefore, damage slows down in these specified samples with increasing cycle numbers whereas damage goes up more rapidly in the others. The initial damage rate also revealed groupwise power-law dependencies on normalised loads. Analysing the damage rates at the defined failure $D = 0.1$ results in another powerlaw dependency (Table 4.8).

$$\frac{\Delta D}{\Delta N}_{initial} = m \times (\sigma/E_0)^n \tag{4.10}$$

m, n: Regression coefficients (see Table 4.8)

Table 4.8: Regression coefficents for Equation 4.10.

Group	m	n	R^2
Human vertebral 0°	5×10^{20}	10.54	0.81
Human vertebral 45°	9×10^{11}	6.63	0.85
Human vertebral 90°	2×10^{16}	8.39	0.88
Human femoral 0°	3×10^{13}	7.41	0.88
Bovine vertebral 0°	3×10^{16}	9.6	0.77

Modeling the course of damage as a function of the normalised load levels can be done through substituting Equation 4.10 and 4.9 in Equation 4.8:

$$D = m \times (\sigma/E_0)^n \times N + k \times (\sigma/E_0)^l \times N^2 \tag{4.11}$$

Fig. 4.15 shows the experimental data for two human vertebral 90° specimens and the computed data for equivalent load levels. Even if the determined relationships are strong, an immense scatter compared to the specimen-specific data was observed. While the relationships work well for the on-axis groups and the human vertebral 90° group, correlations with experimental data from the human vertebral 45° group were poor as specimens failed either with positive or negative damage acceleration.

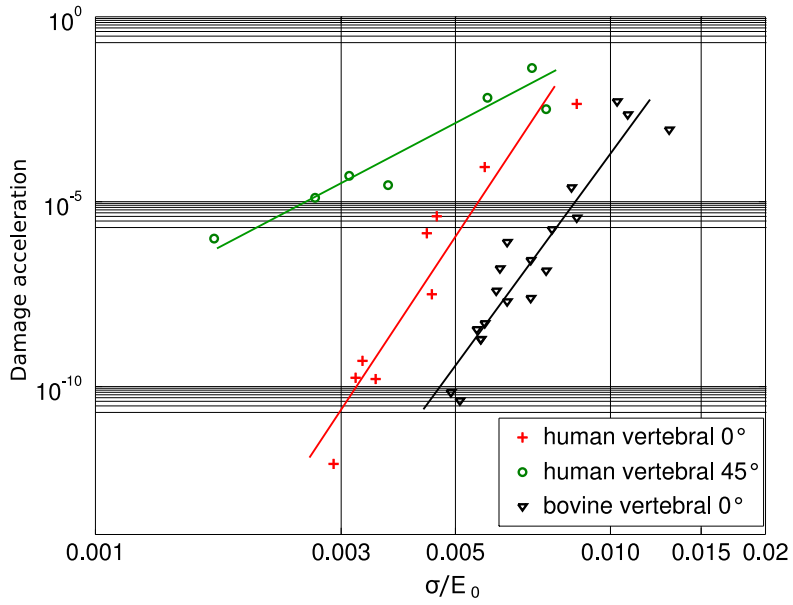

Figure 4.14: Damage acceleration as a function of load for the human vertebral 0°, human vertebral 45° and bovine vertebral 0° groups.

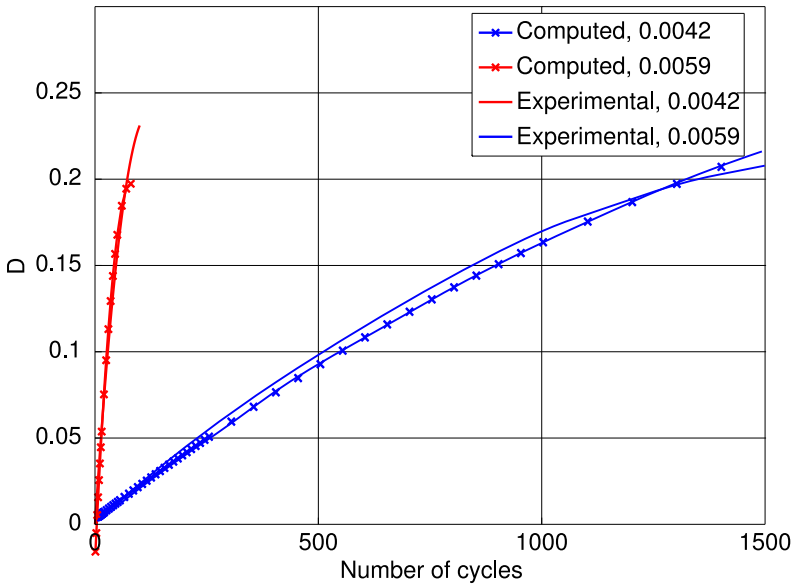

Figure 4.15: D as a function of number of cycles for human vertebral 90° computed with Equation 4.11 and experimental data for two load levels σ/E_0.

Damage acceleration was also assessed for its dependency on cycles to failure. Merging the three 0° groups in one common regression analysis with regard to cycles to failure leads to the strongly correlated powerlaw ($R^2 = 0.98$):

$$N_f = 0.13 \times \left(\frac{\Delta^2 D}{\Delta N^2} \right)^{-0.55} . \tag{4.12}$$

The other groups could not be included in this analysis as they also contained specimens with negative damage acceleration.

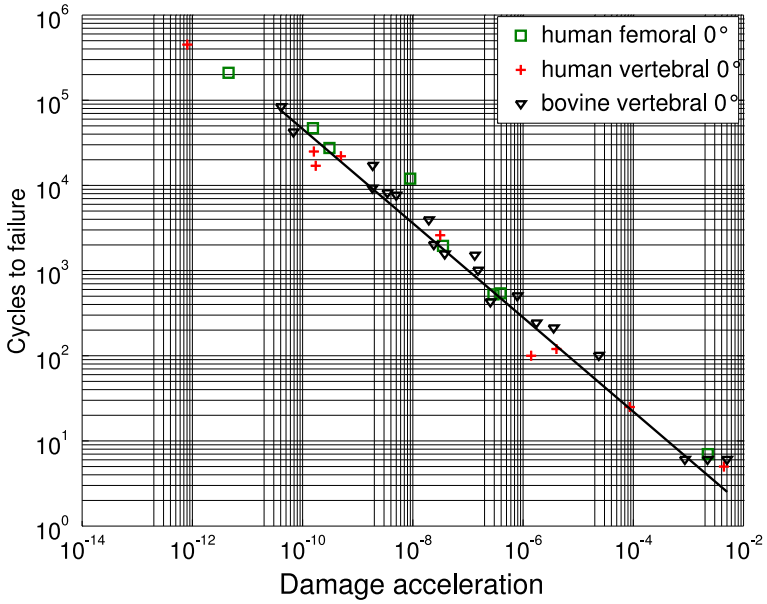

Figure 4.16: Behaviour of cycles to failure as a function of damage acceleration ($\frac{\Delta^2 D}{\Delta N^2}$). One common regression curve was established for the three groups aligned with the main physiological bone axis.

Poisson's ratio

Surface strains were measured on two sides of the specimens for the bovine specimens. This setup allowed for a continuous two-dimensional analysis of the surface deformations. The surface strain components in longitudinal and transverse direction were integrated over the whole surface in order to observe Poisson's ratio defined as

$$\nu = -\frac{\int\int(\varepsilon_{transverse})dxdy}{\int\int(\varepsilon_{longitudinal})dxdy}. \tag{4.13}$$

The optical surface strain analysis revealed two distinctive deformation modes for the bovine vertebral 0° and 90° groups characterised by a variation in Poisson's ratio (established using Equation 4.13) during each test. For the group 0° specimens Poisson's ratio went up with increasing cycle number, indicating a relative increase in the amount of transverse strain. Exactly the opposite behaviour was observed for group 90° specimens: cell deformation increased more rapidly in the longitudinal (along the load axis) direction and thus Poisson's ratio continuously decreased with cycle numbers. This characteristic behaviour was found for almost all specimens, with varying absolute values of the rate of change (Fig. 4.17 shows two typical examples). The large scatter between the specimens did not allow for a quantitative evaluation of this effect. (A second method to quantify Poisson's ratio was also established: binarisation techniques were applied to the images of the optical deformation measurement system. In a self-written routine average extension in the middle section of the specimen was computed and coupled with the longitudinal reduction in the specimens' height. Therefore, the more traditional Poisson's ratio relationship could be established. Likewise, the large inter-specimen scatter did not allow for a quantitative evaluation as transverse deformation appeared rather inhomogeneously.)

Strain localisation

As shown for the monotonic compression behaviour of cancellous bone (Fig. 4.3) also strain localisations were found in specimens exposed to cyclic compression. Optical deformation analyses were utilised to reveal these effects.

Two examples of the evolution of strain concentrations observed during various stages of cyclic compression are given in Fig. 4.18 and Fig. 4.19. In both cases, strains are rather stochastically distributed at the beginning of the saturation region (Fig. 4.18b). As accumulated residual and maximum strains evolve, strain concentrations do further localise (Fig. 4.18c−d). This is followed by the formation of a slip line through the specimen

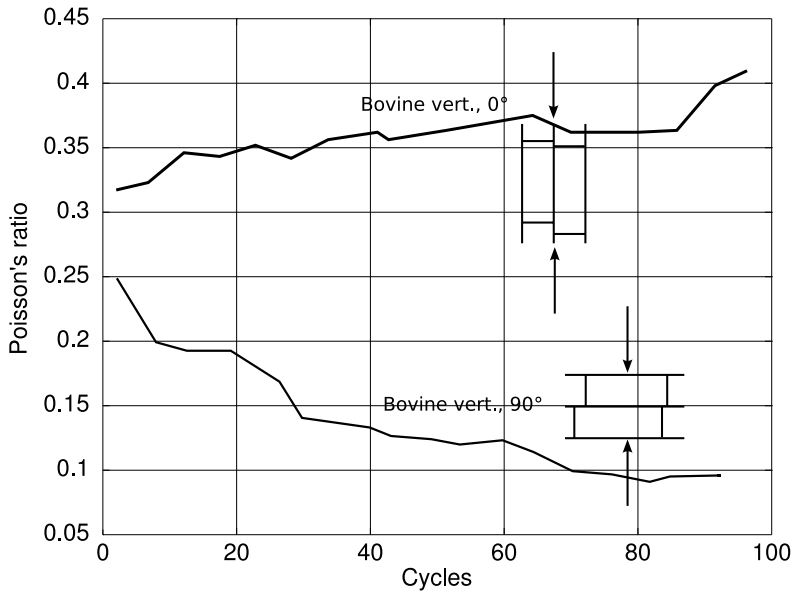

Figure 4.17: Evolution of Poisson's ratio for two specimens with almost equivalent lifetimes (bovine 0°, bovine 90°).

(Fig. 4.18e−f). The strains appear to be highly non-uniformly distributed. The initiation of catastrophic failure with respect to local strains undergoes the following stages: strain localisations right from the beginning; further strain 'hot spots' formations all-over the specimen as integral strains increase; localisation of strains at few regions with initiation of a macroscopic crack through the spongy structure. In the bovine 0° specimen of Fig. 4.20 an example for the connection between strain concentrations and structural failure is given. Fig. 4.20a) shows the distribution of transverse strain components at approximately 18 % of the overall lifetime. Each pair of positive and negative transversal strain components represents the deformation of a cell and its trabeculae, respectively. Many highly strained cells are visible distributed all-over the specimen's surface. In Fig. 4.20c) the von-Mises strains close to the cycle of macroscopic failure are shown. One distinctive region of strain localisation (indicated by the circle) from the earlier detected pattern plays a major role in the initiation of the fracture line whereas regions with initially higher deformations do not contribute to catastrophic failure. The structural element where failure initiates has been located as a trabecula which was orientated in alignment with the specimens' stress axis (Fig. 4.20b).

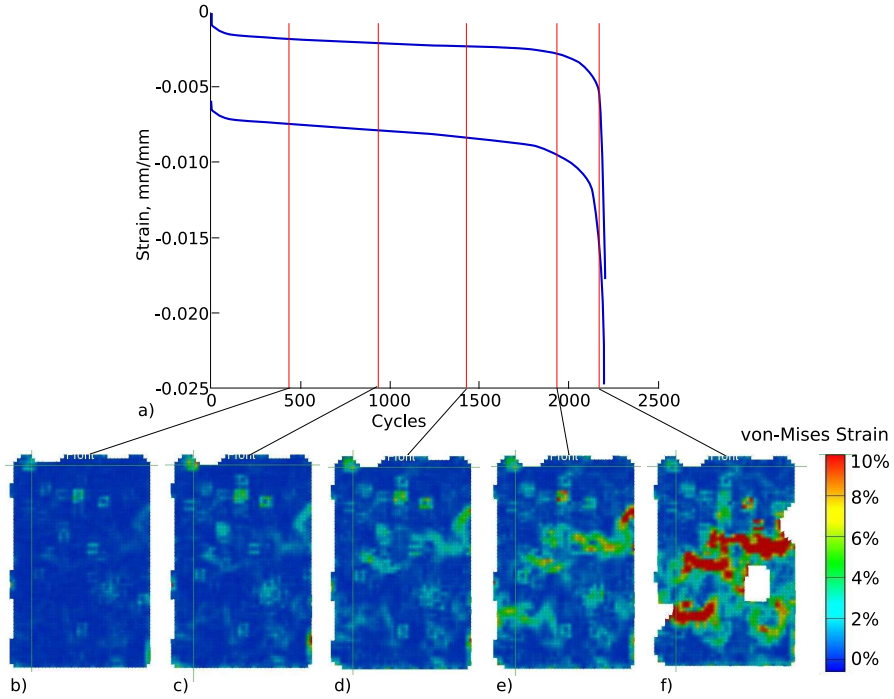

Figure 4.18: Evolution of surface von-Mises strains on a bovine 0° specimen, $\sigma/E_0 = 0.0060$, $N_f = 1550$. (Remark: The absolute strain values are not valid due to distortions in the pattern which are caused by marrow and structural cell collapse).

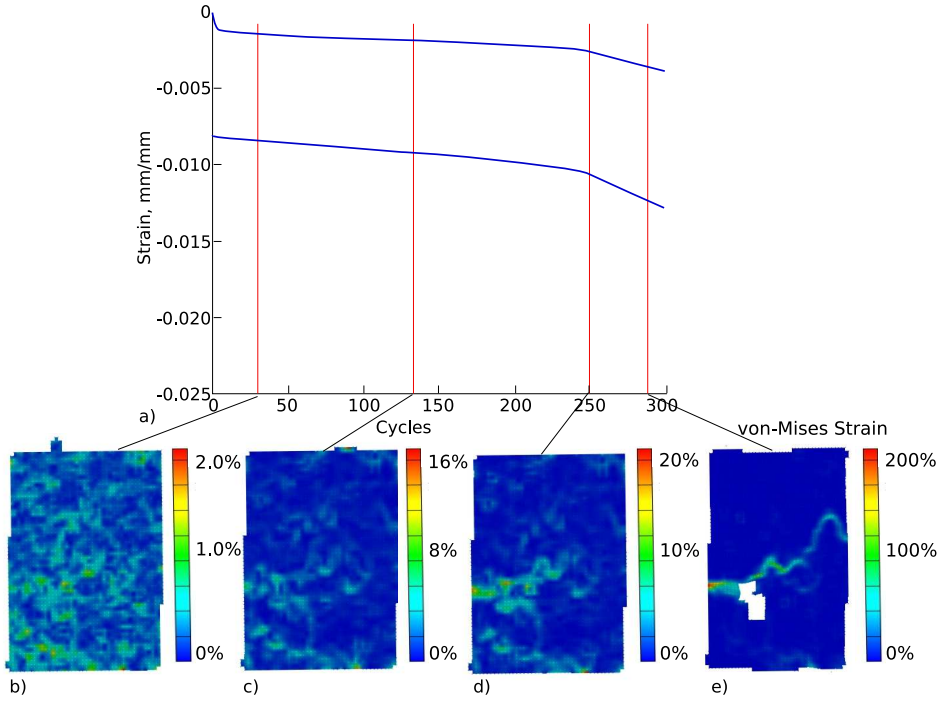

Figure 4.19: Evolution of surface von-Mises strains on a bovine 0° specimen, $\sigma/E_0 = 0.0077$, $N_f = 240$. (Remark: The absolute strain values are not valid due to distortions in the pattern which are caused by marrow and structural cell collapse).

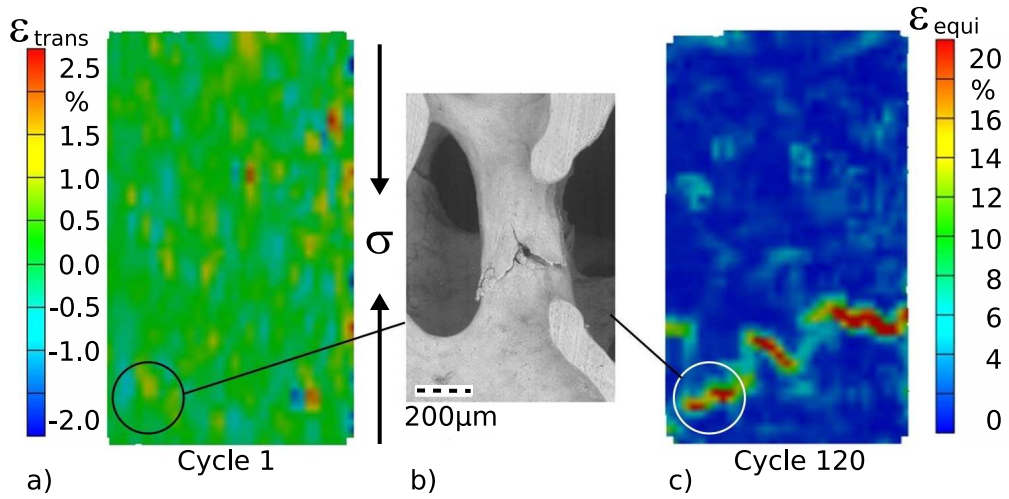

Figure 4.20: Strain distribution on a bovine vertebral specimen 0° (Load σ/E_0 = 0.00414), a) transverse strains at cycle 10,000, b) SEM image of initial failure region after macroscopic failure, c) von-Mises strains at cycle 185,000 (Dendorfer et al., 2005).

Quantitative Assessment of Surface Strains

Surface strains at the bovine specimens were processed in order to analyse the stochastic strain concentrations in a quantitative manner. On-axis, longitudinal and perpendicular, transverse strains were analysed and the total surface area was classified in steps of 1 percent strain bounds from -10 to 10 percent at various stages of each experiment (to study the influence of these rather arbitrary bounds, an analysis of various bounds has been undertaken, and the strain bounds shown below were found to be the most suitable). The percentage of strained area within a certain bound was plotted versus the number of cycles for each specimen (Fig. 4.21). The major strain class is from 0 to -1% (compressive). Its magnitude decreases in the course of the experiment and subsequently more areas are strained with higher strain values. All specimens were merged in a further step by analysing the strained areas at failure (10% reduction in secant modulus) and correlating these values with the corresponding normalised load ratios σ/E_0. Weak linear correlations between the strain classes -1 % to -2 % and -2 % to -3 % and the applied load were observed. The tensile components were found to have the tendency to decrease with increasing nor-

malised load. In the bovine 0° group tensile components do rapidly decrease at a load level of 0.0075 (Fig. 4.22). The specimens transversally loaded to the physiological direction (bovine 90° group) did not exhibit this boundary (Fig. 4.23).

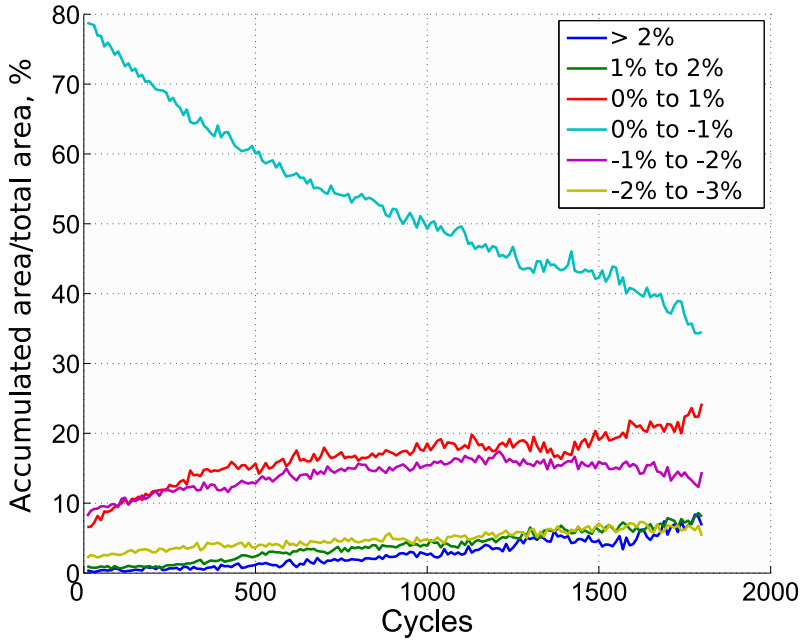

Figure 4.21: Accumulated strained areas as percentage from the total area within different strain classes as a function of the number of cycles of a bovine 0° specimen, $\sigma/E_0 = 0.0075$, $N_f = 1500$.

Trabeculae Level

Strains at the trabeculae level reveal residual components during cyclic loading (Figure 4.24b-e). These are already visible after few load cycles. Increasing the applied loading from almost zero (preload level) (Figure 4.24c) to maximum load in the first cycle causes strain concentrations in the middle of the transverse-oriented trabeculae (Figure 4.24e). Strains between preload level (Figure 4.24b) and peak load (Figure 4.24d) in the 100^{th} cycle (about 15% of the overall lifetime of the specimen) did not differ significantly. Therefore, the load bearing capacity of the trabecula has been reduced by damage accumulation. Damage occurs in the middle section in form of (micro-)cracking (Figure 4.25). The (destructive) magnitude of the strains lies in the range of $4-5\%$. The analysis of trabeculae

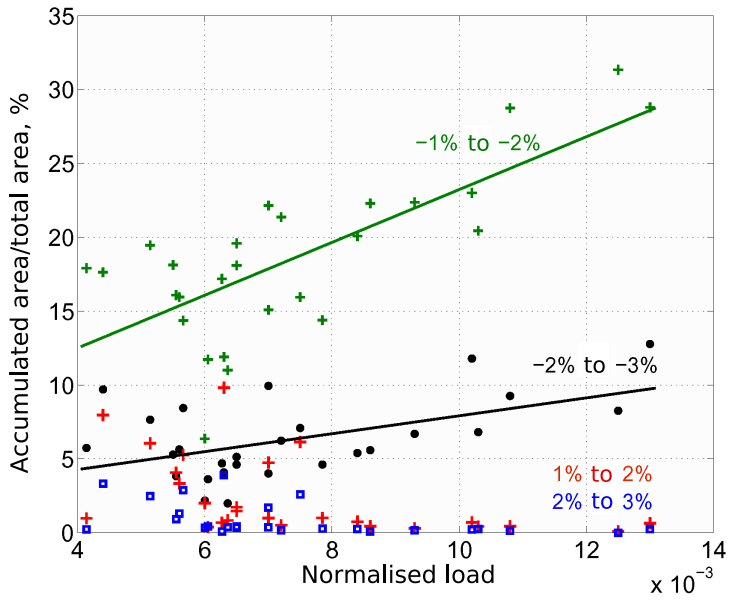

Figure 4.22: Percentage of accumulated strained area from total area within different strain classes at the failure for the bovine 0° group.

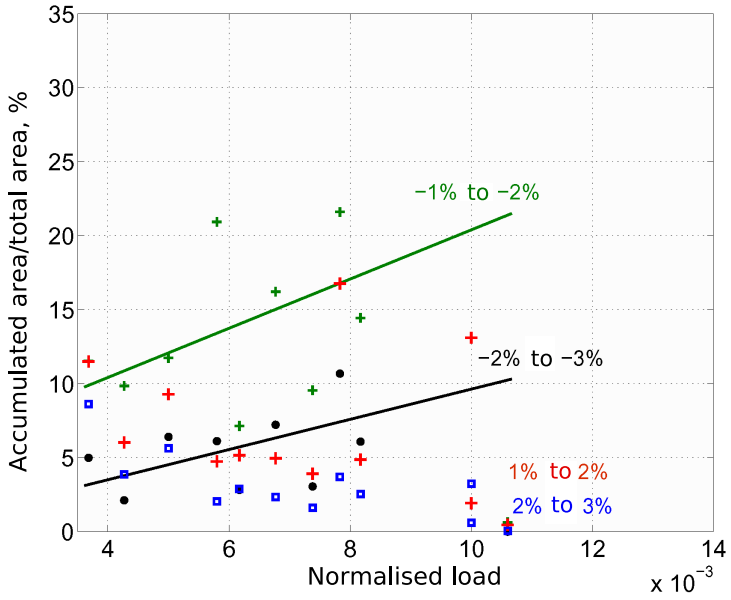

Figure 4.23: Percentage of accumulated strained area from total area within different strain classes at the failure for the bovine 90° group.

orientated in 45° to the load axis revealed bending of the struts and strain concentrations at the joints. Examples for macroscopic damage of cyclic loaded specimens are given in Fig. 4.25, 4.26. In the plate-like structure of the bovine vertebral bone, damage can be found in the transverse struts as well as in the plates. The struts fail mainly due to bending and cracking occurs along the laminary structural compostion of the trabeculae. Furthermore, packages likely from former remodeling activity were found to burst from the trabecula (Fig. 4.25). Failure in the structural elements aligned with the stress axis fail mostly due to compression fractures, perpendicular to the laminar compostion (Fig. 4.26). Also fractures of whole trabeculae (Fig. 4.27, Fig. 4.28) were found.

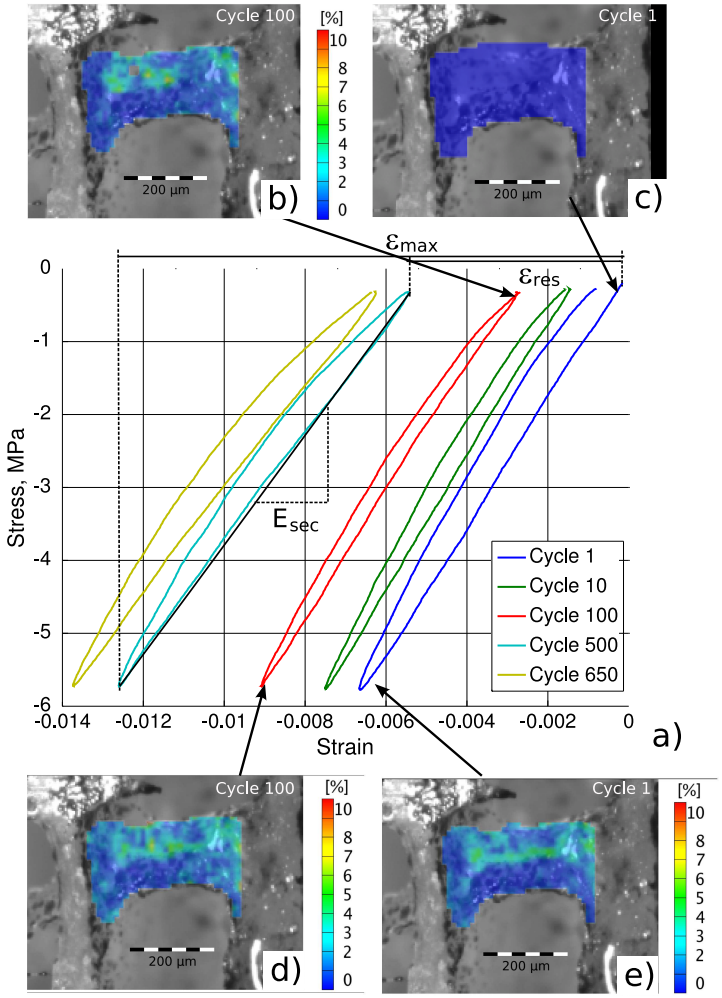

Figure 4.24: a) Stress strain hystereses (human femoral 0° specimen, $\sigma/E_0 = 0.0060$, b) – e) von Mises Strain distribution on a single trabecula during different stages of the experiment.

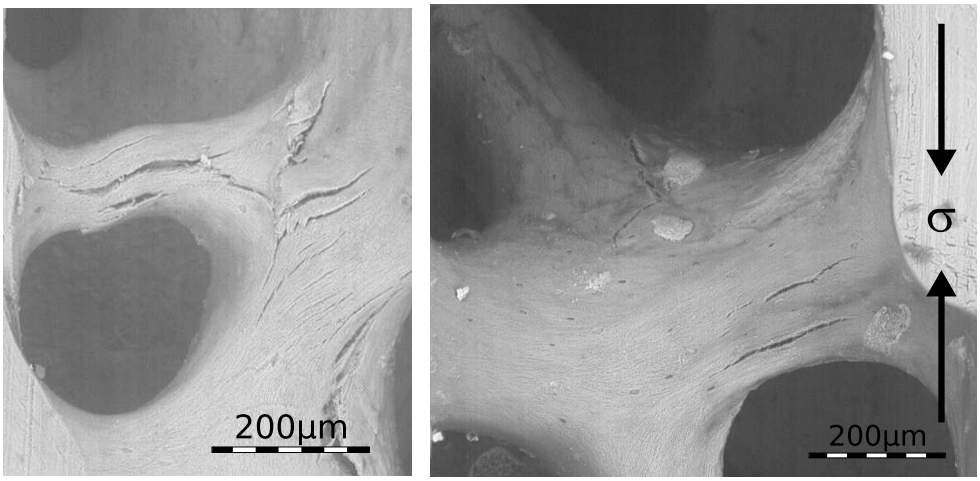

Figure 4.25: (Micro-)Cracking of transversely loaded trabeculae (SEM).

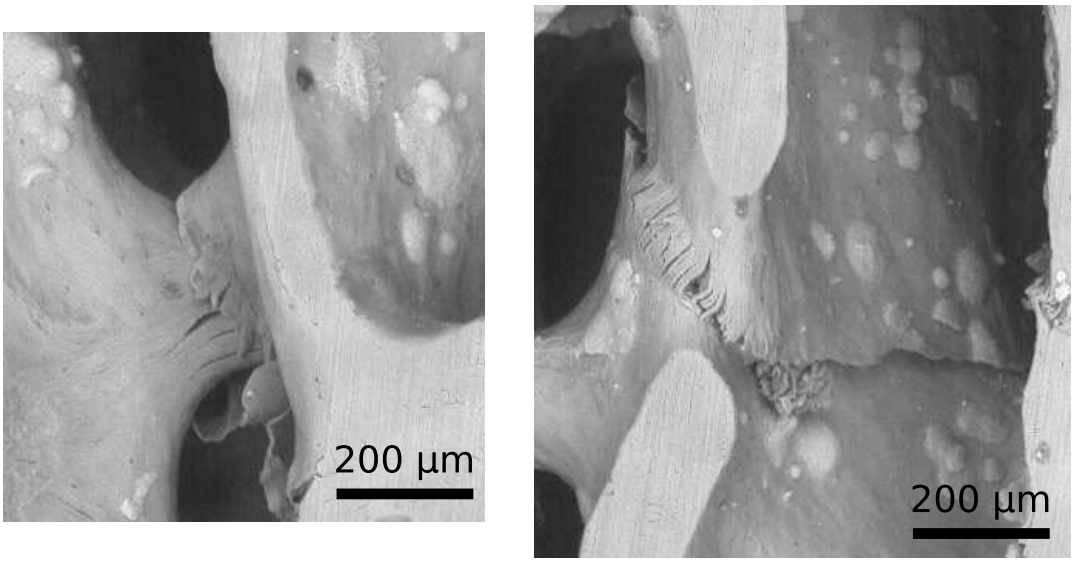

Figure 4.26: Damage in bovine vertebral 0° cancellous bone, $\sigma/E_0 = 0.0041$, $N_f = 185{,}000$, integral strain at examination $\varepsilon_{max} = 1.33$ %, the stress axis lies in the vertical direction (SEM) (Werz, 2005).

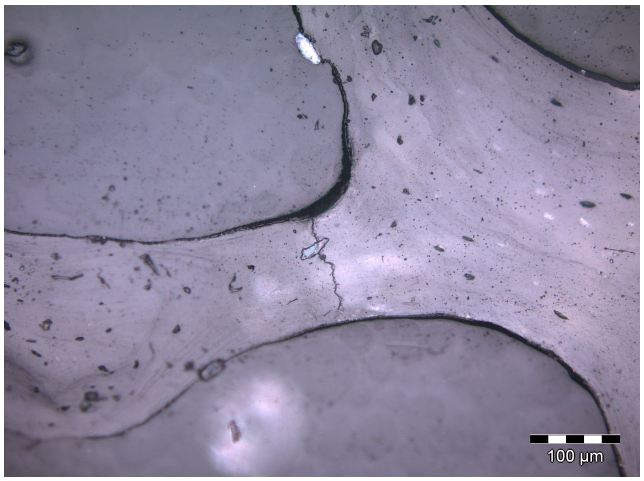

Figure 4.27: Fracture of a trabecula, bovine vertebral specimen, load axis is in vertical direction, specimen has been embedded and sectioned (LM).

Figure 4.28: Rupture of a trabecula joint of a bovine vertebral specimen, load axis is in vertical direction, specimen has been embedded and sectioned (LM).

4.3.3 Lifetime curves

Analysing the relationship between the applied load and the cycles until the (defined) failure results in lifetime curves. For the runout specimens, the cycle number at abort time of the experiment was taken for the analysis. The lifetime curves can be expressed according to a power-law and can therefore be shown in log-log plots as linear functions. Lifetime curves were established for all groups separately. Stress versus cycles to failure regression analyses resulted in very weak correlations. While the groups aligned with the physiological axis showed reasonable trends, off-axis groups behaved rather arbitrarily (Fig. 4.29). Using the normalised stress levels σ/E_0 (as load value) results in strongly correlated power-law relationships for all groups. (Remark: σ/E_0 is used to establish lifetime data, σ refers to the applied maximum compressive stress rather than the stress amplitude.)

$$\sigma/E_0 = a \times N_f^b \tag{4.14}$$

N_f = Cycles to failure

a, b: Regression coefficients (see Table 4.9)

The intersection point at the σ/E_0 axis as well as the gradients of the curves appear to be different between the groups (Fig. 4.30). Lifetimes were highest for the bovine vertebral specimens loaded in physiological direction and lowest for the human vertebral bone loaded at 90° off the physiological axis. A reduction in lifetime was observed for

Table 4.9: Regression coefficients for Equation 4.14.

Group	i	j	R^2
Human vertebral 0°	0.0098	−0.109	0.94
Human vertebral 22°	0.0091	−0.111	0.97
Human vertebral 45°	0.0096	−0.121	0.89
Human vertebral 90°	0.0087	−0.119	0.88
Human femoral 0°	0.0103	−0.108	0.97
Bovine vertebral 0°	0.0133	−0.094	0.91
Bovine vertebral 90°	0.0105	−0.105	0.95

the off-axis groups, both in human and bovine. In the human vertebral groups a larger deviation from the main structural axis of the cancellous bone results also in lower lifetimes. But despite the observed differences, a certain loss of information is associated with the normalisation process (σ/E_0) as it blurs the deviations in the fatigue behaviour between the groups. In order to clearly point out the consequences of non-physiological loading on fatigue lifetime the data was normalised further by the mean modulus of each group (Fig. 4.31). Relating this data specifically to the specimen orientation angle (with respect to the physiological bone axis) results in Fig. 4.32. This modified form of a S-N diagram with the introduction of an anisotropy-based pseudo stress reveals the magnitude of the load bearing capability with respect to the anisotropy. While lifetimes are decreasing rather rapidly within a narrow band of the physiological bone axis, they remain almost constant at higher (deviation) angles.

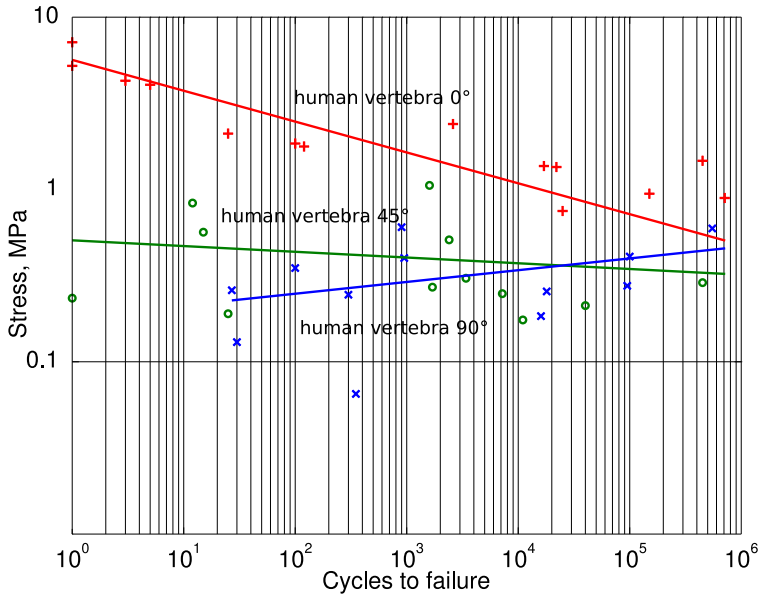

Figure 4.29: Cycles to failure as a function of peak stress σ for human vertebral 0°, 45° and 90° groups.

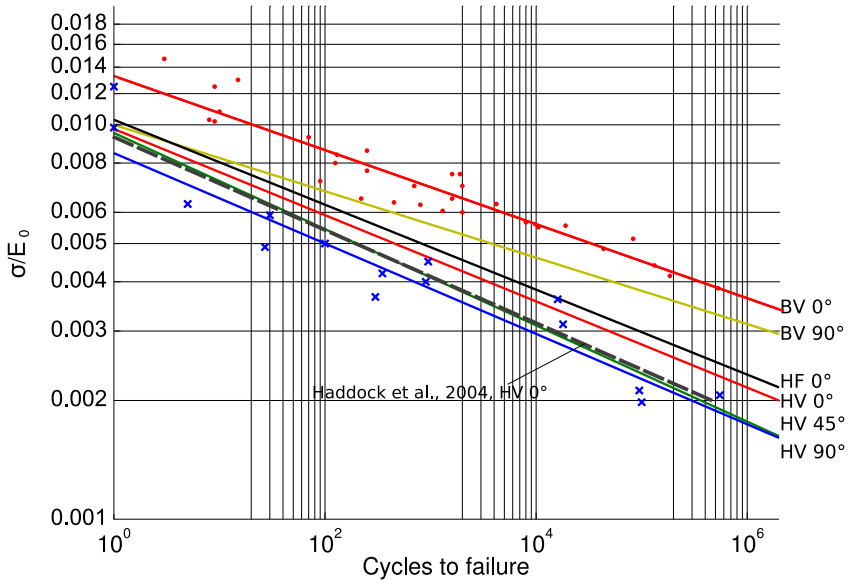

Figure 4.30: Cycles to failure as a function of σ/E_0 for bovine (BV: bovine vertebral, the number refers to the angle between the specimen axis and the physiological bone axis) and human (HV: human vertebral, HF: human femoral) groups. In order to enhance the clarity of the representation only the point data of the bounding groups was included. For comparison with the literature an additional curve taken from Haddock et al. (2004) is plotted in the graph.

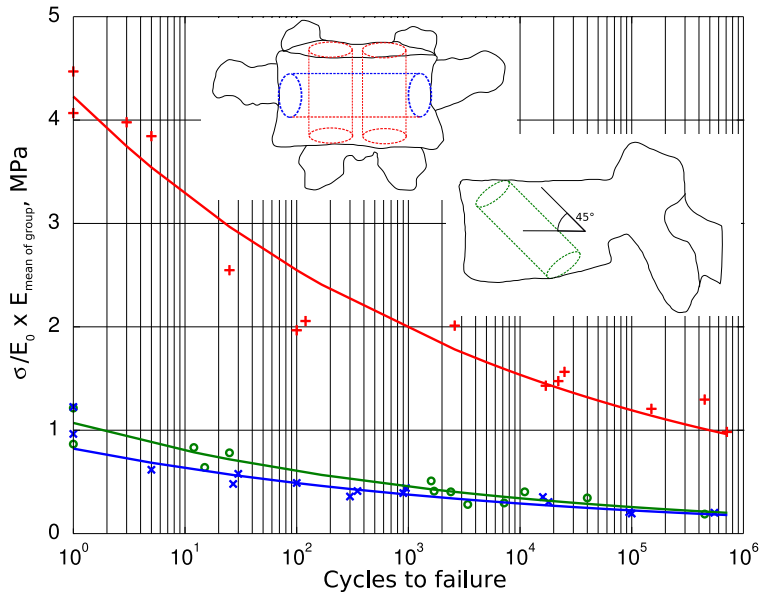

Figure 4.31: Lifetime curves for human vertebral 0°, 45° and 90° groups. Load values were modified by the mean initial modulus of each specimen group.

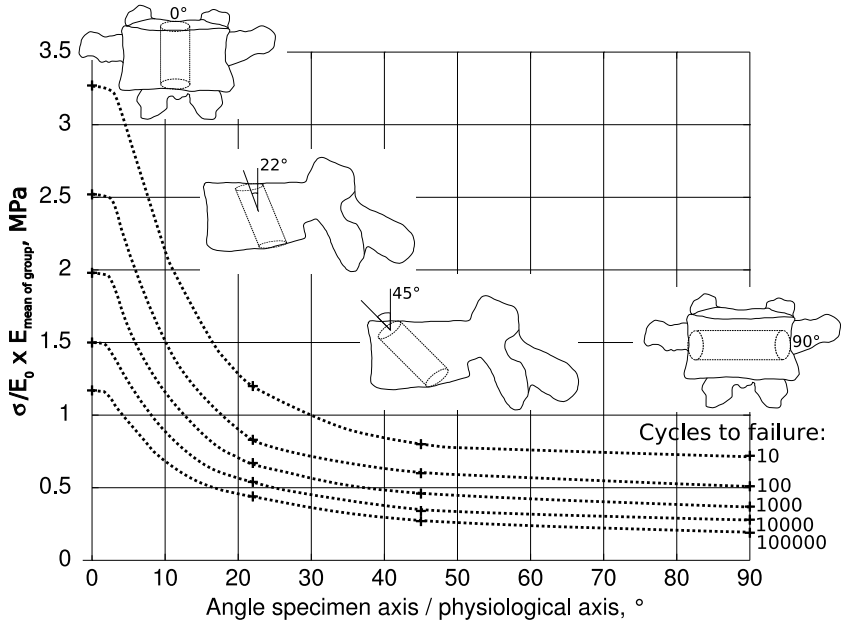

Figure 4.32: Stress values for the corresponding cycle numbers (Fig. 4.30) were modified by the mean initial modulus of each specimen group and plotted as a function of the angle between physiological and specimen axis. (The dashed lines are not based on regression analysis.)

4.4 Age-Related Effects

The influence of age on the mechanical behaviour of cancellous bone is addressed in this chapter. For this reason, human vertebral cancellous bone data was analysed with respect to donor age. No sex-specific differences could be analysed due to vast majority of male donors.

The initial secant modulus of the specimens was found to be highly dependent on donor age (Figure 4.33). For all specimen groups the modulus decreased with increasing age. This holds with the exception of the specimens from the 46 year old male donor of the 0° group, which showed a slightly weaker mechanical performance than the overall trend, as well as one specimen from a 72 year old male donor whose value was exceptionally high. In both cases, the bone samples did not show any (macroscopic) conspicuous features.

The relationships between the decline of the initial secant modulus and the donor's age are represented most suitably as quadratic and cubic polynomials (thus exponential

relationships provide good correlations). While the principle change appears to be similar concerning the different groups, the relative decrease of the modulus appears to be more pronounced in the 45° and 90° groups compared to the 0° group. In these off-axis groups mean modulus drops within 20 years (60 – 80 years) by more than 70 percent from (mean) approx. 180 MPa and 160 MPa to 50 MPa and 20 MPa, respectively, whereas the group aligned with the physiological axis revealed a decrease of 25 percent from approx. 440 MPa to 330 MPa.

The characteristic cyclic deformation behaviour showed no remarkable change with increasing age. All specimens followed the stages of deformation described earlier in fatigue of cancellous bone with an increasing residual deformation, decreasing secant modulus and increasing hysteresis loops during cyclic deformation. Damage evolution, defined as a decrease in secant modulus, did also not appear to be different with increasing donor age. Figure 4.34 shows the evolution of this scalar damage variable as a function of the percentage of total fatigue lifetime for four 45° specimens from two 61 year old and two 80 year old specimens. Damage increases rapidly within a small percentage of lifetime, this transient is followed by a lowered, constant damage rate which increases at approx. 75 to 85 % of the total lifetime indicating macroscopic failure. Similar results can be obtained for the other specimens/groups.

Neither maximum strains at failure nor accumulated residual strains revealed a significant influence of donor age on the results. Specimens with different donor ages showed no tendencies in higher of lower (integral) deformations at failure. Likewise, no influence of donor age on the tendency of earlier or later failure could be observed once initial stiffness was taken into account. Age showed no influence on the probability distribution along the lifetime curves (Figure 4.35). The other groups behaved similar to the 45° group already shown.

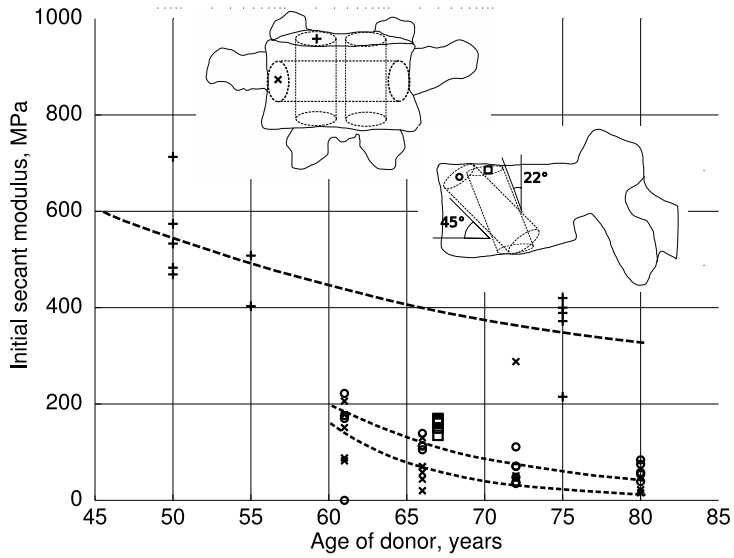

Figure 4.33: Initial (undamaged) secant modulus as a function of donor age for different specimen groups. The groups differed in their coring direction with respect to the physiological axis.

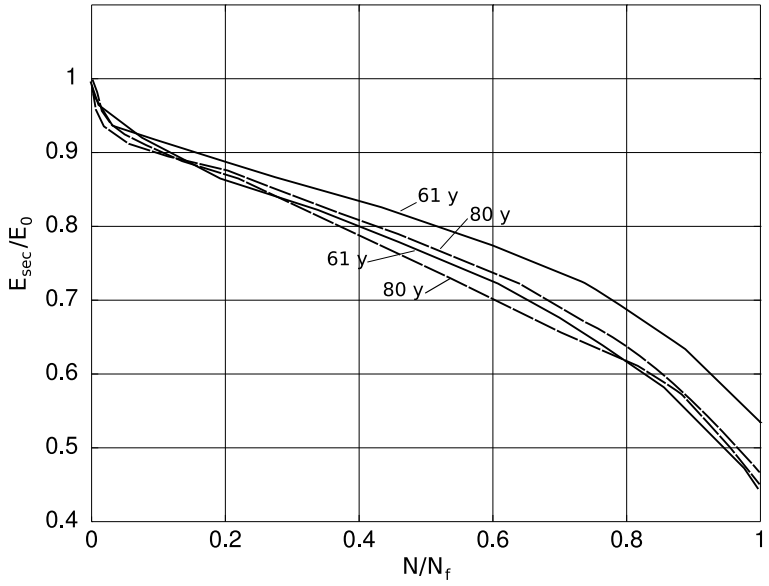

Figure 4.34: Evolution of damage in terms of a decreasing secant modulus as a function of the percentage of fatigue life. The numbers refer to the age of the donors. The lifetimes of the plotted specimens (45 degree group) ranged between 1,600 and 11,000 cycles.

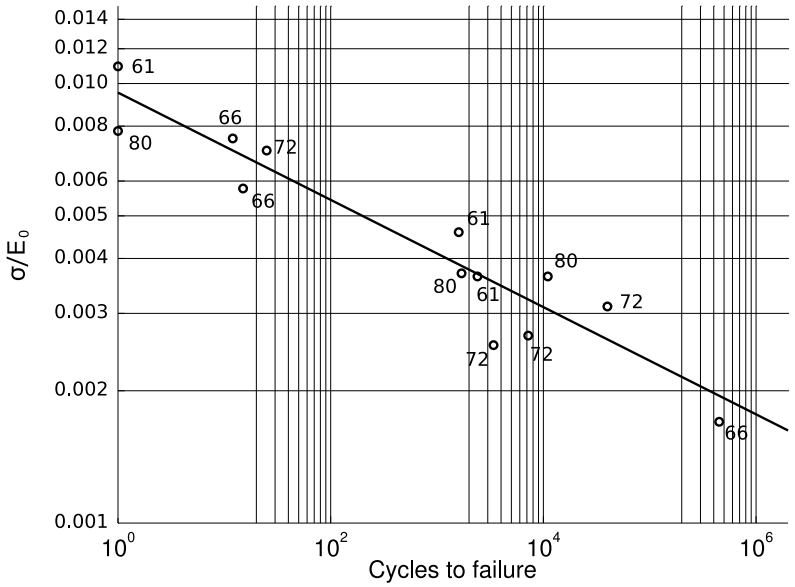

Figure 4.35: Lifetime (S-N) curve for the 45° group. The loads are normalised by the mean initial modulus. The numbers refer to the age of the donor.

5 Discussion

This study focuses on the investigation of the mechanical behaviour of cancellous bone under cyclic compression loading with specific respect to the trabecular bone structure, i.e. orientation of loading axis, species and site. Especially the influence of load components, which are not aligned with the main physiological bone axis has not been addressed yet and is an important issue in understanding bone failure following unphysiological loading (implants, misuse). Besides architecturally dependent lifetime correlations also the deformation and damage behaviour of different cancellous bone structures have been investigated and the influence of load magnitude and direction are shown. The data has been analysed with respect to donor age in order to provide information about the influence of age on lifetime and deformation behaviour of cancellous bone.

5.1 Experimental Set-Up

In this study, no quantitative measure for architectural features was used. Much effort was put into ensuring the proper alignment with respect to the physiological coordinate system. An analysis of the main axes of a group of ten specimens by means of μ CT, analysing the fabric tensor, as well as stereological analyses of microscope images revealed a rather good agreement of the core direction with the main axis of the cancellous structure. As the data was only analysed for few specimens, results were not included in this work. Any inaccuracies concerning the resolution of deformations of the samples under cyclic loading due to the experimental setup were carefully analysed and minimised in preliminary studies. The contribution of the methylmethacrylate layer to the overall deformation of the sample

in terms of a superimposed strain can be regarded as negligible. A certain stiffening effect in the bone boundary layers has been taken into account in the strain calculations. In contrast to most studies on cancellous bone in the literature, which use external extensometers for deformation measurement, the strain data of this study was registered by the internal displacement sensor, i.e. by measuring the grip to grip motion. Nevertheless, the precision of the strain data is assured, for the fixations are clamped in a force-fit manner to the test rig, where slipping is absolutely prevented for the load range of this study. Additionally, individual deformations of all fixing parts aligned within the 'gauge section' of the internal displacement sensor can be neglected due to their high mechanical stiffness. Furthermore, the occurrence of any deformation of these fixing parts were finally analysed and verified by means of external extensometers and by optical deformation measurements. For example, line deformations on the specimens' surface were analysed and the deformational results were extrapolated to the whole specimens' length (as a small percentage was not visible for the optical system). Thus, it is assured that the resolution of strains by the internal deformation measurement system is absolutely reasonable in this study. Secant modulus was chosen instead of other methods (Moore and Gibson, 2001) as its determination appears to have a much higher accuracy (Cotton et al., 2005). Like in all experimental fatigue studies on bone up to now no biological effects in terms of remodeling processes could be included in this study and their influence remains unclear.

5.2 Deformation Behaviour and Damage Mechanisms

Characteristics of Deformation

The principle characteristics of the cyclic deformation behaviour for all groups were found to correspond with the data given in the literature. In accordance with the relations found for bovine tibial (Bowman et al., 1998; Moore et al., 2004) bone and human vertebral bone (Haddock et al., 2004; Rapillard et al., 2006) loaded in the physiological axis of the trabecular architecture stress − strain hysteresis was found to become increasingly nonlinear exhibiting an increased area and a shift along the strain axis. The shift of the

hysteresisis referred to as cyclic creep effect in traditional material sciences (e.g. Schijve (2001)) (but of course may be more related to the phenomena observed in concrete (e.g. Jirasek and Bazant (2002)) rather than metallic materials). It has been discussed in the literature whether or not creep does contribute to fatigue in cancellous bone (Bowman et al., 1998; Moore et al., 2004; Yamamoto et al., 2006). It has been suggested that creep may play a role in habitual loadings, in experimental data, which uses higher loadings, microcracking is dominant (Yamamoto et al., 2006). In the range of this work residual strains were found to be linked to microdamage initiation and growth (Fig. 4.24). Rather large, localised strains were found, even at low load magnitudes (Fig. 4.3), which may also hint at the formation of microcracks. Additionally, quantitative surface strain analysis showed, even at low load levels, relatively large areas with higher strains, so that - at least in the range of this work - microcrack initiation and growth may be the major cause for the evolution of residual strains during cyclic loading, even if the observed mechanisms are not validated with statistical methods. Furthermore, the definition of an elastic regime for cancellous bone may be partly rejected. The terms 'Young's' or 'Elastic modulus' appear to be imprecise as strain localisations in trabecular bone, exposed to monotonic compression, can be found already at very early stages of the experiment, although the stress $-$ strain curve indicates strictly linear elastic behaviour (Fig. 4.3). Deformations in trabecular bone may therefore, even at low magnitude, localise and in consequence be coupled with damage. The secant modulus was found to increase slightly for a part of the specimens during the first few load cycles. In these cases, the secant modulus of the fifth cycle was chosen for the normalisation of the load (σ/E_0). This increase may be induced by stress redistributions in the volume directly beneath the surface to compensate the loss of adjacent trabeculae due to the specimen preparation. Another point may be early inelastic deformation caused by bending and the formation of certain plastic hinges of unfavourably arranged trabeculae. The superposition of both effects causes the observed almost instantaneous random pattern of locally enhanced strain areas, which directly result in an integral loss of the specimen height. Extensive experimental effort has verified that no embedding or other experimental inaccuracies did cause this effect. The definition of the

damage criterion as a ten percent reduction in secant modulus was chosen in accordance with literature (Bowman et al., 1998; Haddock et al., 2004) and did also perform very well in the preliminary studies on bovine vertebral cancellous bone. Therefore it was chosen for the context of this work.

Detailed Cyclic Deformation Behaviour

The cyclic deformation behaviour of cancellous bone can be described, in analogy with the literature on the fatigue behaviour of fibrous composite laminates, as a tripartite process. Starting with stage I, where deformations increase rapidly and damage is initiated, the deformation process stabilises through stage II and in stage III deformations increase leading to catastrophic failure. The definition of damage as a ten percent reduction in secant modulus shifts failure within stage II for all groups. Therefore, stage III is only partly analysed and discussed in the section concerning damage.

Stage I: Initiation

In this initial phase of fatigue behaviour, deformations and damage are initialised and proceeding stabilisation of the deformation behaviour can be observed. The stabilisation of the deformational process is prolonged in the off-axis direction groups. Both strain components, maximum and residual, respectively, at the end of the transient exhibited a linear dependency on the applied load (σ/E_0). The off-axis groups showed increasing strain values with growing deviation from the physiological axis. Even if no (statistically relevant) groupwise differences were observed for the number of cycles within Stage I as a function of the applied load, trends for a varying behaviour can be supposed from Fig. 4.8. Despite this rather weak trend, the percentage of the number of cycles with respect to the cycles to failure is increasing in the off-axis groups. Thus, with rising deviation from the main physiological axis strain deformations as well as the percentage of lifetime during Stage I is increasing. This may be the result of a growing lack of the load-bearing optimum, which the structure has been adapted to during remodeling processes. Therefore, the

highly adapted structure of the bovine 0° group possesses the shortest (relative) initiation duration. As Stage I is also associated with the initiation of microcracks, the prolonged stabilisation process also contributes to this. In the load adapted structures, aligned with the 0° direction, the following mechanism may be present: Microdamage is initiated and microcracks stop relatively rapidly on ultrastructural, collagen fibrils or microstructural, cement lines, boundaries, whereas microcracking in specimens loaded in non-optimised directions may proceed longer until these barriers are reached, depending on the orientation and location (see Trabecular Composition, Fig. 2.3). Furthermore, the trabeculae are increasingly loaded in bending, which results in stress concentration at the trabecular joints and may also produce a higher amount of microdamage.

Stage II: Constant Deformation Rate

The initial transient region is followed by a region with a rather constant deformation rate. This deformation rate was assessed for group differences and analysed as a function of loading. Not all specimens of each group could be used as very high loaded specimens did not reveal a region with constant deformation. The rate of integral strain evolution depends on both, species and direction. In the bovine 0° the lowest deformation rates (with respect to normalised load) were observed, whereas rates increase at bovine 90°. Similar behaviour with an offset on the load axis was found for the human groups. The off-axis groups revealed higher deformation rates. Interestingly, a species-dependent intersection point of the deformation rate regression curves seems to exist. The corresponding load values (σ/E_0) are approximately $0.007-0.008$ for bovine and $0.0045-0.005$ for human vertebral bone, respectively. The human 45° group exhibits some deviation above the threshold, in the bovine 90° group the bearable maximum loads are reduced compared to the bovine 0° group. Therefore, deformation rates increase rapidly beyond a certain load level. Fig. 5.1 shows the deformation rate curves for these two groups of bovine and human bone. Data taken from the literature (Ganguly et al., 2004) on bovine tibial bone shows a similar behaviour, lying between the bovine vertebral and human goups in this study. The behaviour beyond the data range has been assumed. These results point

to a change in the deformation mechanism at the specified load level for each species. Below this load threshold, architectural features accelerate or decelerate the deformation rate which may correspond to increasing microcrack density and length, but most of them being stopped at the materials' internal boundaries. Above the specified load level micro- and ultrastructural barriers may be skipped and therefore their orientation with respect to the stress axis becomes less important. The rates for the maximum strains showed to be very similar, with almost identical regression coefficients. Even if the data is afflicted by remarkable scatter the derived trends are rather clear.

Strains at Failure

Strains at failure were found to be dependent on the specimen group. Even if statistical significance could only be established for the differences between the human vertebral 0° and human vertebral 90° groups, the results indicate the influence of structural orientation as well as species on the deformations at failure. Therefore, an isotropic strain-based failure criterion may not be able to predict fatigue failure. One explanation for this difference can be found in structural cell deformation models. The evolution of Poisson's ratio (Fig. 4.17) revealed predominating transversal deformations in the bovine 0° group, which correspond to bending and/or buckling of the longitudinally oriented trabeculae. Therefore, the main deformational components are oriented in the transversal direction and the longitudinal components are less activated. The cell deformation in transverse loaded specimens (90°) is also dominated by bending of the long struts and thus, large deformations in the longitudinal direction of the specimen accumulate. The observed differences in strains at failure may therefore be caused by geometrical effects as only uniaxial deformational components are used. The analysis of Poisson's ratio was done by integrating the (surface-)strains across the surface for both, transversal and longitudinal components. Even with this advanced method only trends could be observed. Alternatively, the optical data was used to calculate Poisson's ratio in a more traditional sense with extension in the middle of the specimen. This analysis did not result in valuable findings, the damage mechanism in this highly non-uniform structure can can only hardly be described with integrally mea-

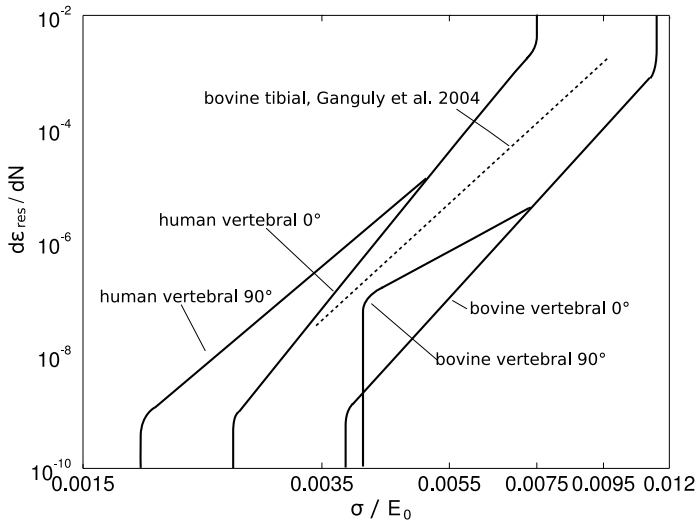

Figure 5.1: Stage II deformation rates (residual strains) as a function of the applied load σ/E_0.

sured deformations as for example cells may collapse either in one or the other direction. In analogy to these findings other researchers reported similar results using extensometer measurements for the orthogonal deformation components of trabecular bone, which were also found to be very difficult and were only partly successful (Bredbenner and Davy, 2006).

Average Cyclic Deformation

By combining the derived relationships for stage I and stage II, cyclic deformation curves can be analysed and established for a set of "average specimens" as the equations are based on regression analyses. All relationships only depend on the applied normalised stress and group. Thus, with the combination of Equation 4.14 (rearranged with respect to cycles to failure), Equation 4.2, Equation 4.3 and Equation 4.4 (with g, h for maximum strains), the deformation behaviour can be modeled for experiments stopped in stage II. Fig. 5.2 shows an example for the computed strains of a human 0° specimen and the comparison to two experimental data sets for specimens which were loaded with equivalent magnitudes. Due to the linear connections between the computed points the smooth appearance of the experimental curves is missing. Unsurprisingly, the computed data represents a mean curve

between the experimental data. The derived equations may be used in order to calibrate and create continuum-based numerical models dealing with cyclic deformation behaviour of cancellous bone. Strain values at the end of stage II, the beginning of the transient to macroscopic failure, were also analysed, but a relatively large scatter in the results was obtained. Therefore, this data was not used for further analyses.

Damage Evolution

The results indicate that damage evolution is dependent on species and structural orientation (with respect to the integral stress axis). The integral loss of structural integrity can be described by a scalar damage parameter D, relating the actual secant modulus to the initial, unharmed secant modulus of the specimen. While it has been shown for cortical (Cotton et al., 2005) and cancellous bone (Moore and Gibson, 2003b; Ganguly et al., 2004) that increasing strains during fatigue testing were associated with a reduction in secant modulus, the effect of the axis of loading has not been addressed so far in the literature. Likewise, direct comparison of the fatigue behaviour between human and bovine cancellous bone has only been discussed sparsely (Haddock et al., 2004).

Specimens loaded in the off-axis direction reached lower overall cycle numbers at comparable load levels for both human and bovine samples (Fig. 4.30, 4.11). In order to assess the qualitatively observed differences in loss of stiffness as a function of number of cycles for the various groups (Fig. 4.11) in a more quantitative manner, D *vs.* N_f data was normalised with respect to percentage lifetime. And the average loss of stiffness was analysed at various percentage values of the lifetime for the specimens (Fig. 4.12). Samples with only few cycles were removed from the analysis as serious damage was already induced during the first load cycle. As N_f is associated with the defined failure criterion of $D = 0.1$ rather than catastrophic failure also N/N_f values beyond 1.0 are possible. While only minor differences in D were observed for normalised cycle numbers N/N_f below 1.0, at higher normalised cycle numbers a deviation between the groups becomes visible. Bovine samples hardly reached higher N/N_f numbers as a stiffness loss of 10 percent was almost suddenly followed by structural failure of the samples. This does not hold for the

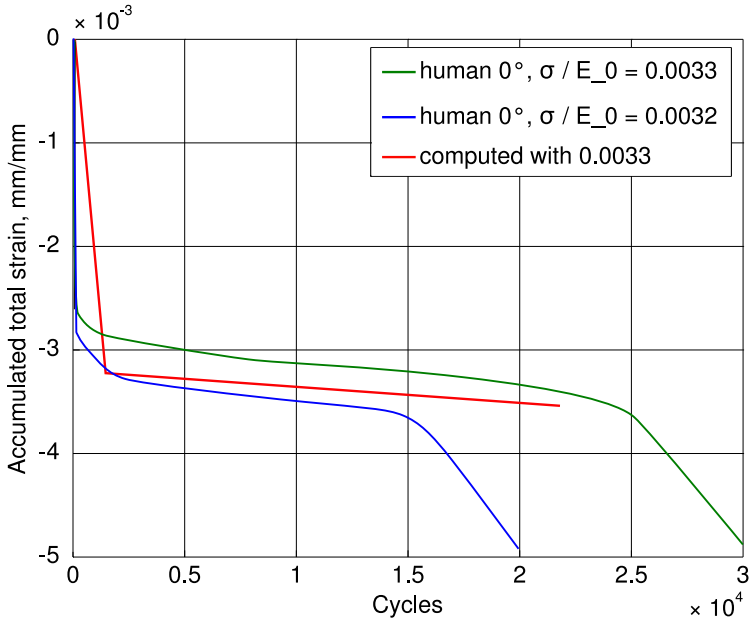

Figure 5.2: The cyclic deformation of a human vertebral 0° specimen is computed with an assumed load of $\sigma/E_0 = 0.0033$ using the equations derived in Section 4. Two sets of experimental data loaded with equivalent magnitude are added.

human groups. Here higher N/N_f values were reached with magnitudes up to 5- to 10-fold for human vertebral 90° samples. The relative lifetimes reached rose with increasing misalignment of the structural axis. Likewise, remarkable differences in the way damage evolved was observed between the groups. For all specimens, a quadratic function did approximate the course of damage very well, at least for the region below twofold normalised lifetimes. Therefore, damage rate is linear and damage acceleration constant for cancellous bone (within the framework of this study). The two parameters have been determined by derivation of D with respect to the number of cycles. Damage evolution was found to be quadratic positive for the bulk of the specimens with exception of the human 90° and a part of the human 45° specimens. Therefore, damage decelerates with increasing cycle numbers for the latter group of specimens, whereas damage rate increases for the others. This does also imply that damage increases more rapidly in the initial phase in the 45°/90° specimens. In their unoptimised structure (with respect to the stress axis) weak structural elements may fail suddenly and microcracks may grow relatively long until they are stopped. Once the structure has found some kind of equilibrium, the damage rate

decreases. The elements/struts transversally oriented to the physiological axis may be the main cause for this effect as it is mainly observed in the human vertebral 90° group. Likewise, stress concentrations in the trabeculae joints are supposed to be more critical in the 45° group, but this is not reflected in the data, which hints at the above mentioned findings. Specimens in the 45° group did fail either with positive or negative damage acceleration manner. This may depend on the real orientation of the trabecular architecture as in this study structural orientation is defined with respect to the physiological bone axis. Therefore, the structure may be not loaded exactly in 45° and either transversal or longitudinal trabeculae are mainly loaded and the corresponding damage acceleration characteristics may be activated. Furthermore, local bone structure in general is very inhomogeneous. Despite the negative damage acceleration in the $45°/90°$ specimens this does not lead to the conclusion that these structures exhibit a higher resistance against damage. Obviously, the bearable stress levels are much lower (Fig. 4.31) and therefore their absolute damage resistance is heavily reduced. (Critical) damage in samples, which are loaded along their optimised structural axes appear to take much longer to be initiated (Fig. 4.11), but once started, damage evolves rapidly to catastrophic failure. The critical level of structural degeneration and loss of stiffness is much lower compared to the $45°/90°$ samples. In the extremal case of the highly organised and optimised structures of the bovine 0° group already a damage level of $D = 0.1$ is critical.

Cotton et al. (2005) found that damage rate is a good predictor of fatigue life for human cortical bone exposed to pure tensile fatigue. Damage rate has been defined in their work as the linear fit to the damage curves within 10 % and 90 % of the specimens' lifetime. Therefore, damage rate has been determined as constant and early damage in the inital transient has been neglected. Ganguly et al. (2004) modelled the reduction in secant modulus during compression fatigue loading of bovine cancellous bone as a function of the maximum strain. They approximated upper and lower bounds for this reduction within normalised stress ranges. It was also suggested that damage is governed by maximum strain and the relationships can be determined with monotonic compression tests, whereas the secondary residual strain accumulation rate (stage II) is governed by the normalised

stress. In this work, the evolution of the residual (and maximum) strains during stage II and damage propagation were approximated as functions of normalised stress. Damage curves were approximated with quadratic fits for the whole course of each specimens' lifetime. Hence, also the initial damage processes were included in the analysis. The main advantage of this approach is that only one parameter (σ/E_0) is needed for the analysis of the deformation and damage process. One weakness of this method is obviously the magnification of any inconsistency of the variables through the integration process. Therefore, well-defined structural responses, as bovine 0°, human 0° and 90° specimens supplied, result in reasonable damage curves, whereas data from the 45° specimens, which exhibit a rather random behaviour with respect to damage acceleration, as discussed above, are only restrictedly suitable for damage predictions. In analogy to (Cotton et al., 2005) one variable for the evolution of damage - in this study acceleration - was found to strongly correlate to the number of cycles to failure. This holds irrespectively of site and species if the samples were loaded along the main physiological axis. Therefore, damage acceleration may be a very good predictor for lifetime, even if there will be hardly a chance to determine this factor in clinical praxis. This relationship may be more valuable for the (numerical) modeling of the fatigue behaviour of cancellous bone and theoretical analyses of the damage process.

As the critical level of stiffness loss was found to be different between the groups also the definition of the damage criterion with a 10 percent reduction in stiffness is somehow arbitrary. Nevertheless, a common measure for failure was applied in this study in order to enable a direct comparison with literature data. Specimens were loaded up to a fixed integral strain level to make post analysis of the structures' architecture possible. That's why the catastrophic failure cycle was not available. Furthermore, sensitivity analyses were conducted with different failure criteria: $D = 0.25$ (25 % reduction in E_{sec}), $D = 0.50$ and end of stage II. Results were similar to the obtained findings with $D = 0.10$, but with weaker correlations concerning each of the relationships.

Damage Mechanisms

The appearance of (surface) damage in cancellous bone was analysed in this study at different scale levels. The main goal was to identify methods for an analysis and to show the underlying damage mechanisms.This study does not claim a rigorous statistically verified analysis of these principles. This lies beyond the scope of this survey and is a field of further research.

The optical deformation measurement system used in this study was found to be capable to analyse strains on the specimen as well as the trabecula level. Even if some researchers applied optical deformation measurements on biological tissues - for example pattern recognition algorithms to track the motion of a random speckle pattern (Sanghavi et al., 2004) or optical strain measurement method (microdisplacements) (Kim et al., 2005) - the application to trabecular bone as well as the analysis of strains at various scales, from specimen to trabeculae level, is novel and shows the potential of these measurements. E.g. through a rigorous statistical analysis of trabeculae strain evolution essential information for precise models of damage in cancellous bone may be provides, which can be used for the increasingly used micro-CT-based finite element computations and may also contribute largely to crack growth models necessary for both, remodeling and damage, respectively. Due to the highly inhomogeneous (apparent) surface of the specimens analysis was in most cases restricted to two dimensions. The influence of the third deformational component was minimised by aligning the object with the analysis plane. Therefore, its contribution may be negligible. The character of the optical system restricts the measurement of strains to the surface of the specimen. Therefore, some deformational components may be included in the analysis of whole surface strains, which originate from deformations at sectioned trabeculae (through the preparation process), not representing the precise structural response. Strain magnitudes at the apparent level are therefore always afflicted with some degree of uncertainty. This does not hold for the analyses of trabeculae deformations. In these cases, trabeculae in the volume (second or third row) of the specimen were monitored. Absolute strain values at the trabecula level are therefore much more accurately

comparable to the apparent specimen level. Nevertheless, surface strain data is found to be very useful in order to explain the evolution of overall damage in the specimen and, as damage is supposed to initiate on the surface of the structure, to detect regions of damage initiation and propagation.

Besides the experimental investigation of the feasibility of these kinds of measurements also principle damage mechanisms could be obtained. Damage was found to appear very localised within cancellous bone specimens under monotonic and cyclic loading. Thus, strain localisations in trabecular bone, exposed to monotonic compression, were found at very early stages of the experiment, although the stress − strain curve indicates strictly linear elastic behavior. Comparable results were obtained with numerical studies, which demonstrated that damage is already visible below apparent compressive yield strain and local tissue yielding initiates at low apparent stress levels (Nagaraja et al., 2005; Morgan et al., 2005). Taken together, the results do reject the assumption of a linear elastic regime in cancellous bone which may result from pure bending deformation modes of the structural elements. Deformations in trabecular bone may therefore, even at low magnitude, localise and in consequence be coupled with damage. Interestingly, local strain concentrations could be detected in the region of later macroscopic damage initiation at very low apparent stress levels (Fig. 4.3). Therefore, flaws (which may also be unfavorable structural elements) are supposed to be pre-existing and if so may also be determined as a measure for bone quality in further studies.

Cyclic loading of trabecular bone results in highly non-uniform deformations. Analysing the integral material behaviour, damage appears in the form of increasing residual strains, often referred to as cyclic creep, an increasing hysteresis area and a decrease in secant modulus. The quantitative measures for these values depend highly on the trabecular architecture. These effects are linked to several (local) damage mechanisms. Singular cell deformations, resulting in bending of trabeculae, are observed within the first few cycles. In combination with the non-uniform loading situation at the single trabecula level (Fig. 5.3) struts fail even at low fractions of the overall lifetime (Fig. 4.24). Therefore, trabeculae are subsequently removed from the load-bearing part of the structure. This is

visible from the appearance of strain 'hot spots' across the specimens' surface. This supports the results from Keaveny et al. (1994) that damaged trabecular bone may be stress protected by redistributing stress to undamaged regions. A critical density of local damage may cause a large increase in crack growth rate, failure of whole trabeculae (initiation of the fracture line) and successive failure of the whole structure in a relatively narrow failure line across the specimen (Fig. 4.18, 4.19). Damage of single trabeculae appears in form of very localised strains, which are linked to microcrack initiation and propagation. As microcracks progress and trabeculae fail, respectively, residual strains accumulate and the secant modulus decreases. Therefore, the observed cyclic creep effect is a result of (microcrack) damage. Friction along the cracks' surfaces may appear in the broadened hysteresis loops. The highly reduced lifetimes of non-physiological loaded specimens are supposed to be a result of architecturally induced stress concentrations, which result in an acceleration of the above mentioned damage mechanism.

Usually studies on trabecular bone exhibit a large scatter in results, for which the heterogeneity of local deformations across the specimen might be an explanation. As this inhomogeneity is (without further refined analyses of the structure) a stochastic value for the bone sample, an adequate specimen size has to be chosen in order to average this effect. But as size is limited (donor bone size, homogeneity of local structure) a decrease in scatter can only be gained with more detailed information.

As deformations and damage appear very localised in trabecular bone structures, in-

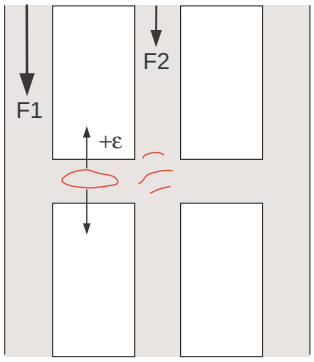

Figure 5.3: Schematic structural cell deformation

tegral approaches may lead to a high amount of uncertainties in deformation and fracture predictability. This may be even more pronounced as structural inhomogeneity increases as it appears in osteoporotic structures. The accumulation of residual strains may be the result of microcracking of individual trabeculae. In order to give more accurate quantitative measures specimen size, tissue quality and, as damage appears local, local structural information should be included in the standard procedures.

5.3 Lifetimes

A traditional approach to lifetime analysis is to establish S-N or lifetime curves. Relating the maximum stress magnitude to the number of cycles to failure for the groups in this work did not result in useful correlations (Fig. 4.29). In accordance to what has been shown in the literature for bovine tibial (Bowman et al., 1998; Moore et al., 2004) and human vertebral bone (Haddock et al., 2004; Rapillard et al., 2006), single power-law relationships could be established for each group by applying a normalisation of the load with the initial modulus of each specimen.

Lifetimes with respect to a normalised load σ/E_0 varied to a large degree between the groups. The group with the highest initial stiffness (bovine 0°) revealed the best performance, whereas in comparison human bone specimens displayed reduced initial stiffness and reduced lifetimes. Non-physiological (off-axis) load application was correlated with a decrease in fatigue strength for both bovine and human bone, respectively. Lifetimes decreased with decreasing mean initial stiffness of the groups. Therefore, bovine specimens performed superior to human specimens. Among human samples femoral bone showed the highest fatigue strength. It should be noted that almost no differences in fatigue lifetime were observed between the human 45° and 90° group. In both cases, the trabecular structure is not optimised for the applied loading. This can result either in shear stress concentration at the strut joints or in failure of the weak transversely oriented trabeculae, also the initial stiffness of both groups is comparable. Similar behaviour has been reported on anisotropic fibre reinforced composites (Hertzberg, 1995), where strength reduced dras-

tically for changes in orientation close to 0° but was similar at 45° and 90°. Therefore, in analogy to engineering methods in composite materials, detailed information about the local bone quality and structure is essential for an improved risk of failure estimation of cancellous bone.

The remarkably higher lifetimes observed for the bovine vertebral 0° groups may be explained by the different architectural structure of this high dense bone type. The trabecular structure is organised in a plate-like manner, aligned with the main loading (0°) direction, whereas in the directions normal to the load axis strut-like elements can be found (Fig. 2.4). In the bovine vertebral 90° group the latter elements are aligned with the integral stress axis. Therefore, lifetimes decrease, but at lower levels the decrease is less pronounced. One explanation may be the combination of the short buckling length of the struts and the rather stiff "floor" plates. While at high load levels struts fail in compression and initiate macroscopic failure, lower stress levels result in a more elastic type of deformation, mainly causing fatigue in the plates. Furthermore, the species-dependent differences may not only be a result of differing architectural structures, but also of the differing donor age. All bovine bones were obtained from young cows (the age of the cows matched the age of a 20-year-old man/woman) with an appropriate bone quality, whereas human donors were middle- to old-aged where quality may be decreased.

The lifetime curves (σ/E_0 vs. N_f) do not exhibit a common endurance limit. In the literature, an endurance limit of approx. $\sigma/E_0 = 0.0035$ has been suggested for cancellous bone, which has been derived from finite element studies (Guo et al., 1994) and low cycle fatigue tests (Moore and Gibson, 2003b). Ganguly et al. (2004) determined a theoretical endurance limit for bovine bone between $\sigma/E_0 = 0.0024 - 0.0032$. While this limit may exist for the bovine data, human specimens failed at much lower load values (e.g. 0.0017 for a human 45° specimen), so the endurance limit is supposed to be smaller for human bone. The in-vivo apparent strain of human vertebral trabecular bone during moderate activity has been estimated to be about 2300 μm (Kopperdahl and Keaveny, 1998). Therefore, the fatigue data of this study does also, at least partly (as the literature deals with on-axis strains), map physiological load magnitudes. Of course, no biological reaction in terms of

remodeling processes is included in the in-vitro experiments. However, the influence of these repair/optimisation processes on the fatigue behaviour remains still controversial in the literature. Beside the well-known repair function the influence of resorption cavities preceding repair may contribute in a negative manner to the structural integrity (Hernandez et al., 2006). So it remains unclear if the experimental fatigue data matches a 'safe engineering design' or not.

As the initial modulus plays a major role in establishing lifetime curves for spongeous structures, the question arises if this structural parameter is sensitive enough to represent the initial mechanical potential of the structure with regard to cyclic loading. The lifetime curves exhibited large differences between the groups, even if the initial modulus was included. Likewise, two groups with similar initial modulus (bovine vertebral 90° and human femoral 0°) behaved differently. Therefore, initial modulus seems to be a good estimator for the fatigue properties of cancellous bone, as correlations for the lifetime curves were found to be very strong, but does fail to fully describe the mechanics of the structure. Haddock et al. (2004) compared data from bovine tibial cancellous and human vertebral cancellous bone. They suggest that one single lifetime curve works well for the combined set of data if the monotonic yield strain is taken into account, which is slightly higher for bovine cancellous bone. The applied load is therefore normalised to a percentage applied strain with respect to yield strain. Fig. 5.4 shows the merged specimen data for five groups of cancellous bone. For the static yield strain the yield strains at the 0.2% offset ($\varepsilon_{0.2}$) from few monotonic compression tests were taken. The overall fit reveals a rather strong correlation of $R^2 = 0.90$, but of course in this approach the information of the lifetime coefficient (b) is missing which decreases the accuracy at higher lifetimes/lower applied loads. Thus, this approach does not seem usefully contribute to the discussion. Further attempts to improve the inter- and intra- groupwise scatter with density (BMD) values did not succeed.

The lifetime data has been investigated in order to reveal differences in the low-cycle (LCF) and high-cycle regime (HCF), respectively, in order to obtain a combined Basquin-Coffin-Manson relationship. Fig. 5.5 shows best fit results on the data from three groups.

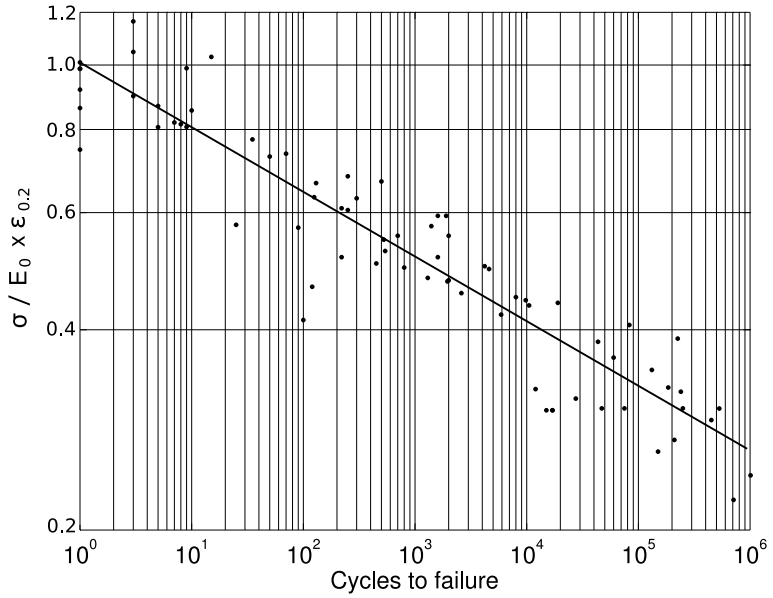

Figure 5.4: Merging specimens from different groups (bovine vertebral $0°$, $90°$ *and human vertebral* $0°$, $90°$ *and human femoral* $0°$ *together by normalisation with monotonic yield strain.*

This means, the boundary between LCF and HCF has been shifted until the specimens of one group were divided in two subgroups with best linear fits in the log-log plot of the lifetime diagram. The relationships are rather poor due to the relatively low amount of specimens within each subgroup analysed. Nevertheless, the transition between the two deformation modes is rather well-defined. For the human vertebral groups a normalised stress level of approximately 0.0045 seems to cause a change in mechanism, whereas in the bovine groups a value of approximately $0.007 - 0.0075$ was obtained. Surface strain analysis on the bovine specimens revealed a normalised stress threshold of the same magnitude, where areas exhibiting certain strain values did disappear (Fig. 4.22). Furthermore, in the analysis of the deformation rates during stage II (saturation regime) corresponding normalised stress values were found for human and bovine specimens, where deformation rates were independent of groups. Taking these results together, a change in the damage mechanism can be obtained at approximately $\sigma/E_0 = 0.0075$ for bovine vertebral bone and $\sigma/E_0 = 0.004 - 0.0045$ for human vertebral bone.

The real effect of the axis of loading with respect to the main physiological axis on

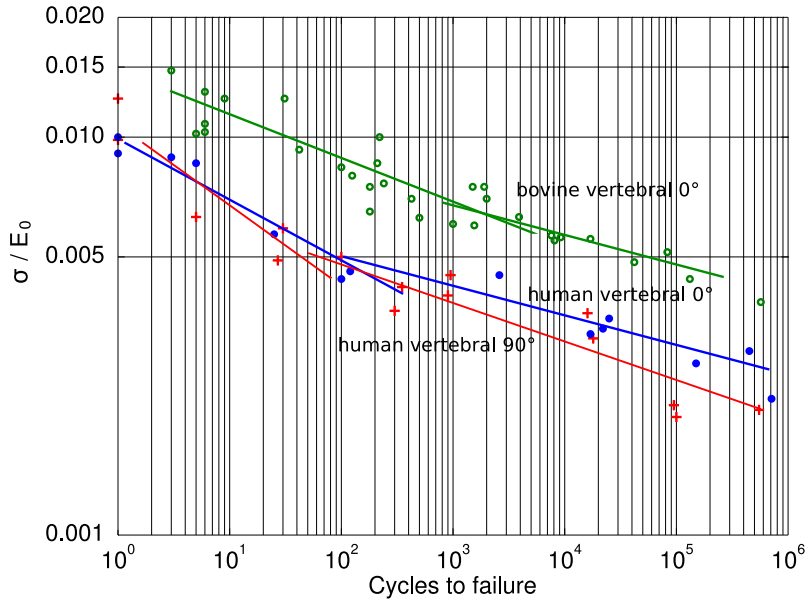

Figure 5.5: Separating the groups bovine vertebral 0° (BV0), bovine vertebral 90° (BV90), human vertebral 0° (HV0) and human vertebral 0° (HV90) with respect to low cycle and high cycle fatigue regions.

the fatigue behaviour is blured in the normalised (σ/E_0) lifetime data. In order to clearly point out the consequences of non-physiological loading on fatigue lifetime the data is normalised by the mean modulus of each group (Fig. 4.31). The so spread lifetime curves are further processed to get an engineering "design diagram". Load values are taken at certain cycle numbers and plotted as a function of the specimen orientation angle (with respect to the physiological bone axis). This modified form of a S-N diagram with the introduction of an anisotropy-based pseudo stress clearly reveals the magnitude of the load-bearing capability with respect to anisotropy. Even small deviations from the physiological axis result in highly reduced bearable stress. Therefore, the oriented, optimised cancellous bone structure is highly sensitive to changes in the load directions. This effect may have direct clinical implications because structural implants in most cases alter local loading conditions in terms of induced stresses acting in non-physiological load axes.

Furthermore, it should be mentioned that the relationships between the applied load and cycles to failure showed comparably good correlations in the off-axis groups which indicates that damage occurs in a reproducible manner. This confirms the assumption that

a damage mechanism related to microstructural properties in terms of microcrack initiation and propagation is operative. The architectural differences cause local stresses which may shorten and thus accelerate the initiation and propagation phases.

Comparing our data for the same bone type (human vertebrae 0°) with the literature (Haddock et al., 2004) showed a good agreement (Fig. 4.30). Another study on human vertebral cancellous bone, cored along the main physiological axis (Rapillard et al., 2006) observed similar trends, but slightly different values (see Table 5.1). Earlier studies did not include embedding of the end surfaces and reported a much higher intercept on the load axis (Michel et al., 1993). Even if the studies shown in Table 5.1 used some similar experimental techniques, direct comparison is limited due to variations concerning the experimental boundary conditions, i.e. surrounding media, temperature, specimen fixing, strain rate etc. In both cases, specimens were smaller than those used in this study (diameter 8.3 mm and 8.0 mm compared to 11.2 mm), also boundary conditions (embedding) were applied in a different manner. Additionally, Rapillard and co-workers used a tempered fluid bath, whereas Haddock et al. tested at room temperature and samples were kept wet with physiological solution. The concluding evaluation, where the differences originate, remains unclear, but may be a combination of experimental boundary conditions and of course donor-specific differences.

5.4 Age Effects

The data of the cyclic deformation experiments was analysed with respect to donor age in order to reveal the influence of age on the fatigue properties of cancellous bone. The

Table 5.1: Coefficients for lifetime curves Equation 4.14.

	a	b
This work	0.0098	-0.109
Haddock et al. (2004)	0.0093	−0.1179
Rapillard et al. (2006)	0.0121	−0.0808

initial secant modulus of the specimens was found to be highly dependent on donor age. The modulus decrease was much more pronounced in the off-axis groups, this increasing mechanical anisotropy indicates also an increased degree of structural anisotropy with age, findings that correspond with data from Nicholson et al. (1997), who showed that there is relative conservation of stiffness in the axial direction compared with the transverse direction.

Initial stiffness is used as a normalisation factor in fatigue analysis of cancellous bone (Bowman et al., 1998; Moore and Gibson, 2003b) and therefore the corresponding relationships are directly related to its magnitude. Consequently, fatigue lifetime is also highly dependent on age and decreases more pronouncedly in the off-axis orientations. This implies that old bone is much more sensitive to (cyclic) failure loads in general but particularly to loads which are not coincident with the physiological main axis. Therefore, for instance the right implant anchorage (which may result in unphysiological local stress) is much more important in older bone. Also changes in the physiological load flow through a change in habitual tasks increase the risk of fatigue fractures for elderly people. Furthermore, these findings suggest that the integrally measured value for bone strength in current routine clinical practice, BMD (Friedman, 2006), may be of decreased predective value concerning older bone as the structural anisotropy becomes increasingly important.

While for human cortical bone modulus degradation profiles were found to be different regarding younger and older bones (Diab et al., 2005), the data in this study did not reveal an effect of age on damage evolution. Additionally, age did not show any further influence on lifetime curves and deformations at failure once initial stiffness has been included. As old bone is known to have reduced quality e.g. in terms of increased microdamage (Schaffler et al., 1995), one could expect older bones to reveal a tendency for reduced lifetimes. At least in the range of the data presented there is no evidence for this, once initial stiffness is included. There may be different explanations for these findings. Firstly, initial stiffness is a highly sensitive parameter of tissue quality, which has also explanatory power for cyclic loadings; secondly, initial (micro-)damage may not be critical for fatigue failure; and thirdly, the range of donor age is too limited to reveal significant

results. O'Brien et al. (2003) found for bovine cortical bone that bone fails by extensive propagation of a few cracks, not the proliferation and coalescence of microcracks, and therefore initial microdamage is not a significant factor in fatigue failure, which may also be true for cancellous bone. Additional microdamage quantification and analysis is needed to confirm this assumption. It has been suggested that damage rates increase with age for cortical bone (Cotton et al., 2005). Whether this is also true for cancellous bone could not be proved with this study due to the limited amount of data.

The deformation mechanism for static failure is reported to depend on the cancellous bone density and therefore age. At lower density values elastic buckling dominates, whereas at higher density levels a lowered slenderness ratio of the trabeculae causes failure by progressive microfracturing (Townsend et al., 1975; Gibson and Ashby, 1997). While these findings hold for static loadings, cyclic loadings much below the static failure values did not result in these critical deformations and may therefore not so strongly depend on the slenderness ratio, which could explain the similarity of the deformation behaviour.

Even if the age range of the donors is limited in this study, it represents the age-group, where bone quality becomes an important issue. The limited number of data points does not allow for an exact determination of the relationships between initial modulus and age, but nevertheless the trends can be shown and are valid.

Concluding, initial modulus and therefore lifetimes were found to be highly dependent on age. The decrease in both with increasing age was much more pronounced in specimens which were not aligned with the main physiological axis.

5.5 Clinical Relevance

The high dependency of fatigue lifetime on the axis of loading may have direct clinical consequences. For instance, fracture treatment through implants should preserve the physiological load axis. In the simple example of a pedicle screw placement in a vertebral body (Fig. 1.2) screw insertion in strictly vertical direction may lead to highest stability in the

long run. In general, implant anchorage should lead to mostly on-axis loading and regions of low structural anisotropy should be preferred. But the results do also indicate that above a certain deviation from the main axis (Fig. 4.32) fatigue strength is almost equal and therefore, if alignment with the physiological direction can not be achieved, other factors may be more important for the choice of implant anchorage. The need for a inclusion of structural information in the determination of the mechanical performance of cancellous bone has been stressed by recent studies (Ulrich et al., 1999; Stauber et al., 2006; Matsuura et al., 2007). This study does support this concept with mechanical data showing the large influence of the axis of loading on the fatigue behaviour of cancellous bone. So, especially for the case of osteoporosis, which incorporates an increased structural anisotropy, it appears to be essential to determine morphological parameters which enhance the predictability of clinical diagnosis. It could be shown in this work that BMD could predict the initial stiffness at least to some degree, when specimens are loaded along their structural main axis, but fails to assess the behaviour of non-axis loaded specimens. Bone Mineral Density alone is therefore not suitable to predict bone strength in trauma treatment situations and provides only weak predictability for the fracture risk. The development of techniques to improve the non-invasive estimation of density and structure of trabecular bone, e.g. quantitative magnetic resonance imaging- (MRI-)based (Lammentausta et al., 2006), are essential.

6 Conclusion

This study shows for the first time the relationship between the cyclic deformation and fatigue behaviour and axis of loading (anisotropy), site, species and age of cancellous bone. Furthermore, damage mechanisms were derived from novel measurement methods for strain analysis on the apparent and tissue level. For this reason, cyclic compression tests were performed on different groups of cancellous bone varying in specimen orientation angle with respect to the physiological bone axis, site and species. Surface strains were analysed by means of optical deformation analysis.

While the characteristics of cyclic deformation were found to be similar for all groups, large deviations were observed for the fatigue lifetimes. Bovine specimens did reveal higher lifetimes compared to human samples and lifetimes decreased with increasing deviation of the specimens' axis from the physiological bone axis. Already small deviations cause a large reduction, whereas deviations above 45° result in a similar fatigue behaviour. Strains at failure were found to be dependent on specimen orientation (with respect to the physiological bone axis). The whole cyclic deformation process as well as damage evolution until defined failure could be shown to be a function of normalised stress and group. The corresponding functional relationships were derived. Damage acceleration was found to be constant for all specimens and different damage mechanisms are acting for on-axis and off-axis groups. Likewise, load thresholds were found, at which damage mechanisms change from low-cycle to high-cycle fatigue. Age appeared to have a large influence on the initial modulus of the specimens. Deformation analysis on the apparent and the trabecular level could be linked to macroscopic damage and microdamage was found to contribute to residual strain accumulation. Concluding, the axis of loading appears to

contribute dominantly to fatigue and cyclic deformation, which may be even more pronounced in cases of increased anisotropy (Osteoporosis). Therefore, local morphological information has to be included in risk of fracture predictions in order to achieve a higher reliability.

Bibliography

Ashman, R. B., Rho, J. Y., 1988. Elastic modulus of trabecular bone material. J Biomech 21 (3), 177–181.

Augat, P., Link, T., Lang, T. F., Lin, J. C., Majumdar, S., Genant, H. K., 1998. Anisotropy of the elastic modulus of trabecular bone specimens from different anatomical locations. Med Eng Phys 20 (2), 124–131.

Basquin, O., 1910. The exponential law of endurance tests. Proceedings of the American Society for Testing and Materials 10, 625–30.

Bauer, T. W., Schils, J., 1999. The pathology of total joint arthroplasty.ii. mechanisms of implant failure. Skeletal Radiol 28 (9), 483–497.

Bayraktar, H. H., Gupta, A., Kwon, R. Y., Papadopoulos, P., Keaveny, T. M., 2004. The modified super-ellipsoid yield criterion for human trabecular bone. J Biomech Eng 126 (6), 677–684.

Borgström, F., Sobocki, P., Ström, O., Jönsson, B., 2007. The societal burden of osteoporosis in sweden. Bone 40 (6), 1602–1609.

Bowman, S. M., Guo, X. E., Cheng, D. W., Keaveny, T. M., Gibson, L. J., Hayes, W. C., McMahon, T. A., 1998. Creep contributes to the fatigue behavior of bovine trabecular bone. J Biomech Eng 120 (5), 647–654.

Bredbenner, T., 2003. Damage modelling of vertebral trabecular bone. Phd thesis, Mechanical & Aerospace Engineering , Case Western Research University, Cleveland, OH.

Bredbenner, T. L., Davy, D. T., 2006. The effect of damage on the viscoelastic behavior of human vertebral trabecular bone. J Biomech Eng 128 (4), 473–480.

Brunet-Imbault, B., Lemineur, G., Chappard, C., Harba, R., Benhamou, C. L., 2005. A new anisotropy index on trabecular bone radiographic images using the fast fourier transform. BMC Med Imaging 5 (1), 4.

Burr, D. B., Forwood, M. R., Fyhrie, D. P., Martin, R. B., Schaffler, M. B., Turner, C. H., 1997. Bone microdamage and skeletal fragility in osteoporotic and stress fractures. J Bone Miner Res 12 (1), 6–15.

Burr, D. B., Martin, R. B., Schaffler, M. B., Radin, E. L., 1985. Bone remodeling in response to in vivo fatigue microdamage. J Biomech 18 (3), 189–200.

Burr, D. B., Turner, C. H., Naick, P., Forwood, M. R., Ambrosius, W., Hasan, M. S., Pidaparti, R., 1998. Does microdamage accumulation affect the mechanical properties of bone? J Biomech 31 (4), 337–345.

Carter, D. R., Caler, W. E., Spengler, D. M., Frankel, V. H., 1981. Uniaxial fatigue of human cortical bone. the influence of tissue physical characteristics. J Biomech 14 (7), 461–470.

Carter, D. R., Hayes, W. C., 1977. The compressive behavior of bone as a two-phase porous structure. J Bone Joint Surg Am 59 (7), 954–962.

Choi, K., Goldstein, S. A., 1992. A comparison of the fatigue behavior of human trabecular and cortical bone tissue. J Biomech 25 (12), 1371–1381.

Coffin, L., 1954. A study of the effects of cyclic thermal stresses on a ductile metal. Transactions of the American Society of Mechanical Engineers 76, 931–940.

Compston, J., 2006. Bone quality: what is it and how is it measured? Arq Bras Endocrinol Metabol 50 (4), 579–585.

Cotton, J. R., Winwood, K., Zioupos, P., Taylor, M., 2005. Damage rate is a predictor of fatigue life and creep strain rate in tensile fatigue of human cortical bone samples. J Biomech Eng 127 (2), 213–219.

Cowin, S., 2001. Bone mechanics handbook. CRC Press Inc., Boca Raton.

Cowin, S. C., 1985. The relationship between the elasticity tensor and the fabric tensor. Mechanics of Materials 4 (2), 137–147.

Cruz-Orive, L., Karlsson, L., Larsen, S., Wainschtein, F., 1992. Characterizing anisotropy: a new concept. Micron and Microscopica Acta 23, 75–76.

Dendorfer, S., Maier, H. J., Hammer, J., 2005. Strain evolution during compressive fatigue of bovine cancellous bone. IFMBE Proceedings of the 3rd European Medical & Biological Engineering Conference, Prague, Czech Vol. 11(1).

Diab, T., Sit, S., Kim, D., Rho, J., Vashishth, D., 2005. Age-dependent fatigue behaviour of human cortical bone. Eur J Morphol 42 (1-2), 53–59.

Ding, M., Odgaard, A., Linde, F., Hvid, I., 2002. Age-related variations in the microstructure of human tibial cancellous bone. J Orthop Res 20 (3), 615–621.

Ebbesen, E. N., Thomsen, J. S., Beck-Nielsen, H., Nepper-Rasmussen, H. J., Mosekilde, L., 1999. Age- and gender-related differences in vertebral bone mass, density, and strength. J Bone Miner Res 14 (8), 1394–1403.

Englert, C., Angele, P., Fierlbeck, J., Dendorfer, S., Schubert, T., Müller, R., Lienhard, S., Zellner, J., Nerlich, M., Neumann, C., 2007. [conductive bone substitute material with variable antibiotic delivery]. Unfallchirurg 110 (5), 408–413.

Fleck, C., Eifler, D., 2003. Deformation behaviour and damage accumulation of cortical bone specimens from the equine tibia under cyclic loading. J Biomech 36 (2), 179–189.

Ford, C. M., Keaveny, T. M., 1996. The dependence of shear failure properties of trabecular bone on apparent density and trabecular orientation. J Biomech 29 (10), 1309–1317.

Fratzl, P., Gupta, H. S., Paschalis, E. P., Roschger, P., 2004. Structure and mechanical quality of the collagen-mineral nano-composite in bone. J. Mater. Chem. 14, 2115–2123.

Friedman, A. W., 2006. Important determinants of bone strength: beyond bone mineral density. J Clin Rheumatol 12 (2), 70–77.

Frost, H. M., 1987. Bone "mass" and the "mechanostat": a proposal. Anat Rec 219 (1), 1–9.

Frost, H. M., 2003. Bone's mechanostat: a 2003 update. Anat Rec 275A (2), 1081–1101.

Fung, Y., 1993. Biomechanics: mechanical properties of living tissues. Springer Verlag, New-York.

Fyhrie, D. P., Schaffler, M. B., 1995. The adaptation of bone apparent density to applied load. J Biomech 28 (2), 135–146.

Ganguly, P., Moore, T. L., Gibson, L. J., 2004. A phenomenological model for predicting fatigue life in bovine trabecular bone. J Biomech Eng 126 (3), 330–339.

George, W. T., Vashishth, D., 2006. Susceptibility of aging human bone to mixed-mode fracture increases bone fragility. Bone 38 (1), 105–111.

Gibson, L. J., 2005. Biomechanics of cellular solids. J Biomech 38 (3), 377–399.

Gibson, L. J., Ashby, M. F., 1997. Cellular solids: structure & properties. Cambridge University Press, Cambridge 2nd.

Goldstein, S. A., Wilson, D. L., Sonstegard, D. A., Matthews, L. S., 1983. The mechanical properties of human tibial trabecular bone as a function of metaphyseal location. J Biomech 16 (12), 965–969.

Guo, X. E., McMahon, T. A., Keaveny, T. M., Hayes, W. C., Gibson, L. J., 1994. Finite element modeling of damage accumulation in trabecular bone under cyclic loading. J Biomech 27 (2), 145–155.

Haddock, S. M., Yeh, O. C., Mummaneni, P. V., Rosenberg, W. S., Keaveny, T. M., 2004. Similarity in the fatigue behavior of trabecular bone across site and species. J Biomech 37 (2), 181–187.

Haeussler, B., Gothe, H., Goel, D., Glaeske, G., Pientka, L., Felsenberg, D., 2007. Epidemiology, treatment and costs of osteoporosis in germany–the bone eva study. Osteoporos Int 18 (1), 77–84.

Harrigan, T. P., Jasty, M., Mann, R. W., Harris, W. H., 1988. Limitations of the continuum assumption in cancellous bone. J Biomech 21 (4), 269–275.

Harrigan, T. P., Mann, R. W., 1984. Characterization of microstructural anisotropy in orthotropic materials using a second order rank tensor. Journal of Materials Science 19, 761–767.

Hazenberg, J., Taylor, D., Lee, T., 2007. The role of osteocytes and bone microstructure in preventing osteoporotic fractures. Osteoporos Int 18 (1), 1–8.

Hernandez, C. J., Gupta, A., Keaveny, T. M., 2006. A biomechanical analysis of the effects of resorption cavities on cancellous bone strength. J Bone Miner Res 21 (8), 1248–1255.

Hertzberg, R., 1995. Deformation and fracture mechanics of engineering materials. John Wiley and Sons, Inc.

Hodgskinson, R., Currey, J. D., 1990. The effect of variation in structure on the young's modulus of cancellous bone: a comparison of human and non-human material. Proc Inst Mech Eng 204 (2), 115–121.

Hoffler, C. E., Moore, K. E., Kozloff, K., Zysset, P. K., Goldstein, S. A., 2000. Age, gender, and bone lamellae elastic moduli. J Orthop Res 18 (3), 432–437.

Homminga, J., Van-Rietbergen, B., Lochmueller, E.-M., Weinans, H., Eckstein, F., Huiskes, R., 2004. The osteoporotic vertebral structure is well adapted to the loads of daily life, but not to infrequent "error" loads. Bone 34 (3), 510–516.

Jess, W., 1990. The skeletal tissue. in book: Cell and tissue biology: A textbook of histology, edited by: Weiss, l. Urban & Schwarzenberg, Baltimore.

Jirasek, M., Bazant, Z. P., 2002. Inelastic analysis of structures. John Wiley and Sons, Ltd, Chinchester, England.

Kanis, J. A., Johnell, O., Oden, A., Borgstroem, F., Zethraeus, N., Laet, C. D., Jonsson, B., 2004. The risk and burden of vertebral fractures in sweden. Osteoporos Int 15 (1), 20–26.

Kaplan, S. J., Hayes, W. C., Stone, J. L., Beaupre, G. S., 1985. Tensile strength of bovine trabecular bone. J Biomech 18 (9), 723–727.

Keaveny, T. M., Borchers, R. E., Gibson, L. J., Hayes, W. C., 1993. Theoretical analysis of the experimental artifact in trabecular bone compressive modulus. J Biomech 26 (4-5), 599–607.

Keaveny, T. M., Morgan, E. F., Niebur, G. L., Yeh, O. C., 2001. Biomechanics of trabecular bone. Annu Rev Biomed Eng 3, 307–333.

Keaveny, T. M., Pinilla, T. P., Crawford, R. P., Kopperdahl, D. L., Lou, A., 1997. Systematic and random errors in compression testing of trabecular bone. J Orthop Res 15 (1), 101–110.

Keaveny, T. M., Wachtel, E. F., Guo, X. E., Hayes, W. C., 1994. Mechanical behavior of damaged trabecular bone. J Biomech 27 (11), 1309–1318.

Keaveny, T. M., Wachtel, E. F., Zadesky, S. P., Arramon, Y. P., 1999. Application of the tsai-wu quadratic multiaxial failure criterion to bovine trabecular bone. J Biomech Eng 121 (1), 99–107.

Kim, D. G., Brunski, I. B., Nicolella, D. P., 2005. Microstrain fields for cortical bone in uniaxial tension: optical analysis method. Proc Inst Mech Eng 219 (2), 119–128.

King, A. I., Evans, F. G., 1967. Analysis of fatigue strength of human compact bone by the weibull method.

Kopperdahl, D. L., Keaveny, T. M., 1998. Yield strain behavior of trabecular bone. J Biomech 31 (7), 601–608.

Lammentausta, E., Hakulinen, M. A., Jurvelin, J. S., Nieminen, M. T., 2006. Prediction of mechanical properties of trabecular bone using quantitative mri. Phys Med Biol 51 (23), 6187–6198.

LeBlanc, A. D., Spector, E. R., Evans, H. J., Sibonga, J. D., 2007. Skeletal responses to space flight and the bed rest analog: a review. J Musculoskelet Neuronal Interact 7 (1), 33–47.

Lee, T. C., Staines, A., Taylor, D., 2002. Bone adaptation to load: microdamage as a stimulus for bone remodelling. J Anat 201 (6), 437–446.

Levenston, M. E., Carter, D. R., 1998. An energy dissipation-based model for damage stimulated bone adaptation. J Biomech 31 (7), 579–586.

Li, J. P., Li, S. H., Van Blitterswijk, C. A., de Groot, K., 2006. Cancellous bone from porous ti6al4v by multiple coating technique. Journal of Materials Science: Materials in Medicine 17 (2), 179–185.

Linde, F., Hvid, I., 1989. The effect of constraint on the mechanical behaviour of trabecular bone specimens. J Biomech 22 (5), 485–490.

Liu, X., Wang, X., Niebur, G. L., 2003. Effects of damage on the orthotropic material symmetry of bovine tibial trabecular bone. J Biomech 36 (12), 1753–1759.

Lotz, J. C., Hayes, W. C., 1990. The use of quantitative computed tomography to estimate risk of fracture of the hip from falls. J Bone Joint Surg Am 72 (5), 689–700.

Makiyama, A. M., Vajjhala, S., Gibson, L. J., 2002. Analysis of crack growth in a 3d voronoi structure: a model for fatigue in low density trabecular bone. J Biomech Eng 124 (5), 512–520.

Manson, S. S., 1954. Behaviour of materials under conditions of thermal stress. NACA TN 2933.

Martin, R. B., Burr, D. B., Sharkey, N. A., 1998. Skeletal tissue mechanics. Springer Verlag, New York.

Martin, R. B., Gibson, V. A., Stover, S. M., Gibeling, J. C., Griffin, L. V., 1997. Residual strength of equine bone is not reduced by intense fatigue loading: implications for stress fracture. J Biomech 30 (2), 109–14.

Matsuura, M., Eckstein, F., Lochmueller, E.-M., Zysset, P., 2007. The role of fabric in the quasi-static compressive mechanical properties of human trabecular bone from various anatomical locations. Biomech Model Mechanobiol Jan, in print.

McCalden, R. W., McGeough, J. A., Court-Brown, C. M., 1997. Age-related changes in the compressive strength of cancellous bone. the relative importance of changes in density and trabecular architecture. J Bone Joint Surg Am 79 (3), 421–427.

Michel, M. C., Guo, X. D., Gibson, L. J., McMahon, T. A., Hayes, W. C., 1993. Compressive fatigue behavior of bovine trabecular bone. J Biomech 26 (4-5), 453–463.

Mohsin, S., O'Brien, F. J., Lee, T. C., 2006. Osteonal crack barriers in ovine compact bone. J Anat 208 (1), 81–89.

Moore, T. L., Gibson, L. J., 2001. Modeling modulus reduction in bovine trabecular bone damaged in compression. J Biomech Eng 123 (6), 613–622.

Moore, T. L., Gibson, L. J., 2003a. Fatigue microdamage in bovine trabecular bone. J Biomech Eng 125 (6), 769–776.

Moore, T. L., Gibson, L. J., 2003b. Fatigue of bovine trabecular bone. J Biomech Eng 125 (6), 761–768.

Moore, T. L., O'Brien, F. J., Gibson, L. J., 2004. Creep does not contribute to fatigue in bovine trabecular bone. J Biomech Eng 126 (3), 321–329.

Morgan, E. F., Bayraktar, H. H., Keaveny, T. M., 2003. Trabecular bone modulus-density relationships depend on anatomic site. J Biomech 36 (7), 897–904.

Morgan, E. F., Yeh, O. C., Chang, W. C., Keaveny, T. M., 2001. Nonlinear behavior of trabecular bone at small strains. J Biomech Eng 123 (1), 1–9.

Morgan, E. F., Yeh, O. C., Keaveny, T. M., 2005. Damage in trabecular bone at small strains. Eur J Morphol 42 (1-2), 13–21.

Mosekilde, L., 1989. Sex differences in age-related loss of vertebral trabecular bone mass and structure–biomechanical consequences. Bone 10 (6), 425–432.

Mosekilde, L., 2000. Age-related changes in bone mass, structure, and strength–effects of loading. Z Rheumatol 59 Suppl 1, 1–9.

Mosekilde, L., Mosekilde, L., 1986. Normal vertebral body size and compressive strength: relations to age and to vertebral and iliac trabecular bone compressive strength. Bone 7 (3), 207–212.

Mugrabi, H., 1985. Disclocations in fatigue. Dislocations and properties of real materials, Book No. 323, The Institute of Metals, London, 244–261.

Mullender, M. G., Tan, S. D., Vico, L., Alexandre, C., Klein-Nulend, J., 2005. Differences in osteocyte density and bone histomorphometry between men and women and between healthy and osteoporotic subjects. Calcif Tissue Int 77 (5), 291–296.

Nagaraja, S., Couse, T. L., Guldberg, R. E., 2005. Trabecular bone microdamage and microstructural stresses under uniaxial compression. J Biomech 38 (4), 707–716.

Nagaraja, S., Lin, A. S. P., Guldberg, R. E., 2007. Age-related changes in trabecular bone microdamage initiation. Bone 40 (4), 973–980.

Nalla, R. K., Kinney, J. H., Ritchie, R. O., 2003. Mechanistic fracture criteria for the failure of human cortical bone. Nat Mater 2 (3), 164–168.

Nalla, R. K., Kruzic, J. J., Kinney, J. H., Ritchie, R. O., 2004. Effect of aging on the toughness of human cortical bone: evaluation by r-curves. Bone 35 (6), 1240–1246.

Nazarian, A., Muller, R., 2004. Time-lapsed microstructural imaging of bone failure behavior. J Biomech 37 (1), 55–65.

Nicholson, P. H., Cheng, X. G., Lowet, G., Boonen, S., Davie, M. W., Dequeker, J., der Perre, G. V., 1997. Structural and material mechanical properties of human vertebral cancellous bone. Med Eng Phys 19 (8), 729–737.

Niemeyer, P., Weinberg, A., Schmitt, H., Kreuz, P. C., Ewerbeck, V., Kasten, P., 2006. Stress fractures in the juvenile skeletal system. Int J Sports Med 27 (3), 242–249.

O'Brien, F. J., Taylor, D., Lee, T. C., 2003. Microcrack accumulation at different intervals during fatigue testing of compact bone. J Biomech 36 (7), 973–980.

Odgaard, A., Jensen, E. B., Gundersen, H. J., 1990. Estimation of structural anisotropy based on volume orientation. a new concept. J Microsc 157 (Pt 2), 149–162.

Ohrndorf, A., Krupp, U., Christ, H.-J., 2006. Metallic open-cell foams–a promising approach to fabricating good medical implants. Technol Health Care 14 (4-5), 201–208.

Penzkofer, R., 2005. Quantitative charakterisierung struktureller und experimenteller einflussgroessen auf das wechselverformungsverhalten von spongiosa. Diplomathesis, University of Applied Sciences Regensburg.

Prendergast, P. J., Taylor, D., 1994. Prediction of bone adaptation using damage accumulation. J Biomech 27 (8), 1067–1076.

Rajapakse, C. S., Thomsen, J. S., Espinoza Ortiz, J. S., Wimalawansa, S. J., Ebbesen, E. N., Mosekilde, L., Gunaratne, G. H., 2004. An expression relating breaking stress and density of trabecular bone. J Biomech 37 (8), 1241–1249.

Rapillard, L., Charlebois, M., Zysset, P. K., 2006. Compressive fatigue behavior of human vertebral trabecular bone. J Biomech 39 (11), 2133–2139.

Rice, J. C., Cowin, S. C., Bowman, J. A., 1987. On the dependence of the elasticity and strength of cancellous bone on apparent density. Journal of biomechanics 21 (2), 155–168.

Rohl, L., Larsen, E., Linde, F., Odgaard, A., Jorgensen, J., 1991. Tensile and compressive properties of cancellous bone. J Biomech 24 (12), 1143–1149.

Roux, W., 1895. Gesammelte abhandlungen ueber die entwicklungsmechanik der organismen. W. Engelmann, Leipzig.

Rubin, M. A., Jasiuk, I., Taylor, J., Rubin, J., Ganey, T., Apkarian, R. P., 2003. Tem analysis of the nanostructure of normal and osteoporotic human trabecular bone. Bone 33 (3), 270–282.

Sanghavi, P., Bose, D., Kerrigan, J., Madeley, N. J., Crandall, J., 2004. Non-contact strain measurement of biological tissue. Biomed Sci Instrum 40, 51–56.

Schaffler, M. B., Choi, K., Milgrom, C., 1995. Aging and matrix microdamage accumulation in human compact bone. Bone 17 (6), 521–525.

Schaffner, G., Guo, X.-D. E., Silva, M. J., J., G. L., 2000. Modelling fatigue damage accumulation in two-dimensional voronoi honeycombs. International Journal of Mechanical Sciences 42, 645–656.

Schijve, J., 2001. Fatigue of structures and materials. Kluwer Academic Publishers, Dordrecht, Nl.

Schuetz, W., 1996. A history of fatigue. Eng. Fracture Mechanics 54, 263–300.

Snyder, R. A., Koester, M. C., Dunn, W. R., 2006. Epidemiology of stress fractures. Clin Sports Med 25 (1), 37–52, viii.

Sobelman, O. S., Gibeling, J. C., Stover, S. M., Hazelwood, S. J., Yeh, O. C., Shelton, D. R., Martin, R. B., 2004. Do microcracks decrease or increase fatigue resistance in cortical bone? J Biomech 37 (9), 1295–1303.

Sormaala, M. J., Niva, M. H., Kiuru, M. J., Mattila, V. M., Pihlajamaeki, H. K., 2006. Bone stress injuries of the talus in military recruits. Bone 39 (1), 199–204.

Sowers, M. F., 2000. Lower peak bone mass and its decline. Baillieres Best Pract Res Clin Endocrinol Metab 14 (2), 317–329.

Stauber, M., Rapillard, L., van Lenthe, G. H., Zysset, P., Mueller, R., 2006. Importance of individual rods and plates in the assessment of bone quality and their contribution to bone stiffness. J Bone Miner Res 21 (4), 586–595.

Stone, J. L., Beaupre, G. S., Hayes, W. C., 1983. Multiaxial strength characteristics of trabecular bone. Journal of biomechanics 16 (9), 743–747.

Suresh, S., 1998. Fatigue of materials. University Press Cambridge 2nd.

Taylor, D., 1998. Fatigue of bone and bones: an analysis based on stressed volume. J Orthop Res 16 (2), 163–169.

Taylor, D., Hazenberg, J. G., Lee, T. C., 2003a. The cellular transducer in damage-stimulated bone remodelling: a theoretical investigation using fracture mechanics. J Theor Biol 225 (1), 65–75.

Taylor, D., Hazenberg, J. G., Lee, T. C., 2007. Living with cracks: damage and repair in human bone. Nat Mater 6 (4), 263–268.

Taylor, D., O'Reilly, P., Vallet, L., Lee, T. C., 2003b. The fatigue strength of compact bone in torsion. J Biomech 36 (8), 1103–1109.

Townsend, P. R., Rose, R. M., Radin, E. L., 1975. Buckling studies of single human trabeculae. J Biomech 8 (3-4), 199–201.

Turner, C. H., 1989. Yield behavior of bovine cancellous bone. J Biomech Eng 111 (3), 256–260.

Turner, C. H., Cowin, S. C., 1988. Errors induced by off-axis measurement of the elastic properties of bone. J Biomech Eng 110 (3), 213–215.

Ulrich, D., van Rietbergen, B., Laib, A., Ruegsegger, P., 1999. The ability of three-dimensional structural indices to reflect mechanical aspects of trabecular bone. Bone 25 (1), 55–60.

Vajjhala, S., Kraynik, A. M., Gibson, L. J., 2000. A cellular solid model for modulus reduction due to resorption of trabeculae in bone. J Biomech Eng 122 (5), 511–515.

van der Linden, J. C., Birkenhager-Frenkel, D. H., Verhaar, J. A., Weinans, H., 2001. Trabecular bone's mechanical properties are affected by its non-uniform mineral distribution. J Biomech 34 (12), 1573–1580.

van Rietbergen, B., Weinans, H., Huiskes, R., Odgaard, A., 1995. A new method to determine trabecular bone elastic properties and loading using micromechanical finite-element models. J Biomech 28 (1), 69–81.

Vashishth, D., 2004. Rising crack-growth-resistance behavior in cortical bone: implications for toughness measurements. J Biomech 37 (6), 943–946.

Wang, X., Masilamani, N., Mabrey, J., Alder, M., Agrawal, C., 1998. Changes in the fracture toughness of bone may not be reflected in its mineral density, porosity, and tensile properties. Bone 23, 67–72.

Wenzel, T. E., Schaffler, M. B., Fyhrie, D. P., 1996. In vivo trabecular microcracks in human vertebral bone. Bone 19 (2), 89–95.

Werz, T., 2005. Rasterelektronenmikroskopische bruchcharakterisierung biologischer materialien nach zyklischer wechselbelastung. Diplomthesis, University of Applied Sciences Regensburg.

Whitehouse, W. J., 1974. The quantitative morphology of anisotropic trabecular bone. Journal of Microscopy 101 (2), 153–168.

Whitehouse, W. J., Dyson, E. D., 1974. Scanning electron microscope studies of trabecular bone in the proximal end of the human femur. J Anat 118 (3), 417–444.

Whitehouse, W. J., Dyson, E. D., Jackson, C. K., 1971. The scanning electron microscope in studies of trabecular bone from a human vertebral body. J Anat 108 (3), 481–496.

W.H.O., 1994. World health organisation: Assessment of fracture risk and its application to screeening for postmenopausal osteoporosis. Report of a W.H.O. Study Group, World Health Organisation, Geneva, Switzerland.

Williams, J. L., Lewis, J. L., 1982. Properties and an anisotropic model of cancellous bone from the proximal tibial epiphysis. J Biomech Eng 104 (1), 50–56.

Wolff, J., 1892. Das gesetz der transformation der knochen. Hirschwald, Berlin.

Yamada, H., 1970. Strength of biological material. Williams & Wilkins, Baltimore.

Yamamoto, E., Crawford, R. P., Chan, D. D., Keaveny, T. M., 2006. Development of residual strains in human vertebral trabecular bone after prolonged static and cyclic loading at low load levels. J Biomech 39 (10), 1812–1818.

Yang, G., Kabel, J., van Rietbergen, B., Odgaard, A., Huiskes, R., Cowin, S. C., 1998. The anisotropic hooke's law for cancellous bone and wood. J Elast 53 (2), 125–146.

Yeni, Y. N., Fyhrie, D. P., 2002. Fatigue damage-fracture mechanics interaction in cortical bone. Bone 30 (3), 509–514.

Yeni, Y. N., Fyhrie, D. P., 2003. A rate-dependent microcrack-bridging model that can explain the strain rate dependency of cortical bone apparent yield strength. J Biomech 36 (9), 1343–1353.

Yeni, Y. N., Hou, F. J., Vashishth, D., Fyhrie, D. P., 2001. Trabecular shear stress in human vertebral cancellous bone: intra- and inter-individual variations. J Biomech 34 (10), 1341–1346.

Zioupos, P., Casinos, A., 1998. Cumulative damage and the response of human bone in two-step loading fatigue. J Biomech 31 (9), 825–833.

Zioupos, P., Currey, J. D., 1998. Changes in the stiffness, strength, and toughness of human cortical bone with age. Bone 22 (1), 57–66.

Zysset, P. K., 2003. A review of morphology-elasticity relationships in human trabecular bone: theories and experiments. J Biomech 36 (10), 1469–1485.

Zysset, P. K., Curnier, A., 1996. A 3d damage model for trabecular bone based on fabric tensors. J Biomech 29 (12), 1549–1558.

Appendix

Group	Load (σ/E_0)	Cycles to failure	E_0
Human vertebral 0°	0,0091	1	574
	0,0100	1	713
	0,0086	5	469
	0,0045	2600	533
	0,0089	3	483
	0,0044	100	420
	0,0035	25000	215
	0,0046	120	389
	0,0022	711000	400
	0,0057	25	372
	0,0033	22000	403
	0,0029	450000	508
	0,0032	17000	430
	0,0027	150000	350
Human vertebral 22°	0,0068	2	170
	0,0036	5600	165
	0,0042	1300	135
	0,0026	32500	167
	0,0035	9800	150
	0,0063	35	162
	0,0048	145	160
	0,0023	180000	165
Human vertebral 45°	0,0058	15	98
	0,0017	450000	170
	0,0075	12	111
	0,0109	1	233
	0,0036	2400	140
	0,0046	1600	230
	0,0031	40000	68
	0,0070	25	27
	0,0025	3400	120
	0,0027	7200	93
	0,0078	1	30
	0,0036	11000	48
	0,0037	1700	73

Group	Load (σ/E_0)	Cycles to failure	E_0
Human vertebral 90°	0,0063	5	20
	0,0037	300	70
	0,0021	95000	130
	0,0125	1	44
	0,0049	27	58
	0,0050	100	70
	0,0098	1	178
	0,0040	900	151
	0,0045	950	88
	0,0020	100000	206
	0,0031	18000	82
	0,0021	550000	288
	0,0036	16000	51
	0,0059	30	22
	0,0042	350	15,6
Human femoral 0°	0,0031	12000	845
	0,0029	47000	600
	0,0082	1	1118
	0,0045	1950	1720
	0,0078	7	1600
	0,0071	1	1395
	0,0026	210000	1440
	0,0030	27500	1008
	0,0052	525	1262
	0,0050	540	1280
	0,0029	250000	230
	0,0029	75000	308
	0,0023	1010000	601
	0,0060	300	890

Group	Load (σ/E_0)	Cycles to failure	E_0
Bovine vertebral 0°	0,0100	220	2746
	0,0125	31	1880
	0,0075	180	2170
	0,0068	14000	2330
	0,0080	125	2600
	0,0075	1500	2500
	0,0086	210	3300
	0,0125	9	1917
	0,0039	570000	2700
	0,0063	500	2340
	0,0060	1550	2250
	0,0070	425	1580
	0,0070	2000	2700
	0,0077	240	2470
	0,0057	7600	2145
	0,0056	9200	2604
	0,0055	8100	2050
	0,0049	42000	3250
	0,0147	3	1636
	0,0102	5	1957
	0,0093	42	2573
	0,0061	1000	1900
	0,0044	132000	3082
	0,0051	83000	83000
	0,0130	6	2004
	0,0084	100	2500
	0,0065	180	2559
	0,0063	3900	3562
	0,0056	17000	3205
	0,0103	6	2370
	0,0108	6	2715
Bovine vertebral 90°	0,0100	1	550
	0,0100	1	850
	0,0062	220	860
	0,0043	5900	1120
	0,0068	500	503
	0,0106	3	1520
	0,0058	1400	3080
	0,0050	4600	1700
	0,0082	5	470
	0,0074	50	1550
	0,0078	35	1038
	0,0037	60000	1480